

Christian BRANDSTÄTTER, B.Sc.

DETAILED ANALYSIS OF PCM-ALUMINIUM STORAGE MODULES

MASTERARBEIT

zur Erlangung des akademischen Grades

Diplom-Ingenieur

Masterstudium Maschinenbau

eingereicht an der

Technischen Universität Graz

Betreuer

Dipl.-Ing. Dr.mont. Hermann SCHRANZHOFER
Institut für Wärmetechnik

Beurteiler

Ao.Univ.-Prof. Dipl.-Ing. Dr.techn. René RIEBERER
Institut für Wärmetechnik

Graz, im Mai 2017

EIDESSTATTLICHE ERKLÄRUNG AFFIDAVIT

Ich erkläre an Eides statt, dass ich die vorliegende Arbeit selbstständig verfasst, andere als die angegebenen Quellen/Hilfsmittel nicht benutzt, und die den benutzten Quellen wörtlich und inhaltlich entnommenen Stellen als solche kenntlich gemacht habe. Das in TUGRAZonline hochgeladene Textdokument ist mit der vorliegenden Masterarbeit identisch.

I declare that I have authored this thesis independently, that I have not used other than the declared sources/resources, and that I have explicitly indicated all material which has been quoted either literally or by content from the sources used. The text document uploaded to TUGRAZonline is identical to the present master's thesis.

30.05.2017

Datum / Date



Unterschrift / Signature

KURZFASSUNG

Titel: Detaillierte Analyse von PCM/Aluminium Speichermodulen

Autor: Christian Brandstätter

1. Stichwort: Paraffin
2. Stichwort: Leistungsbestimmung
3. Stichwort: latente Wärme

Phasenwechselmaterialien (PCM) in Wärmespeichersystemen besitzen die Möglichkeit, Wärme sowohl in sensibler als auch latenter Form zu speichern. Dies erhöht die Speicherdichte im Vergleich zu Wasserspeichern und die Größe des Wärmespeichers kann damit reduziert werden. Es gibt viele unterschiedliche Phasenwechselmaterialien die in Abhängigkeit der chemischen Zusammensetzung eine bestimmte Phasenwechseltemperatur aufweisen. Durch eine gezielte Auswahl des Phasenwechselmaterials können dadurch verschiedene Temperaturniveaus für Speicherkonzepte in technischen Anwendungen abgedeckt werden. Der Betrag der freiwerdenden latenten Wärme während des Phasenwechsels kann je nach Art des verwendeten Phasenwechselmaterials (organisches oder anorganisches PCM) sowie der chemischen Reinheit variieren. Ein Nachteil von Phasenwechselmaterialien ist die geringe Wärmeleitfähigkeit im festen Zustand. Eine Kombination aus Phasenwechselmaterial mit Aluminiumschaum, der zur Verbesserung der Wärmeleitfähigkeit eingesetzt wird, kann die Leistung des Speicherkonzepts dabei maßgeblich verändern. Anhand von Labormessungen wurde eine Leistungsbestimmung eines experimentellen Speichermoduls durchgeführt, sowie anschließend mithilfe eines Simulationsmodells verglichen. Die Messungen konnten mithilfe der Simulation reproduziert werden und zeigten äquivalente Ergebnisse. Weitere Möglichkeiten und/oder Einschränkungen der Kombination PCM/Aluminiumschaum soll anhand dieser Masterarbeit untersucht und bewertet werden.

ABSTRACT

Title: Detailed analysis of PCM/Aluminium storage modules

Author: Christian Brandstätter

1st keyword: Paraffin

2nd keyword: Heat delivery

3rd keyword: Latent heat

Phase Change Materials (PCM) are capable of storing thermal energy in sensible and latent state with the advantage of increased storage density in comparison with water storage modules with the side-effect of minimizing storage size. Many different PCMs, which possess quite different phase change temperatures depending on their chemical composition, have been invented in recent years. Additionally these PCMs (either based on organic or anorganic structure) cover a large variety of temperature level which allows for raising the thermal performance in lot of applications. The amount of heat of fusion of the PCM is dependent on the chemical structure and the chemical purity of the PCM, which additionally extends the application range. One of the downsides of PCMs is the decreased heat conduction when it is in solid state. A combination of phase change material with aluminium foam, which complies as heat spreader, is able to increase the heat conduction to maximise the thermal output. An experimental storage module has been analysed in terms of thermal heat delivery and compared with a simulation model. The measurements could be reproduced with the simulation and the results are showing similar thermal behaviour. Determining the capabilities and/or limitations of this storage concept is part of this masters thesis.

VORWORT

Die Arbeit entstand im Rahmen des nationalen Forschungsprojektes Tes4Set (Thermal Energy Storages for Sustainable Energy Technologies; FFG Projektnummer: 845020) und wurde am Institut für Wärmetechnik der TU Graz durchgeführt. Alle Messutensilien sowie das umfangreiche Messequipment wurden vom Institut für Wärmetechnik zur Verfügung gestellt. Spezieller Dank geht daher in erster Linie an die leitenden Personen des Instituts für Wärmetechnik sowie an das Werkstättenpersonal, das mir immer mit Rat und Tat zur Verfügung stand und die anstrengenden und umfangreichen Tage im Labor mit willkommenen Konversationen auflockerte.

Ein besonderer Dank gebührt Hermann Schranzhofer, der mich seit vielen Jahren am Institut begleitet und mir diese Masterarbeit erst ermöglicht hat. Weiters hat er es verstanden, mich in den richtigen Momenten zu motivieren und stand mir mit seinem hervorragenden fachlichen Wissen immer hilfreich zur Seite. Hermann hat sehr viel seiner Freizeit geopfert diese Masterarbeit zu begutachten und mir sehr wertvolle Anmerkungen gegeben. Eine Masterarbeit wäre ohne seine Hingabe in dieser Form nicht möglich gewesen.

Weiters möchte ich meiner liebenswerten Freundin Maria, meiner geschätzten Familie, sowie meinen Freunden und Studienkollegen meinen Dank aussprechen, die mich all diese Jahre begleitet und unterstützt haben.

Graz, 31.05.2017



Brigitte Müller

TABLE OF CONTENTS

1	INTRODUCTION	1
1.1	Literature research	2
1.1.1	Porosity level	2
1.1.2	Natural convection	2
1.1.3	Numerical simulation	2
1.1.4	Effective thermal conductivity	3
1.2	Case of application (London subway system)	1
2	FUNDAMENTALS	4
2.1	Phase change material	4
2.2	Advantage of paraffin in comparison with water storage systems	6
2.3	Aluminium foam	8
2.4	Thermodynamic abstraction	10
2.4.1	Sensible heat	10
2.4.2	Latent heat	10
2.4.3	Sensible heat of the aluminium matrix	12
2.4.4	Sensible heat of additional components	12
2.4.5	Predominant flow condition (laminar or turbulent)	12
2.4.6	Heat delivery	14
2.4.7	Thermal gains	14
3	TRNSYS SIMULATION TYPE 842	15
4	MEASUREMENTS	18
4.1	Experimental box	18
4.2	Measurement strategy	21
4.3	Parallel tests	21
4.4	Measurement VS simulation for parallel flow configuration	24
4.5	Serial tests	31
4.6	Measurement VS simulation for serial flow configuration	33
4.7	Thermal gains of parallel and serial box experiments	39
4.8	Comparison of PCM/Aluminium modules with initial parametrization of type 842	40
4.9	Tube tests	44
4.9.1	Theoretical background	44
4.9.2	Tube composition	46
4.9.3	Measurement setup	47
4.9.4	Measurement strategy	49
4.9.5	Heat delivery of the tube tests	52
4.9.6	Thermal gains	54
4.9.7	Conclusion of the tube measurements	55
4.10	Measurement uncertainties	55
4.10.1	Random errors	56
4.10.2	Systematic errors	56
4.10.3	Error propagation	56
4.10.4	Propagation of uncertainties	58

5	CONCLUSION	60
6	REFERENCES	61
7	APPENDIX	A-1
7.1	Parametrization of the TRNSYS type 842	A-1
7.2	Parametrization of the flow distributor within the simulation	A-1
7.3	Calibration protocol of the PT100 temperature sensors	A-2
7.4	Calibration protocol of the Thermocouple sensors	A-3
7.5	Error estimation of the flow meter Endress + Hauser Promag 50P25	A-3
7.6	Tech data sheet Rubitherm RT5HC	A-4
7.7	Glysofor N – Specifications part I	A-5
7.8	Glysofor N – Specifications part II	A-6
7.9	AF/Armaflex insulation material	A-7
7.10	RS Components – Heat transfer paste RS217-3835	A-8

1 INTRODUCTION

During summer several subway tunnel systems may have problems with impact to overheating. This is reinforced by the thermal discharge of the HVAC cooling systems of the subway carriage and the undersized ventilation system of the tunnels, which cannot remove the excessive heat out of the system in an adequate amount of time. Also out of date HVAC systems are not capable of handling the increased amount of passenger volumes as the average lifespan of subway carriage are way above 10 years according to Lynch (2014). Additional ventilation fans would improve the hygienic change of air, but increase the temperature of the tunnel systems by thermal dissipation. To minimize thermal losses to the ambient and to enhance the power output of the air conditioning system of sub way carriages, combinations of heat exchanger with added PCMs are investigated. The charging of the modules could be provided either at each subway station or at the end of the line, when the subway carriage is inspected and/or cleaned.

Thermal energy storage systems (TES) using Phase Change Materials (PCM) are capable of storing and releasing large amounts of energy. These systems use the physical property of the shift in phase of the material, by using the sensible and the latent heat (water storage systems often use the sensible heat), and to increase the specific thermal output within a wide range of temperatures. As a result thermal energy storage systems can be reduced in size, which lead to more compact and heat efficient thermal energy storage systems. Unfortunately the thermal conductivity of the PCM is low when it is changing into solid state. This leads to extended charging/discharging durations with the side-effect of minimizing the power outcome. To compensate the effect of decreasing thermal conductivity in solid state metal foams are one possibility to increase the heat transfer, as the heat is spread over a larger surface area. The increased heat conduction by adding aluminium foam into the storage concept opens up new fields of applications by cutting costs for storage modules and more lightweight and rigid constructions.

The possibility of storing thermal energy within PCM storage systems has been investigated within the doctoral thesis of Heinz (2007). Different PCMs are characterised concerning the relevant physical properties and different possibilities for the integration of the materials into storage units are presented and tested experimentally. Simulation tools for different types of PCM storage tanks and heat exchangers have been developed and verified with experimental measurements.

Further applications on thermal energy storage systems in combination with PCM materials are successfully tested by Furbo et al. (2012), who investigated seasonal storage systems. PCMs used for heat pipe materials for mobile devices were tested by Tomizawa et al. (2015) and PCMs for automotive applications was investigated by Kim et al. (2008). In this master thesis an alternative approach for using thermal energy storage systems for increasing the performance of air conditioning systems of subway carriages is invested. A positive side-effect of combining the air conditioning system with PCM is, that the power consumption of the air conditioning system can be reduced, which leads to less heat losses and reduces the average temperature of the tunnel system itself. For this purpose a thermal energy storage system by using paraffin as PCM in combination with aluminium foam as containment matrix, was designed. An aluminium matrix is not only used to encapsulate the PCM but also to increase the thermal conductivity and the specific thermal output by reducing the charging/discharging duration. If one considers applications with lightweight construction as well, an aluminium matrix can be used to reinforce the fatigue of structure parts while enhancing thermal capabilities.

1.1 Literature research

Several research and developer teams have put their effort in improving and optimizing thermal energy systems by replacing ordinary storage materials with PCMs. Great success of using aluminium foam for improving thermal management in Li-Ion batteries has been documented by Wang et al. (2014). The team could show that the theoretical effective thermal conductivity of the composite PCM is almost 200 times larger than using pure paraffin and that the mechanisms of heat conduction and natural convection dominate the melting process. Additionally the enhancement of heat conduction is more dominant than the reduction of natural convection caused by the aluminium foam. According to the experimental results, additional amount of aluminium foam can accelerate the melting process. The experimental results also indicate that the temperature distribution in the composite PCM is more uniform than that in pure paraffin. Bauer and Wirtz (2000) could confirm the positive effect of increased thermal conductivity caused by using aluminium foam as heat conductor.

1.1.1 Porosity level

The porosity level of aluminium foam was investigated by Atal et al. (2015) and Mahdi and Nsofor (2016) who detected that metal foam with less porosity (higher metal content) resulted in faster charging/discharging cycles due to a higher overall thermal conductivity. This difference becomes more significant when the specific heat transfer rate is low so less energy can be transferred to the PCM. A substantial improvement on heat transfer rate could be shown when the metal foam is in direct contact to the inner wall of the heat exchanger tube. Less porous aluminium foam can enhance and accelerate the phase change process without significantly reducing the total amount of storable energy capacity inside the aluminium foam.

1.1.2 Natural convection

Research in natural convection inside metal foams was performed by Han et al. (2012) with experimental and numerical analysis of PCM flows inside aluminium foam cavities. Paraffin flows, caused by density differences inside the foam, are significantly low in comparison to heat conduction. A variation in porosity grade of the aluminium foam was negligible as the flow resistance and the viscosity of the paraffin limits the effect of natural convection.

1.1.3 Numerical simulation

Analysis on bulk PCM tanks with an immersed water-to-air heat exchanger have been performed by Heinz (2007). A TRNSYS storage model was validated based on experimental measurements. The model uses finite differences in the explicit formulation. The modelling of the phase change from solid to liquid is based on the enthalpy method by Claußen and Visser (1993). Additional simulations have been performed by Zang and He (2016) as a three-dimensional numerical abstraction for phase change material within open-celled aluminium foam. The velocity field distribution and the melting volume fraction within the composite PCM as a function of different porosities were acquired. It could be shown that during heat up phase the heat conduction was the dominating factor for the heat-transfer process but convection terms slightly increased as the viscosity of the paraffin decreased. The investigations of Nada and Alshaer (2015) focus on thermal management systems (under consideration of constant heat flux) of metal or carbon foam structures with different porosities which are saturated with

PCM. The outcome of this work is, by using a validated finite element numerical model based on volume averaging technique, that if the foam porosity is increasing the average thermal density is increasing as well and the temperature distribution across the porous medium is more regular.

Gao et al. (2017) developed a Lattice-Boltzmann simulation model to describe the melting process based on heat conduction of PCMs within porous metal foams. Different foam porosities hugely effect the overall heat transfer and the melting process.

1.1.4 Effective thermal conductivity

It is very difficult to estimate the thermal conductivity of PCM/metal foam composites as the porous structure cannot be properly abstracted within a simulation model. Xiao et al. (2013) determined the effective thermal conductivity, thermal diffusivity and thermal capacity of copper and nickel foams with embedded paraffin by testing metal foams with four different porosities and pore sizes by using a transient plane heat source method. The effective thermal conductivity is increasing by factor 25 in comparison to pure paraffin and it could be shown that the effective thermal conductivity is depending on porosity of the metal foam.

1.2 Case of application (London subway system)

As mentioned within the introduction subway tunnel systems, especially the subway tunnel system of London, are dealing with overheating issues during the hot summer months. So a maximum temperature of 47 °C has been reported in the year 2006. The outcome of the energy balance is that around 79 % of the energy input within the tunnel system is absorbed by the tunnels walls, 10 % is removed by ventilation and 11 % remain inside the tunnel system. These numbers have been publicised in the article of Plant engineer (2017). As the subway tunnel system of London is the oldest tunnel system in the world, a proper cooling or ventilation strategy was not part of the design when construction work started in the year 1863. Also due to the limited technical capabilities of that time the tunnels are very narrow, which are now limiting modern ventilation systems. So ventilation systems which are mounted over the circumference of the tunnel can be used in the minority of cases. To illustrate the small dimensions of the old subway tunnel system in comparison with modern subway carriages Figure 1-1 shows a carriage leaving one of the so called “tube” which has been built in the 19th century.



Figure 1-1: A modern subway carriage leaving a narrow tunnel built in the 19th century
source: https://de.wikipedia.org/wiki/London_Underground#/media/File:Why_London_Underground_is_ni cknamed_The_Tube.jpg

The main heat input into the tunnel system is caused by the braking/acceleration power of the subway carriage itself and the thermal waste of the HVAC system of the subway carriage. But also increased passenger numbers intensify the heat accumulation within the tunnel system. A thermal image of a subway carriage entering a station highlights this circumstance (Figure 1-2).



Figure 1-2: Thermal image of a subway carriage entering a station
 source: <https://www.welt.de/wissenschaft/article157165282/Darum-ist-es-in-der-U-Bahn-so-heiss.html>

It can be seen that the bottom of the subway carriage is dissipating much heat radiation which is caused by the hot braking disc. An overview of the most concerned tunnel lines suffering thermal issues is shown in Figure 1-3.

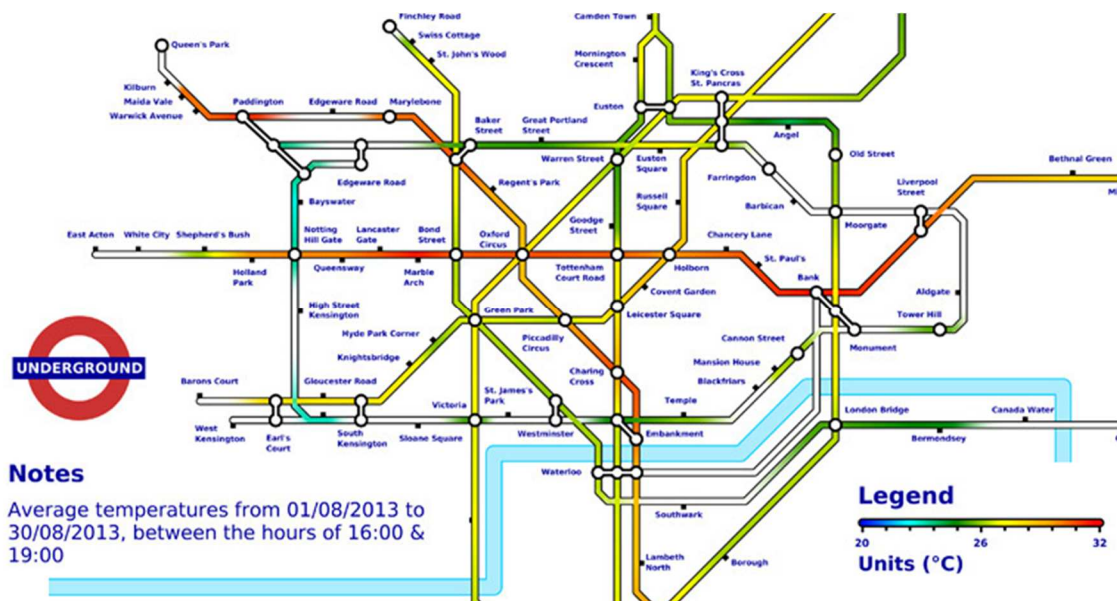


Figure 1-3: Temperature hotspots of the subway lines of London during August 2013
 source: <http://www.citymetric.com/transport/which-london-s-hottest-tube-line-1186>
<http://blog.loot.com/wp-content/uploads/2015/07/Underground.jpg>

The thermal investigation of the tunnel system was performed during August 2013 and it could be shown, that especially the ancient lines (such as the central line, built in 1900) are most concerned with overheating issues. As it is expected that the overheating issue is getting worse, several approaches have been tested and investigated. Some of these measures, such as combinations of ice cooling within the ventilation system or efforts of minimising thermal losses of the braking system by using magnetic brakes with energy recuperation, have been successfully tested. A different approach by minimizing the power consumption of the build in HVAC system can be achieved by using PCMs. The advantage of storing high amounts of energy within a compact storage system by using PCM aluminium modules, as available space is limited within a subway carriage, will now be discussed.

An approach investigated in the research project Tes4Set is the integration of a PCM storage directly in the HVAC system of a subway carriage. In terms of charging and discharging strategy for the subway carriages of London, it is best to include the PCM/Aluminium storage modules within the HVAC system of the carriage. So when the HVAC system is providing cool air for the passenger cabin the exhaust heat can be stored inside the PCM/Aluminium modules during the way through the tunnel. When the train is leaving the tunnel system the excessive heat can be released to the outside environment and the modules can be re-charged. When the subway carriage is again entering the tunnel system, the HVAC system can benefit from the stored energy inside the PCM/Aluminium modules which helps to minimize the power consumption of the HVAC system and minimizes the heat losses to the tunnel system.

2 FUNDAMENTALS

The main benefit of using phase change materials within thermal applications is its capability of providing additional energy by changing its physical state at a nearly constant temperature. This process is called latent heat conversion. A general overview of different types of PCMs as well as their specific physical parameter is described in the following chapter.

2.1 Phase change material

A phase change material based on paraffin was chosen for the application because it is nontoxic, non-corrosive and long-time stable. Additionally it can be combined with all sorts of materials and paraffins can be used in a widespread of applications and temperature ranges for example in domestic heat water preparations or storing thermal energy. Depending on length and uniformity of the carbon chains of the paraffin molecule it possesses a wider or smaller temperature range where phase change occurs according to Mehling and Cabeza (2008). In general it can be said that pure paraffins have a narrower temperature range than different blends of paraffin, but they do not have exact melting points. An overview of different PCMs in terms of phase change temperature can be seen in Figure 2-1.

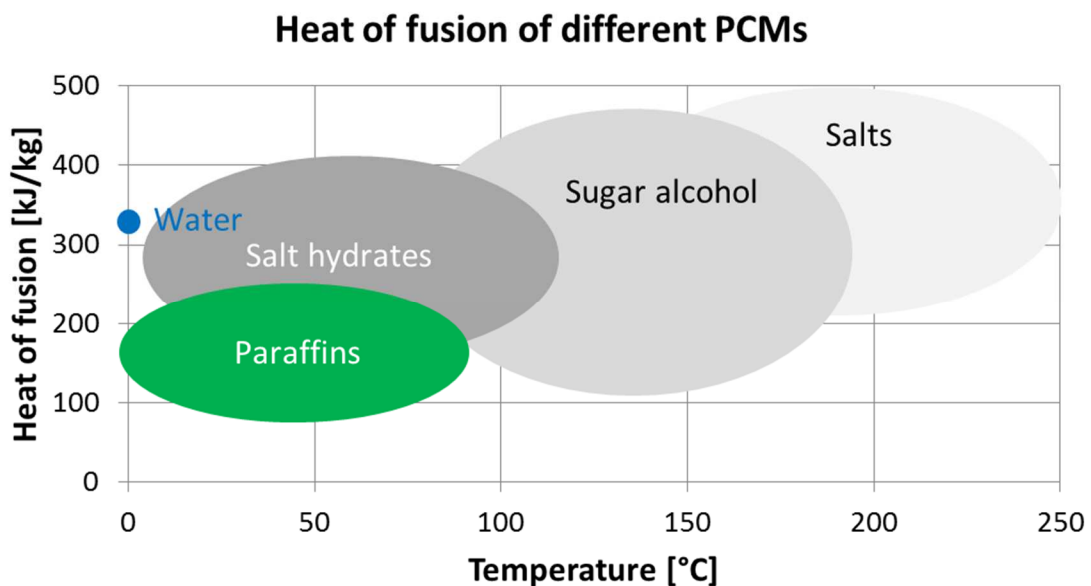


Figure 2-1: Heat of fusion of different PCMs depending on temperature
source: Mehling and Cabeza (2008)

Downsides of paraffins are their low density, their inflammability and their limited potential in cost saving applications as the price of paraffins is rather high in comparison to other PCMs. Also the price is increasing with higher purity of the used PCM. An investigation on investment costs have been performed by Cao (2013). The price range for paraffins varies from 2 €/kg up to 55 €/kg (for high purity laboratory grade paraffins). The average cost of inorganic PCMs, such as salt hydrates, is about 0.13 €/kg to 4 €/kg.

According to Figure 2-1 paraffins have a wide range where phase change occurs (-10 °C to +90 °C). In terms of maximum performance for technical cooling, reducing the phase change temperature would lead to increased thermal performance of the HVAC system. When considering technical and financial aspects then providing heat at lower temperature is much more cost intensive as providing heat at moderate levels. Therefore the decision was made, that paraffins with a phase change temperature of +5 °C seem to be best suited for the HVAC

system of the subway carriage. A symmetrical temperature range between +1 °C and +9 °C was chosen for the following experiments because the phase change temperature of the paraffin occurs at +5 °C. When providing a heat transfer fluid with a temperature difference of ± 4 K above and below the phase change temperature adequate heat deliveries from the heat exchanger to the paraffin should be achievable as well. Also the necessary heat delivery for providing the cooling heat is within acceptable ranges.

Out of the manufacturer sheet of Rubitherm (2016) there are different paraffins that can be used within a temperature range from -10 °C up to +90 °C and these paraffins provide a high specific heat storage capacity. Different heat of fusion enthalpies depending on phase change temperature can be seen in Figure 2-2.

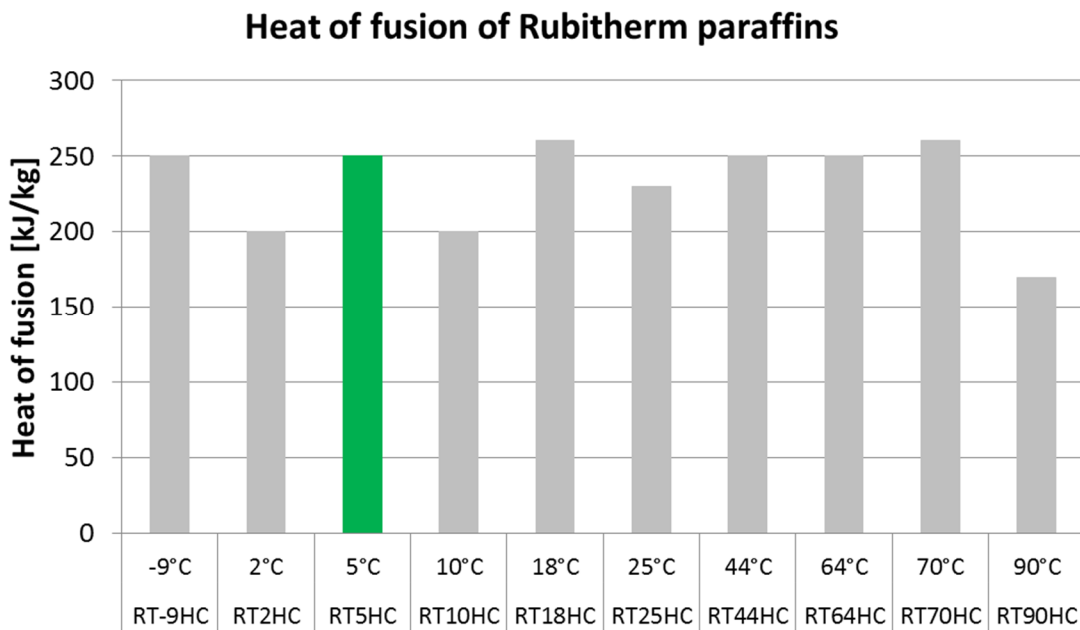


Figure 2-2: Heat of fusion of Rubitherm paraffins depending on phase change temperature source: Rubitherm (2016)

The selected paraffin type RT5HC Rubitherm (2016) should possess positive characteristics in terms of maximum performance, consistent specific thermal heat capacity and chemical purity. Paraffin Rubitherm RT5HC is an organic phase change material which shows no subcooling effects while performing its phase change within a temperature range between +3 °C and +6 °C. Subcooling is the effect that a temperature is significantly below the melting temperature of the paraffin, until the material begins to solidify and release heat. When operating the paraffin at operating temperatures greater than +30 °C the amount of crystallisation particles is decreasing, leading to subcooling effects. These subcooling effects are difficult to predict and usually not favoured within technical applications. As the paraffin RT5HC possesses a particular composition with high chemical purity it is possible to gain greater values of heat of fusion within a narrow temperature range. Additionally it is chemical inert and the phase change is constant over the time. As illustrated in Figure 2-2 paraffin Rubitherm RT5HC does possess a heat of fusion of 250 kJ/kg with a phase change temperature of +5 °C. An overview of all relevant physical properties of paraffin Rubitherm RT5HC is shown in Table 2-1.

Table 2-1: Physical properties of the phase change material Rubitherm RT5HC

Phase change temperature	Specific heat capacity of solid phase	Specific heat capacity of liquid phase	Heat of fusion	Thermal conductivity
[°C]	[kJ/(kg.K)]	[kJ/(kg.K)]	[kJ/kg]	[W/(m.K)]
5	15	2	250*	0.2
Density of solid phase	Density of liquid phase	Volumetric expansion	Max. operating temperature	Flash point
[g/dm ³]	[g/dm ³]	[%]	[°C]	[°C]
880	760	13	30	115

source: Rubitherm (2016)

* The combination of latent and sensible heat within a temperature range of -2 °C to 13 °C according to Figure 2-8.

Noticeable is the rather low thermal conductivity of about 0.2 W/(m.K), while metals such as aluminium possess significant higher values.

2.2 Advantage of paraffin in comparison with water storage systems

Two main advantages of PCM over conventional water storage techniques for thermal energy storage are according to IEA (2005)

- a) Relatively constant temperature during charging and discharging
- b) Higher thermal energy storage capacity compared to the sensible energy storage in water. This leads to smaller required storages but this is only advantageous when small temperature ranges are used to charge/discharge the storage system

The advantage in heat storage capacity of 1 kg paraffin in comparison with 1 kg water within a certain temperature range is illustrated in Figure 2-3. All values within this figure consider the paraffin Rubitherm RT5HC with a phase change temperature of +5 °C, when varying the temperature within ±1 K (4 °C to 6 °C), ±4 K (1 °C to 9 °C) and from 0.01 °C to 30 °C.

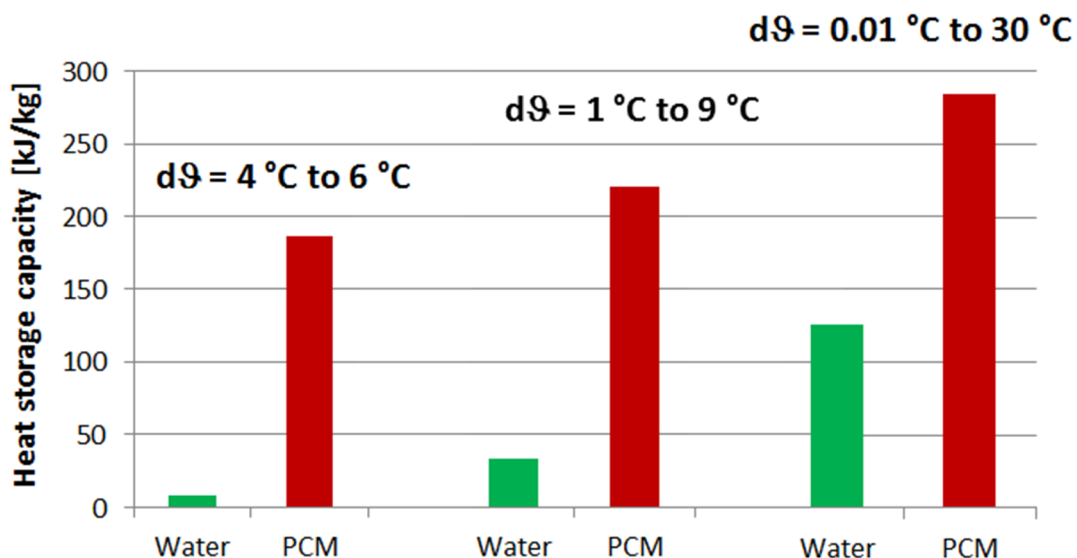


Figure 2-3: Heat storage capacity of 1 kg PCM in comparison with 1 kg water within certain temperature ranges

As thermal energy of liquid water can only be stored within sensible state, the PCM shows its advantage of storing energy within sensible and latent state. Therefore the energy storage capacity of PCM in comparison with water is much larger when performing a phase change within this temperature range, but this advantage is slowly decreasing when the temperature difference is increasing from $\Delta\vartheta = 2\text{ K}$ to $\Delta\vartheta = 6\text{ K}$. This can be explained by the fact, that the specific heat capacity of water is double the specific heat capacity of the paraffin.

As the chosen temperature difference can depend on thermal application Figure 2-4 shows the progression of energy content when a PCM/Aluminium module (with 10.7 kg paraffin and 6.72 kg Aluminium foam) will be compared with a water storage tank of the same storage volume. This particular paraffin and aluminium mass has been chosen as it represents the experimental PCM/Aluminium box which is described and explained in the chapter 4.1 later on. Table 2-2 gives a quick overview of the energy content of each storage concept depending on the temperature range, where charging/discharging of the storage occurs. As the PCM/Aluminium module consists of paraffin and Aluminium foam, the energy content of the aluminium foam has been considered as well. The energy content of the housing and periphery of both storage types have been neglected, as equivalent storage volume for both storage types have been assumed.

Table 2-2: Improvement of the storage energy content comparing a PCM/Aluminium module with a water tank of the same storage volume

$\Delta\vartheta$	Energy content water	Energy content PCM	Energy content Al-foam	Σ PCM + Al-foam	Improvement
	[kJ]	[kJ]	[kJ]	[kJ]	[-]
(4-6 °C)	156.7	2000.9	12.1	2013.0	12.8
(3-7 °C)	313.3	2017.9	24.2	2042.1	6.5
(2-8 °C)	470.0	2034.5	36.4	2070.9	4.4
(1-9 °C)	626.6	2051.9	48.2	2100.1	3.4
(0.01-10 °C)	782.5	2068.8	60.2	2129.0	2.7

When analysing the progression of the storage energy contents of the PCM/Aluminium module in comparison with a water storage (according to Figure 2-4), it can be seen that the beneficial effect of using heat of fusion is decreasing with a wider temperature range.

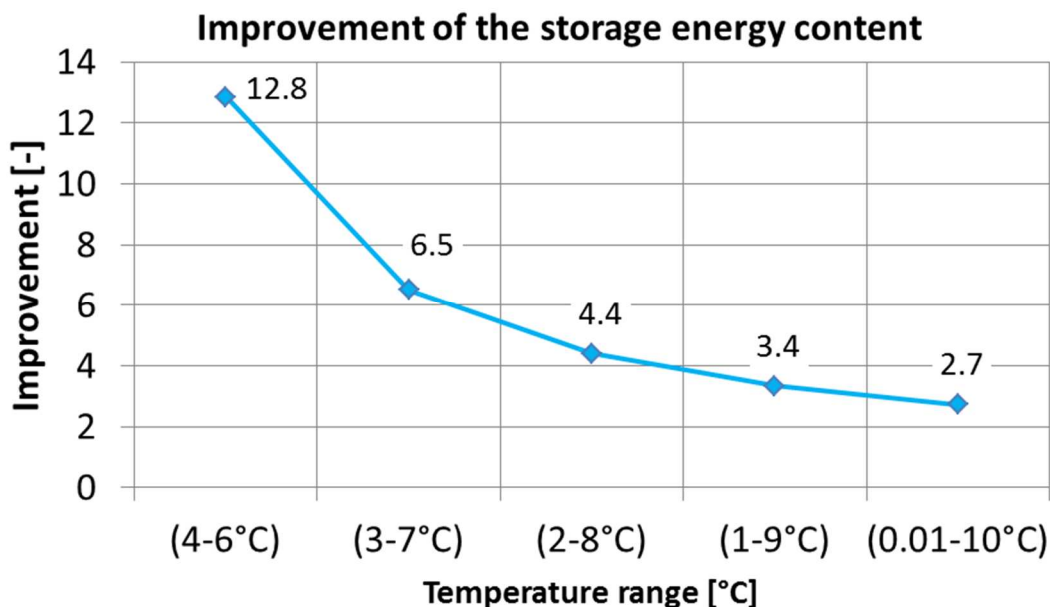


Figure 2-4: Improvement of the storage energy capacity of paraffin in comparison with water depending on different temperatures ranges

For a chosen temperature range, starting with initial temperatures of +9 °C and finishing at a temperature of +1 °C, the expected improvement of available energy content inside the thermal energy storage by using a PCM/Aluminium storage concept is expected to be 3.4 times better in comparison with a water storage tank of same volume. When the temperature range is increasing the amount of sensible heat within a water storage tank equals the effect of the latent heat of the PCM material because of the larger specific heat capacity of the water. Therefore PCM/Aluminium storage systems show best performances within small temperature ranges.

Four main disadvantages of PCM compared to conventional water storage techniques are according to IEA (2005)

- a) Higher investment costs
- b) The peak power during discharging is limited due to limited heat conduction in the solid state of the PCM. This is the main limit for determining an acceptable size for the PCM storage modules
- c) Limited experience with long-term operation of many thousands of charge-discharge cycles
- d) Risks of loss of stability of the solution and deterioration of the encapsulation material. As the temperatures level of the chosen application is low, deterioration issues of the PCM should not cause any problems.

2.3 Aluminium foam

According to Mehling and Cabeza (2008) the heat transfer depends on the heat transfer area, the mode of heat transfer (convection, conduction, radiation) the corresponding heat transfer coefficient and the temperature gradient. When trying to improve the heat transfer, one method is to increase the surface area. As foam like structures (such as Aluminium foam) consist of a large surface area, this characteristic can be useful to increase the heat transfer rate from the heat transfer fluid to the PCM material.

Aluminium foam is a porous structure consisting of numerous cavities which can be sealed (closed cell foam) or interconnected with each other (open cell foam). Aluminium foam combines good thermal conductivity and large surface area within a lightweight design. Typical fields of application are structural parts, filtration applications, acoustic and vibration damping as well as energy absorption for automotive applications. The main benefits of using aluminium foam are applications where a lightweight and rigid structure is used. Aluminium foams are usually manufactured by melting the aluminium and injecting gases or blowing agents into the liquid aluminium. By varying several process parameters it is possible to produce aluminium foams with different porosity level. After solidification the aluminium foam can undergo further processing steps such as cutting, drilling or milling. According to Banhart and Seelinger (2008) there are several types of aluminium foam as can be seen in Figure 2-5.

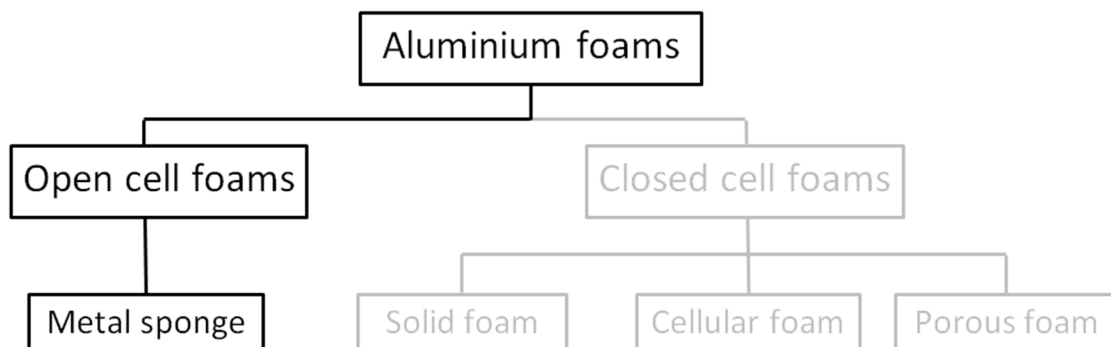


Figure 2-5: Types of aluminium metal foams

A metal sponge consists of interconnected voids (open cell foam) which are necessary to ensure proper infiltration of paraffin inside its aluminium structure. An aluminium metal sponge foam with a porosity of 69.4 % and a pore diameter between 3 mm and 12 mm was used for this application. A cross-sectional image of the used aluminium foam can be seen in Figure 2-6.



Figure 2-6: Internal structure of the aluminium foam

An overview of relevant physical properties of the aluminium foam in comparison with other materials within thermal applications is shown in Table 2-3. The porosity of the aluminium foam has been calculated out of the fraction of the density of the aluminium foam and the density of solid aluminium.

Table 2-3: Physical properties of materials used in thermal storage systems

Material	Density	Specific heat	Thermal conductivity	Melting point
	[g/dm ³]	[kJ/(kg.K)]	[W/(m.K)]	[°C]
Aluminium foam AlSi10	826.2 69.4 % porosity	0.897	71.6	660
Copper	8920	0.385	401	1358
Polypropylen	915	1.920	0.2	130
Rockwool	200	1.012	0.03 – 0.045	1250
AF/Armaflex	45 – 100	0.840	0.033	240

The thermal conductivity λ_f of the PCM/Aluminium matrix can be calculating by the volume fraction of each substance, according to equation (2-1) and it is assumed, that the aluminium foam is totally soaked with paraffin.

$$\lambda_f = (1 - p) \cdot \lambda_{Al} + p \cdot \lambda_{PCM} \quad (2-1)$$

The porosity of the aluminium matrix is denoted as p and λ_{Al} and λ_{PCM} are the thermal conductivities of the aluminium matrix and the paraffin. This equation does not account for natural convection between the paraffin and the aluminium foam or the pore size. According to equation (2-1) it is evident, that the thermal conductivity λ_f increases when the porosity p of the aluminium matrix is decreasing.

2.4 Thermodynamic abstraction

To classify and evaluate a thermal energy storage system in terms of heat delivery a few thermodynamic fundamentals have to be defined. A good overview of all flow situations within cylindrical pipes gives the literature VDI Wärmesatlas (2006).

2.4.1 Sensible heat

For an isobaric change of state the amount of stored energy Q can be calculated by a multiplication of the mass m , the specific heat capacity cp and the temperature difference between final and initial state ($T_f - T_i$).

$$Q = m \cdot cp \cdot (T_f - T_i) \quad (2-2)$$

Heat transferred to the storage medium, according to equation (2-2), results in a change of temperature of the storage medium. Sensible heat is the most common form of storing heat in thermal storage modules, but storage types which combine both sensible and latent heat are also considered within storage concepts. The specific heat capacity is assumed to be constant over the chosen temperature range, or does not change significantly.

2.4.2 Latent heat

The storage capacity of PCMs is not only based on a sensible temperature change but also on a change of state of the material itself. This means the change of state from either solid to liquid or liquid to gaseous state. The progression of stored specific enthalpy as a function of the temperature is shown in Figure 2-7. When summarizing the specific enthalpies out of Figure 2-7, starting at a temperature of -2 °C , the incremental enthalpies of a temperature increase of 1 K , can be arranged to create a heat storage capacity chart as shown in Figure 2-8. The heat of fusion for undergoing a phase transition is the amount of energy that must be added to the system in order to change the physical state of the material from solid to liquid. As pure systems perform an instant phase change impure materials such as paraffins, perform the phase change in a temperature range, where both solid and liquid phase occur simultaneously. This physical effect can be seen in Figure 2-8. Unfortunately the change of state often results in an additional volumetric change of the material. This circumstance must be taken into consideration when performing a phase change. The volumetric change of Rubitherm RT5HC is considered to be 13% according to the manufacturer's tech data sheet Rubitherm (2016). In comparison the change in volume of water/ice is 8.9% and the heat of fusion of water/ice is 334 kJ/kg . Minimal to zero hysteresis effects, (when the specific enthalpies of charging and discharging process possess different values at the same temperature) can be seen in Figure 2-8.

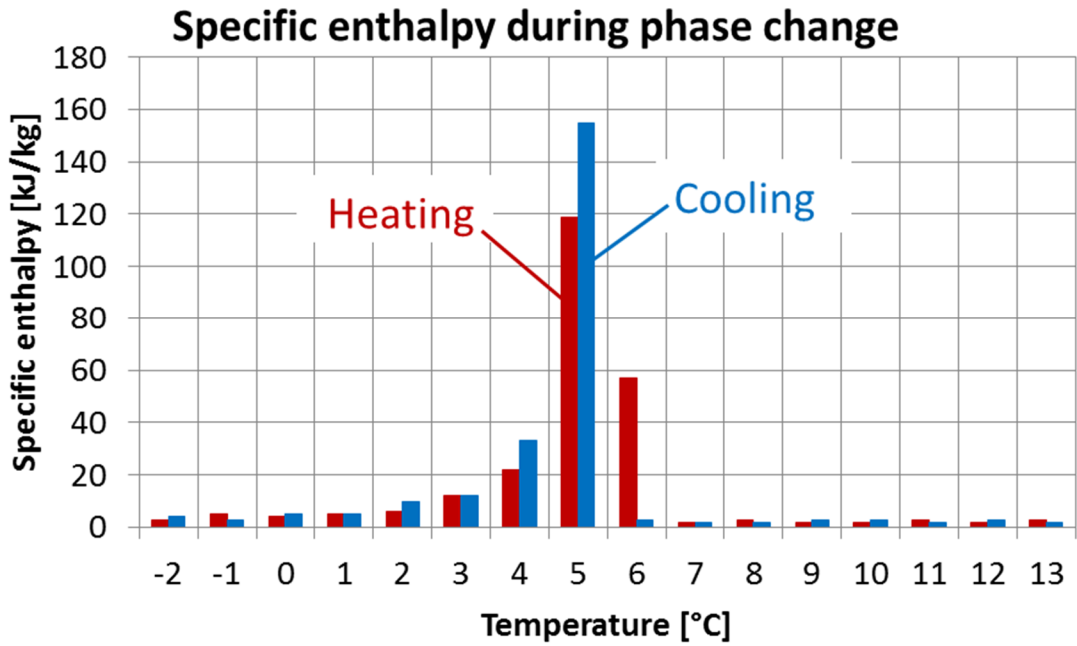


Figure 2-7: Specific enthalpy of paraffin Rubitherm RT5HC within a temperature range of -2 °C to +13 °C
source: Rubitherm (2016)

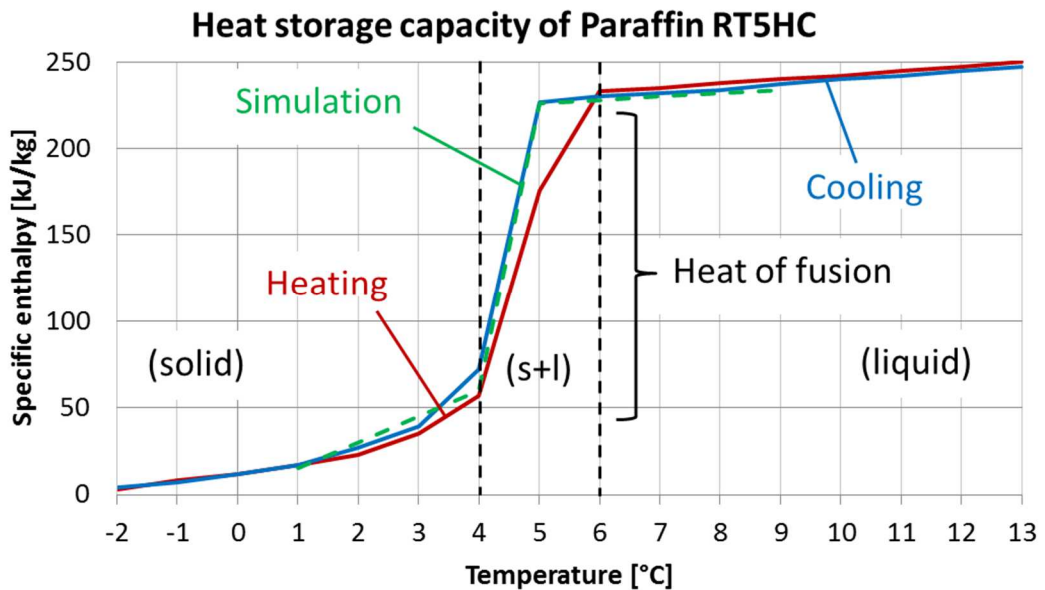


Figure 2-8: Sensible and latent heat progression of paraffin RT5HC within a temperature range of -2 °C to +13 °C
source: Rubitherm (2016)

The slight difference in energy balance (according to Figure 2-8) is probably caused by measurement uncertainties when determining the thermal behaviour of the paraffin via a DSC (Differential Scanning Calorimetry) analysis. As the cooling process is more technical relevant for the HVAC system of the subway carriage the cooling curve of the paraffin RT5HC has been reproduced for the parameters within the simulation (according to Table 3-1). This curve can be seen in Figure 2-8 and represents the green dashed curve. Noticeable is that the gradient of specific enthalpy of sensible energy in solid state is higher as the gradient of specific enthalpy of sensible energy in liquid state. At temperatures below zero degrees the gradient of specific enthalpy has the same value than at liquid state. It can be assumed that the total phase change is finished at temperature below zero degrees, but the major part of heat of fusion occurs

between +4 °C and +6 °C. This fact has to be considered when using the paraffin within certain temperature level.

The total heat content of a PCM performing a phase change defines as

$$Q_{PCM} = Q_{Sensible_{solid}} + Q_{Latent} + Q_{Sensible_{liquid}} \quad (2-3)$$

$$Q_{PCM} = m_{PCM} \cdot \left[cp_{PCM_{sensible_{solid}}} \cdot (T_{f_{solid}} - T_{i_{solid}}) + h_{PCM_{latent}} + \right. \\ \left. + cp_{PCM_{sensible_{liquid}}} \cdot (T_{f_{liquid}} - T_{i_{liquid}}) \right]$$

According to equation (2-3) m_{PCM} denotes the mass of the PCM and cp_{PCM} denotes the specific heat capacity of sensible heat of the PCM. $h_{latent_{PCM}}$ denotes the heat of fusion of the PCM and the difference $(T_f - T_i)$ denotes the temperature of initial and final state where heat has been exchanged.

2.4.3 Sensible heat of the aluminium matrix

As the PCM/Aluminium storage module consists of PCM and a certain amount of aluminium foam, the sensible heat content of the aluminium foam has to be abstracted as well.

$$Q_{Al_{foam}} = m_{Al_{foam}} \cdot cp_{Al_{foam}} \cdot (T_f - T_i) \quad (2-4)$$

The energy of the aluminium foam $Q_{Al_{foam}}$ according to equation (2-4) calculates by a multiplication of the mass of the aluminium foam $m_{Al_{foam}}$, the specific heat capacity of the aluminium foam $cp_{Al_{foam}}$ and the temperature difference between final and initial state $(T_f - T_i)$.

2.4.4 Sensible heat of additional components

As there are also additional thermal masses such as the housing or the steel pipes, passing through the experimental storage module, these thermal masses can be abstracted by additional energy contents.

$$Q_{add} = m_{add} \cdot cp_{add} \cdot (T_f - T_i) \quad (2-5)$$

The energy of the additional thermal masses Q_{add} , according to equation (2-5), calculates by a multiplication of the mass of the additional thermal masses m_{add} , an average specific heat capacity of the additional masses cp_{add} and the temperature difference between final and initial state $(T_f - T_i)$.

2.4.5 Predominant flow condition (laminar or turbulent)

As the Nusselt Number (characterizes the physical effect between convection and heat conduction) for a flowing liquid within a cylindrical pipe (see equation (2-6) to equation (2-9)) is dependent on the Prandtl number according to equation (2-10) it is evident that increased Reynolds numbers, see equation (2-11), lead to increased Nusselt numbers and therefore to reduced charging/discharging durations.

for turbulent flows with $Re > 10^4$, according to chapter G of VDI Wärmeatlas (2006)

$$Nu_{d_{turb}} = \frac{\left(\frac{\xi}{8}\right) \cdot Re_d \cdot Pr}{1 + 12.7 \cdot \sqrt{\frac{\xi}{8}} \cdot \left(Pr^{\frac{2}{3}} - 1\right)} \cdot f_1 \cdot f_2 \quad (2-6)$$

$$\xi = [1.8 \cdot \log(Re_d) - 1.5]^{-2} \quad (2-7)$$

$$f_1 = 1 + \left(\frac{d_i}{l}\right)^{\frac{2}{3}} \quad (2-8)$$

$$f_2 = \left(\frac{Pr}{Pr_W}\right)^{0.11} \quad (2-9)$$

It has to be mentioned that the Nusselt number can be defined for turbulent flows as well as for laminar flows and these Nusselt numbers are acquired out of experiments.

As the heat transfer coefficient is direct proportional to the Reynolds number of the streaming fluid, increased Reynolds numbers lead to larger heat capacities that can be transferred to the PCM material. The thermal output of thermal energy storage systems can therefore be increased by either changing the Prandtl number of the heat exchanging fluid or due to increased flow velocity within the pipe. Due to increased pressure resistance, (the pressure resistance is rising with square of the flow velocity according to equation (2-12)), it is evident that there are technical limits where a further increase in flow velocity is not reasonable.

The Prandtl number, as defined in equation (2-10), denotes the velocity diffusion coefficient divided by the temperature diffusion coefficient and is only dependent on the physical properties of the heat transfer fluid such as thermal conductivity λ , the specific heat capacity c_p and the dynamic viscosity μ .

$$Pr = \frac{v}{a} = \frac{\mu \cdot c_p}{\lambda} \quad (2-10)$$

The Reynolds number according to equation (2-11) is defined as the velocity w multiplied with the characteristic length d (for a cylindrical pipe this equals its inside diameter) of the heat transfer fluid divided by the kinetic viscosity ν of the heat transfer fluid.

$$Re = \frac{w \cdot d}{\nu} \quad (2-11)$$

The pressure drop is dependent on length of the pipe l_{pipe} , the drag coefficient of the pipe λ_{pipe} , the density ρ of the fluid multiplied by the square of the velocity of the fluid divided by the diameter d of the pipe.

$$\Delta p = \frac{l_{pipe} \cdot \lambda_{pipe}}{d} \cdot \frac{\rho}{2} \cdot w^2 \quad (2-12)$$

Large changes in pressure resistance can be achieved if the flowing velocity w , the length of the pipe l_{pipe} or the diameter d of the pipe is varied. The roughness of the pipe has also an effect on the drag coefficient λ_{pipe} . A detailed description of the flow situations inside cylindrical pipes can be found in chapter G according to VDI Wärmeatlas (2006).

The flow velocity and the diameter remain constant during a measurement with a chosen mass flow rate (Law of continuity) but the kinetic viscosity varies with the temperature of the heat transfer fluid. According to Table 2-4 the Reynolds numbers differs with a percentage of 28.8 % when cooling the heat transfer fluid from +9 °C to +1 °C. This results in increased pressure drop and has to be taken into consideration when defining the hydraulic system.

Table 2-4: Physical properties and according Reynolds number of the heat transfer fluid Glysofor N with 70vol% water and 30vol% Monoethylenglycol for a estimated mass flow rate of 3000 kg/h at +9 °C and +1 °C

Fluid temperature [°C]	Fluid velocity [m/s]	Inside diameter [m]	Kinematic viscosity [m ² /s]	Reynolds number [-]
9	3.95	0.016	4.45x10 ⁻⁶	19914
1	3.95	0.016	3.17x10 ⁻⁶	14186

For Reynolds numbers greater than $Re_{crit} > 2300$ it can be assumed that the flowing situation is turbulent. For Reynolds numbers smaller than $Re_{crit} < 2300$ every turbulence inside a pipe is slowly diminishing over the length of the pipe.

2.4.6 Heat delivery

The heat delivery from the heat transfer fluid to the encapsulated PCM according to equation (2-13) calculates by multiplying the mass flow rate \dot{m}_{Glycol} with its specific heat capacity cp_{Glycol} and the temperature difference between input and output of the system ($T_{in} - T_{out}$).

$$\dot{Q}_{system} = \dot{m}_{Glycol} \cdot cp_{Glycol} \cdot (T_{in} - T_{out}) \quad (2-13)$$

The achievable temperature difference is dependent on the flow situation inside the tube as mentioned in the previous sections.

2.4.7 Thermal gains

Thermal gains can be estimated by measuring the incremental temperature rise over a certain time by knowing the total amount of all thermal masses inside the system.

$$\dot{Q}_{loss} = \frac{(m_{water} \cdot cp_{water} + m_{PCM} \cdot cp_{PCM} + m_{steel} \cdot cp_{steel}) \cdot dT}{dtime} = UA \cdot (T_{amb} - T) \quad (2-14)$$

As the total energy content of the experimental module is known, any temperature increase over a certain time represents thermal gains driven by natural convection at the outside of the module according to equation (2-14). The thermal gains decrease when the average temperature of the module is approaching ambient temperature.

3 TRNSYS SIMULATION TYPE 842

To not only collect raw data from experimental measurements but also to compare the outcome of the measurements with simulation results, a suitable TRNSYS type has to be defined. The TRNSYS simulation studio (version 17.02.0004) was used for the simulations. Preceding work has been accomplished by Heinz (2007), who compared several PCM storage modules in his doctoral thesis and programmed the TRNSYS storage type 842 (a model for the transient simulation of bulk PCM tanks with an immersed water-to-air heat exchanger; IWT TU Graz (2007)). This type 842 should provide an equivalent abstraction of the PCM/Aluminium storage concept within this application. It is known that the model type 842 is lacking in abstraction compared to the real measurement as it is assumed that the temperature within each node is constant for each iteration step. This simplification is incorrect because due to the three-dimensional heat transfer processes and the resulting temperature gradients between tubes, the aluminium foam and the PCM, identical temperatures at one certain area of the module cannot be expected. But despite lacking in exact abstraction of heat flux between the simulation and the real measurement this model should give quick results for estimating the heat delivery of equivalent storage modules. Additionally several parameters of type 842 can be adjusted to accomplish similar results as the measurements of the PCM/Aluminium storage module and can be used for further investigations of the systems via thermal system simulations.

The TRNSYS type 842 represents an air heat exchanger, which is not exposed to air as heat transporting fluid, but to PCM between its aluminium fins, and the flow configuration can be adjusted in parallel as well as serial configuration. The description of the model for the transient simulation of the bulk PCM tank, representing an immersed water-to-air heat exchanger, can be seen in chapter 6.3 within the doctoral thesis of Heinz (2007). When the type 842 is parametrized with the physical properties of paraffin and the used aluminium foam basically replicates the PCM/Aluminium matrix which has been used within the tested experimental modules. Additionally the TRNSYS type 842 has been validated and also used in simulations prior these experiments by Nagano et al. (2005).

According to Figure 3-1 it is intended to abstract the porosity level of the aluminium foam with the built in simulation parameter t_f (distance between each fin) and s_f (thickness of each fin), as the aluminium foam consists of cavities, which represent the distance between the fins, and a thin aluminium shell representing the thickness of the aluminium fins. The distance between the heat transporting tubes can be adjusted by the parameter t_l (vertical distance between the pipes) and t_q (horizontal distance between the pipes). The exact volume of the aluminium foam cannot be specified within the simulation type, but based on the volume of the PCM (density and mass of the PCM are well known) and the calculated volume of the heat exchanger tubes, simulation type 842 is replacing the rest of the available space within the simulation module with aluminium fins. These aluminium fins represent the aluminium foam of the experimental box. After adjusting the mass of the PCM, the mass of additional thermal capacities of the experimental modules, density of the PCM and the aluminium foam, and the thermal conductivity parameters of PCM and aluminium the TRNSYS type 842 is a quite good abstraction of the experimental modules. Figure 3-1 gives a quick overview of the modified PCM/air heat exchanger as well as the most important parameter used within the simulation. All other parameter of the type 842, which have been modified to suit the experimental modules, can be found in the appendix and in Table 3-1.

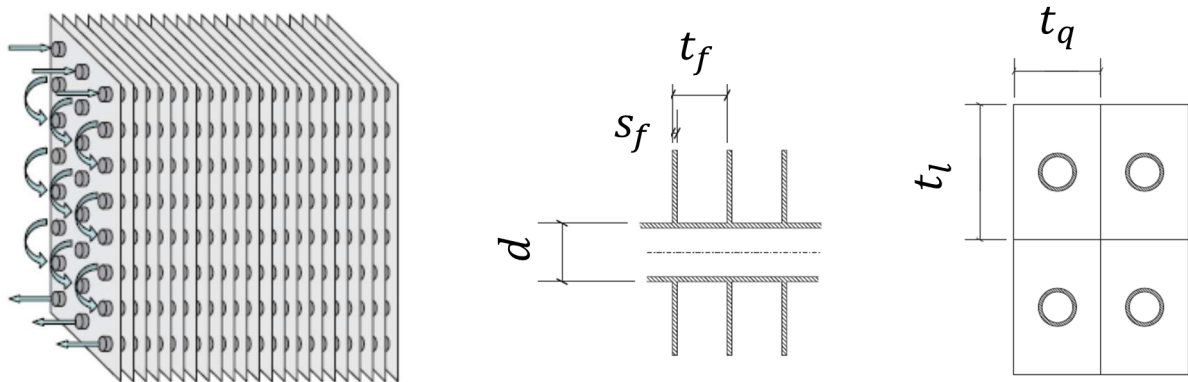


Figure 3-1: TRNSYS type 842 and relevant parameters

Length t_l and width t_q of the “elementary cell” of the surrounding tube area are equal to the average distance between the tubes of the experimental box in vertical and horizontal direction. The dimensions of the box as well as the distance between the tubes are shown in Figure 4-3. Unfortunately the thermal conductivity of the PCM cannot be separated in thermal conductivity of solid and liquid state but only as general parameter for both phases. This seems to be the only disadvantage of using this simulation model.

Table 3-1: Relevant parameter to parametrize the TRNSYS storage type 842

Masses contained in the module			Thermal properties of the used materials		
m_{PCM}	10.7	kg	λ_t	15	W/(m.K)
m_{add}	18	kg	ρ_t	7850	kg/m ³
			cp_t	477	J/(kg.K)
			λ_f	70.6	W/(m.K)
			ρ_f	660	kg/m ³
			cp_f	897	J/(kg.K)
Dimensions of the module					
length of the tubes	0.5	m	cp_{add}	477	J/(kg.K)
Nr. of parallel tubes	1 or 14*	-	ρ_{PCM}	760	g/dm ³
Nr. of serial tubes	1 or 14*	-	λ_{PCM}	0.2	W/(m.K)
d	18	mm	cp_{sPCM}	15	kJ/(kg.K)
t_w	1	mm	cp_{lPCM}	2	kJ/(kg.K)
t_l	41.667	mm	Δhm_{PCM}	163	kJ/kg
t_q	37.5	mm	T_{start}	8.3...9.1	°C
t_f	5	mm	T_{m1}	4	°C
s_f	2	mm	T_{m2}	5	°C

* depending on parametrizing the experimental box in parallel or serial flow configuration

trepresents parameter considering the tube

frepresents parameter considering the fin

cp_{add}specific heat of additional thermal capacity

PCMrepresents parameter considering the PCM material

T_{start}initial temperature of the module

T_{m1}temperature at which melting of the storage medium begins

T_{m2}temperature at which storage medium is fully melted

The most important notations are shown below Table 3-1 and a detailed description of all parameters as well as the numerical abstraction of the TRNSYS type 842 can be found in chapter 6.3 of the doctoral thesis of Heinz (2007).

Input data to the TRNSYS simulation have been flow temperature, as well as the mass flow rate and the ambient temperature and were collected out of the measurement data. Also the surface

temperatures of the box measurements are transferred to the simulation (with type9c) to check for charging/discharging progress and for comparison with the PCM node temperatures of the simulation. As the experimental box measurements in parallel flow orientation are provided with a flow distributor in flow and return stream (Figure 4-5) the simulation has to be adapted to these additional masses. This can be done by abstracting the flow distributor by using a water storage tank model (type4c) which has to be parametrized with the physical properties of the heat transfer fluid and a storage volume of 6.75 dm³. All simulated values and results (PCM node temperatures, calculated heat deliveries, return flow temperature of the simulation...) have been collected with an online plotter (type65c and type25c) and written to an output file for further analysis and data visualization. The time steps of measurements and simulations have been 1 second. A quick overview of the TRNSYS components within the simulation gives Figure 3-2 in the TRNSYS STUDIO view. In general the TRNSYS components of both parallel and serial simulations were identical, but the volume of the flow distributor and the flow configuration of type 842 (parallel versus serial measurements) have been changed.

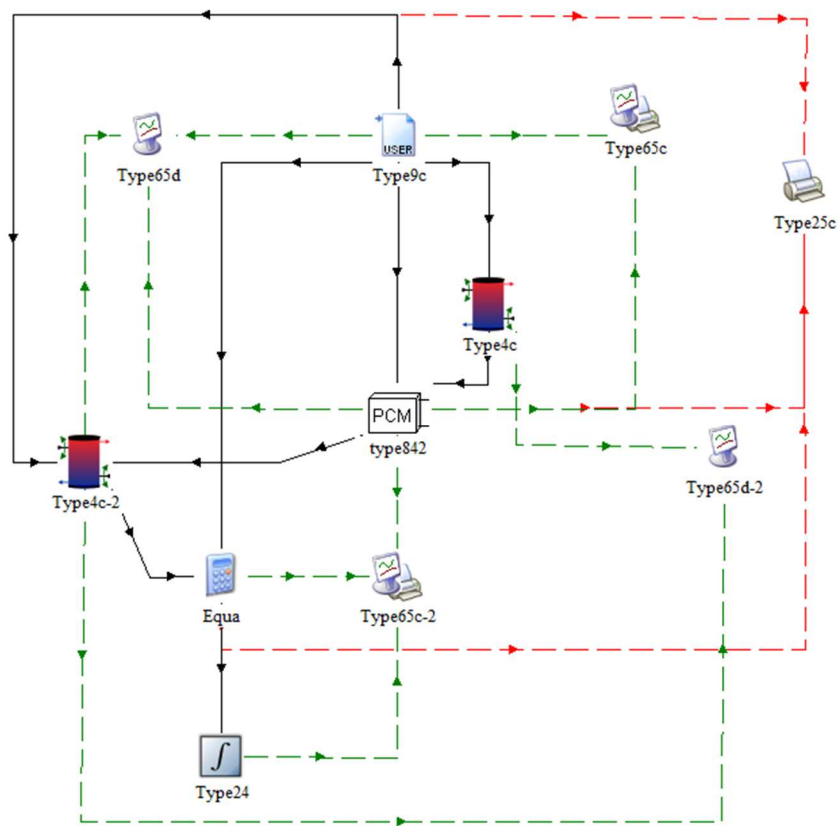


Figure 3-2: Overview of the used components within the TRNSYS simulation

As a very small temperature difference between flow and return has been recognized during the measurements of the experimental tube tests (see chapter 4.9), TRNSYS simulations for experimental tube tests would lead to imprecise results. For this reason, it has not been intended to simulate the experimental tube tests, but as described in chapter 4.9.5 an alternative approach for estimating heat delivery of the experimental tubes has been investigated.

4 MEASUREMENTS

As the thermal behaviour and the power performance of the combination aluminium foam and encapsulated paraffin is not known yet, an optimum operating area, where maximum heat delivery occurs, has to be identified. With the outcome of the measurements it is intended also to parametrize TRNSYS type 842 for the system simulations. Numerous geometric variations can then be performed within the simulation with the benefit of reduced development costs. As the necessary measurement data has to be collected prior to the simulation, several prototype storage modules have been manufactured and prepared for the measurements. These experimental PCM modules have either the shape of a tube, representing an “elementary cell” surrounded by aluminium foam and PCM, as well as a storage box design with 14 tubes through a cuboid housing. These PCM/Aluminium modules have been measured and analysed in the laboratory of the Institute of Thermal Engineering of TU Graz. To give a quick overview, Figure 4-1 shows both measured experimental modules. A more detailed explanation of either internal structure as well as dimensions is discussed in the chapters 4.1 and 4.9.

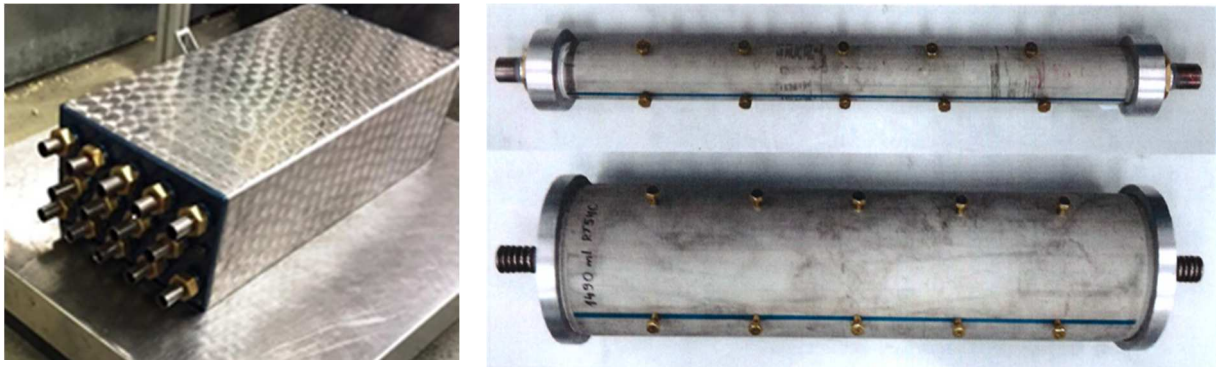


Figure 4-1: Picture of experimental box on the left and the experimental tube on the right side

As there is a difference in heat delivery as well as varying charging/discharging durations when circulating through the experimental box with different hydraulic settings, it is intended that the heat transfer fluid carries a water / glycol mixture and flows through the experimental box either in parallel or serial configuration. It has to be mentioned that all modules have been equipped with surface temperature sensors and are covered with a proper insulation.

4.1 Experimental box

To analyse the thermal capabilities of the experimental box several power performance measurements, with different mass flow rates, were performed. The PCM box was tested as first attempt in parallel flow configuration and afterwards in serial flow configuration, to check for optimum operating characteristics for further applications.

The experimental box PCMM18 (representing a **PCM Module** with **18** mm outside tube diameter) consists of a stainless steel housing with 14 parallel cylindrical tubes across the surface (according to Figure 4-2). The total mass of the experimental box is 29.34 kg. The aluminium foam has been casted within the stainless steel box and afterwards filled with 10.7 kg of the PCM material Rubitherm RT5HC via two separated filling screws, one screw is providing a vacuum and the other screw is providing the PCM, which is sucked inside the box. The mass of the Aluminium foam inside the box is 6.72 kg. Sealed brass sleeves at the end of the tubes prevent the PCM from leaking out of the box.

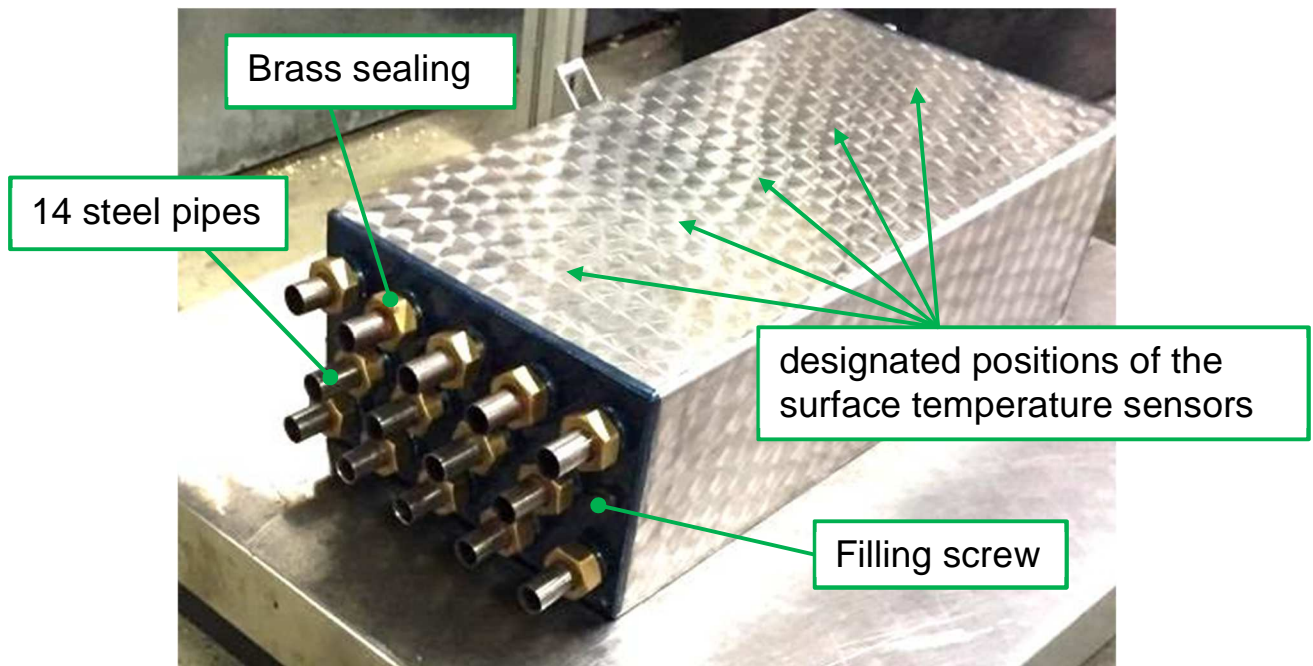


Figure 4-2: Experimental box PCMM18

The main dimensions as well as the distribution of the tubes across the front surface of the experimental box are shown in Figure 4-3.

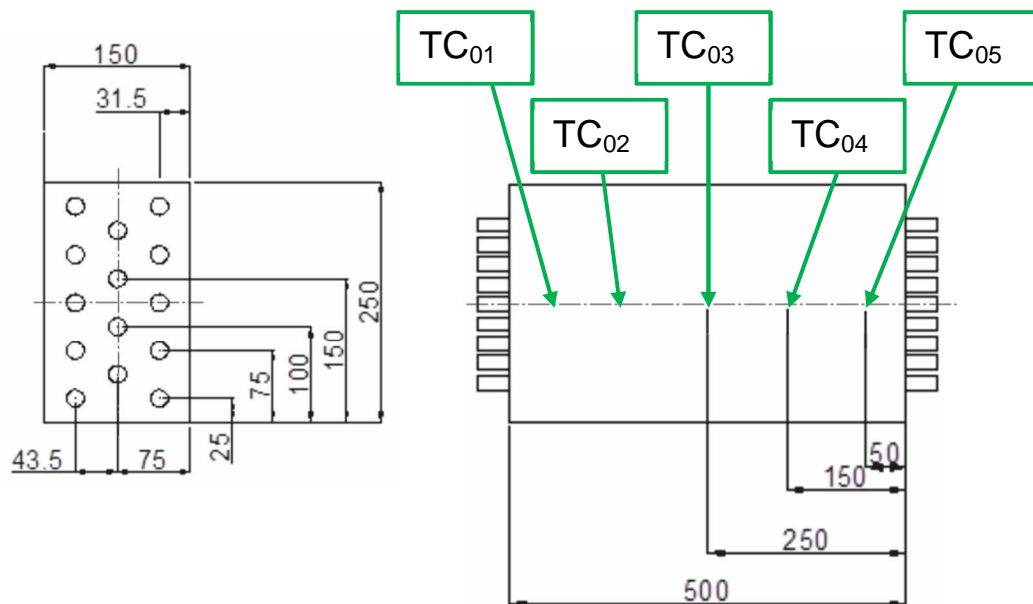


Figure 4-3: Dimensions of the experimental box PCMM18 and positions of the surface temperature sensors

The measurement setup (shown in Figure 4-4) consists of a mobile heat source/sink-system "MegaLauda", an internal pump in the return stream, a magnetic inductive flow meter (Endress Hauser (2016) Promag 50P25) as well as a bypass valve to set mass flow rates to values from 600 kg/h to 5000 kg/h. The magnetic inductive flow meter is located in the flow stream of the experiment modules and has a hydraulic lamination zone of 15 times the inside diameter. Two PT100 temperature sensors (VL_PT100 and RL_PT100) are used to calculate the heat delivery to the PCM tube. The positioning of the PT100 sensors can be seen in the according chapter for parallel tests (chapter 4.3) and for serial tests (chapter 4.5).

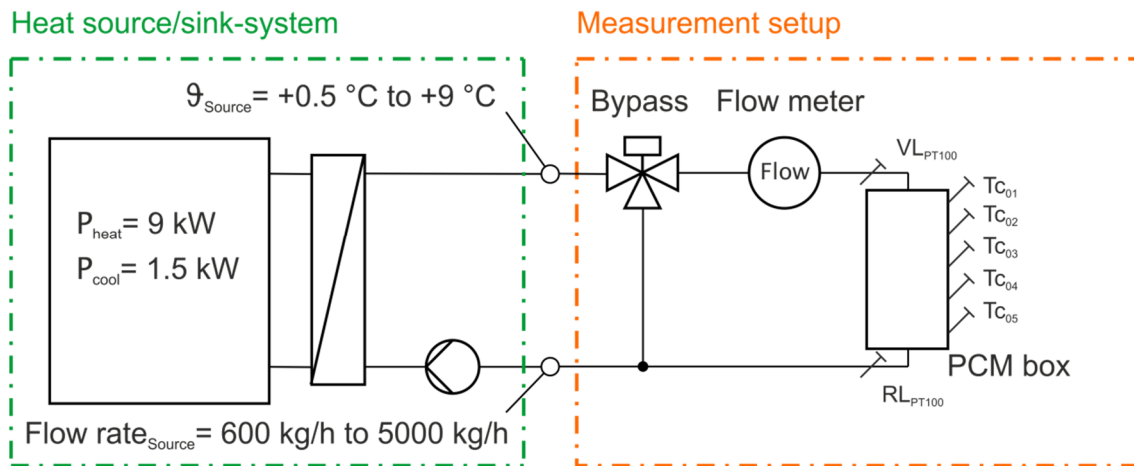


Figure 4-4: Measurement setup for the experimental box

The “MegaLauda” (heat source/sink-system) is capable of providing a heating temperature of +9 °C at 9 kW and a cooling temperature of +0.5 °C with a heat output of 1.5 kW. Flow rates can be chosen between 600 kg/h and 5000 kg/h. All hydraulic tubes connecting the “MegaLauda” and the experimental box have an inside diameter of 1” and are covered with 16 mm AF/Armaflex (2015) in the flow and 9.5 mm AF/Armaflex in the return stream. As the operating temperatures are close to the freezing point of water, the risk of partial freezing inside the heat exchanger should be avoided. Freezing inside the heat exchanger would result in dramatic drops in mass flow rates. As precautionary measure a mixture of 70 % water and 30 % Glysofor N, which is based on Monoethylenglykol Antifrogen (2016), was filled inside the hydraulic system. Physical properties of the heat transfer fluid are shown in Table 4-1.

Table 4-1: Physical properties of the heat transfer fluid

Freezing point	Temperature	Thermal conductivity	Specific heat capacity	Density	Kinematic viscosity
[°C]	[°C]	[W/(m.K)]	[kJ/(kg.K)]	[kg/dm ³]	[mm ² /s]
-16	0	0.448	3.78	1.052	4.45
-16	10	0.458	3.82	1.049	3.17

source: Glysofor N (2016)

5 surface temperature sensors (TC₀₁, TC₀₂...TC₀₅; Thermocouple type K) are measuring the surface temperature distribution of the box. This is necessary to check charging/discharging progression or when the charging or discharging cycle is finished. The temperature sensors are positioned in the centre line of the box and evenly distributed over the length of the box (see figure Figure 4-3 and Figure 4-5). An ambient temperature sensor has been used to determine thermal gains of the experimental as can be seen in chapter 4.7.

The PCM box and its periphery have been insulated with AF/Armaflex with a thickness of 19mm for minimizing thermal gains from the ambient. The thermal conductivity of the AF/Armaflex material is $\lambda_{ARMAFLEX} \leq 0.033 \frac{W}{m \cdot K}$ (a datasheet of the insulation material can be found in the Appendix). The absolute pressure of the circulating heat transfer fluid was set to 0.2 MPa (to avoid cavitation effects and mass flow fluctuations) and checked via a manometer in the return stream. The flow configuration through the box is shown in Figure 4-5.

To ensure reproducible charging/discharging cycles the heat transfer fluid was preconditioned with the “MegaLauda” to the same temperature level by circulating over the bypass channel. Data recording was carried out by the measurement equipment Solartron IMP UNIVERSAL 3595J and a calibration protocol can be found in the Appendix. The sampling rate of the IMP 3595J was set to 1 second for all box measurements. Estimating the heat delivery of the experimental box was performed at different mass flow rates starting at 600 kg/h and was only limited by reaching the maximum mass flow rate of the circulating pump of the “MegaLauda”.

Cooling and heating capacities of the box were typically measured with mass flow rates of 600 kg/h, 1500 kg/h and 3000 kg/h. As the hydraulic resistance for parallel box tests were significantly lower, also a heat delivery at a maximum mass flow rate of 5000 kg/h was performed. Average heat delivery of the parallel box tests are shown in Table 4-2 and for the serial tests in Table 4-3.

4.2 Measurement strategy

All measurements have been performed with the mobile heat source/sink-system "MegaLauda". Prior to the measurement the box has been cooled down to a starting temperature of +9 °C. The box has then been charged with cooling temperatures of 0.5 °C (± 0.5 K) and different mass flow rates (from 600 kg/h up to 5000 kg/h (± 15 kg/h)). When the temperatures of the surface sensors were below +1 °C it can be assumed that the encapsulated paraffin performed its phase change and the charging cycle is finished. Subsequent to the charging cycle the temperatures in the circulating stream of the heat changer fluid are set to +9 °C (± 0.5 K). This can be achieved via a bypass stream parallel to the measurement box and takes about 8 minutes. Due to thermal gains from the ambient the surface temperatures rise about +0.2 K. This small increase in surface temperature has to be accepted as it is assumed that the paraffin inside the tube is still in solid state. Discharging of the box occurs again with the same mass flow rate as chosen for the charging process. This measurement procedure was kept for all measurements of the experimental box. There was only a variation in hydraulics flow over the experimental box (parallel and serial flow configuration). These flow configurations are discussed in detail in the chapter 4.3 and chapter 4.5.

4.3 Parallel tests

As first test setting the experimental box was investigated in parallel flow configuration. As the experimental box has 14 parallel pipes through the box a flow distributor had to be fabricated (according to Figure 4-5). This distributor is necessary to connect each tube in parallel flow configuration. As first simplification it has to be assumed that the heat transfer fluid is perfectly mixed inside the distributor, so the temperature of the fluid into the distributor is equal to the fluid temperatures of all tubes flowing into the experimental box. To connect the flow distributor with the experimental box 28 PVC pipes (inside diameter 3/4") with same length have been slid over the pipes and sealed with hose clamps. These PVC pipes can be seen in Figure 4-5 and exact positioning of the surface temperatures onto the box is shown in Figure 4-3. The ambient temperature sensor has been positioned nearby the measurement setup, but it has been considered that the ambient temperature sensor is not exposed to draft or waste heat.

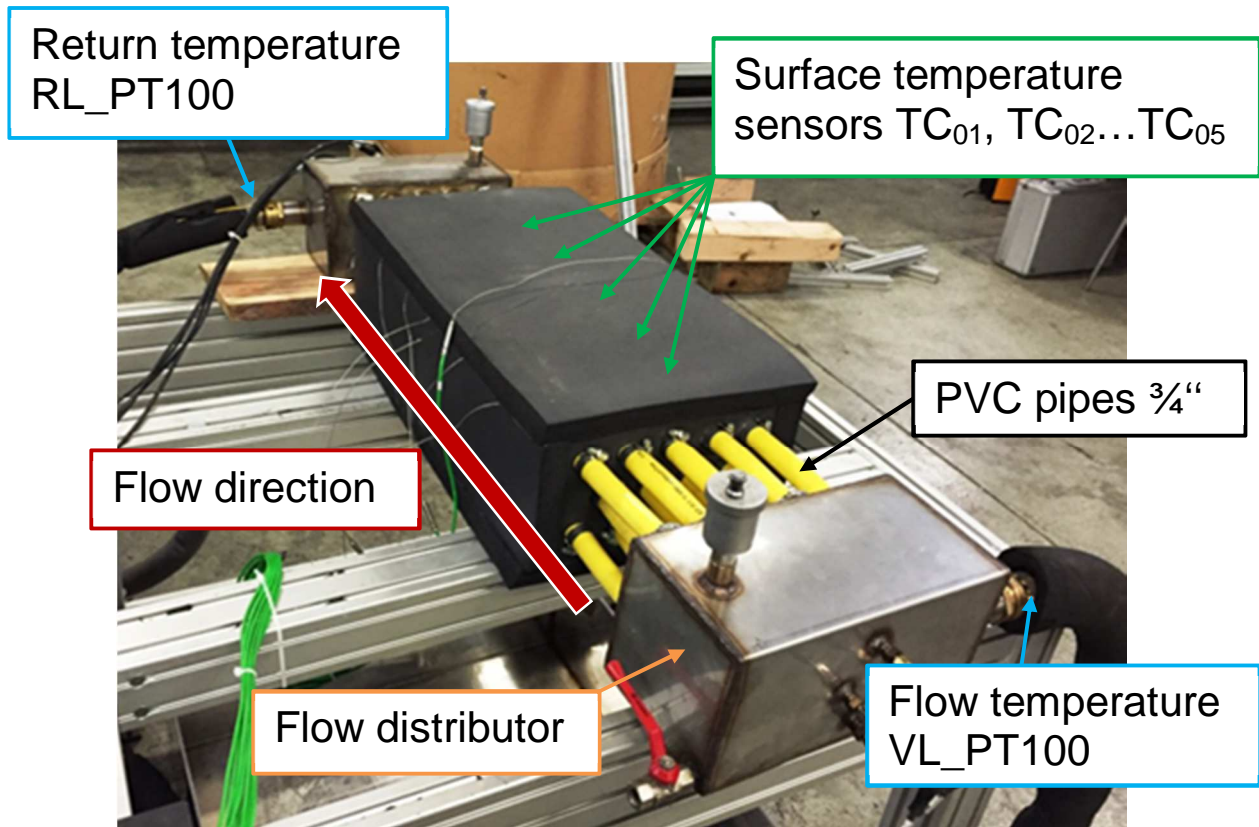


Figure 4-5: Experimental setup of parallel flow configuration measurements

Flow and return stream connectors were oriented opposite to each other to ensure that individual distances through each of the 14 parallel pipes are identical. The flow distributors were made out of stainless steel and possess four clamp connections for temperature sensors (for the possibility of measuring temperatures inside PVC tubes) as well as a breather valve. The volume of each flow distributor was 6.75 dm^3 and the flow distributor has been abstracted as small cylindrical water storage tank within the simulation.

An exemplary charging/discharging cycle in parallel flow configuration shows Figure 4-6. The charging cycle takes about 180 minutes and the discharging cycle about 120 minutes. The mass flow rate was about 1500 kg/h and the initial temperature of the box prior to the measurement was set to $8.7 \text{ }^\circ\text{C}$. From 185 min to 193 min the heat transfer fluid was set to $+9 \text{ }^\circ\text{C}$ via the bypass channel to prepare for the discharging cycle (that is why the measured mass flow rate is zero in this time interval).

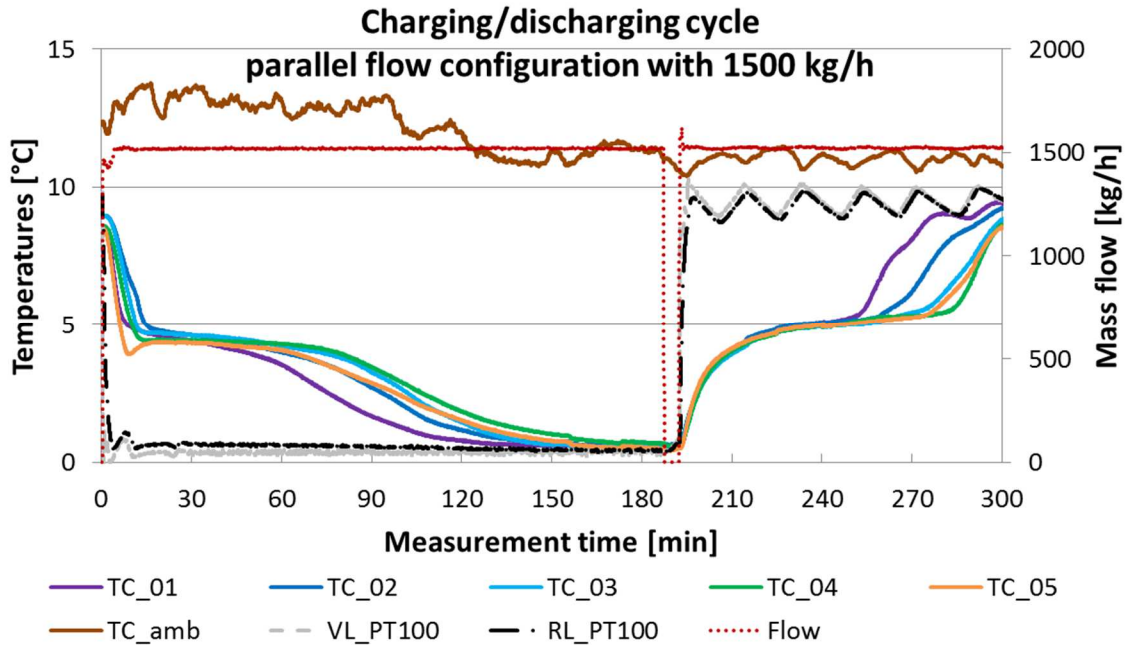


Figure 4-6: Exemplary charging/discharging cycle of parallel box measurements

It has to be mentioned that the discharging cycle is highly influenced by the slow behaviour of the controller of the “MegaLauda”, as the temperature of flow stream is varying about ± 0.6 K. But as the charging cycle is more relevant for the HVAC subway application the discharging cycle will be neglected and only charging cycles are shown in further diagrams.

The heat delivery from the heat transfer fluid to the experimental box can be estimated by measuring flow and return temperatures and the mass flow rate. As the specific heat capacity of the glycol/water mixture is well known the heat delivery can be calculated. According to Figure 4-7 the heat delivery to the experimental box is low. This results in a small temperature difference between flow and return stream which does not change significantly throughout all measurements, despite changing mass flow rates. Also due to laminar flow situation inside the pipes (according to the corresponding Reynolds number in Table 4-2) heat delivery is limited.

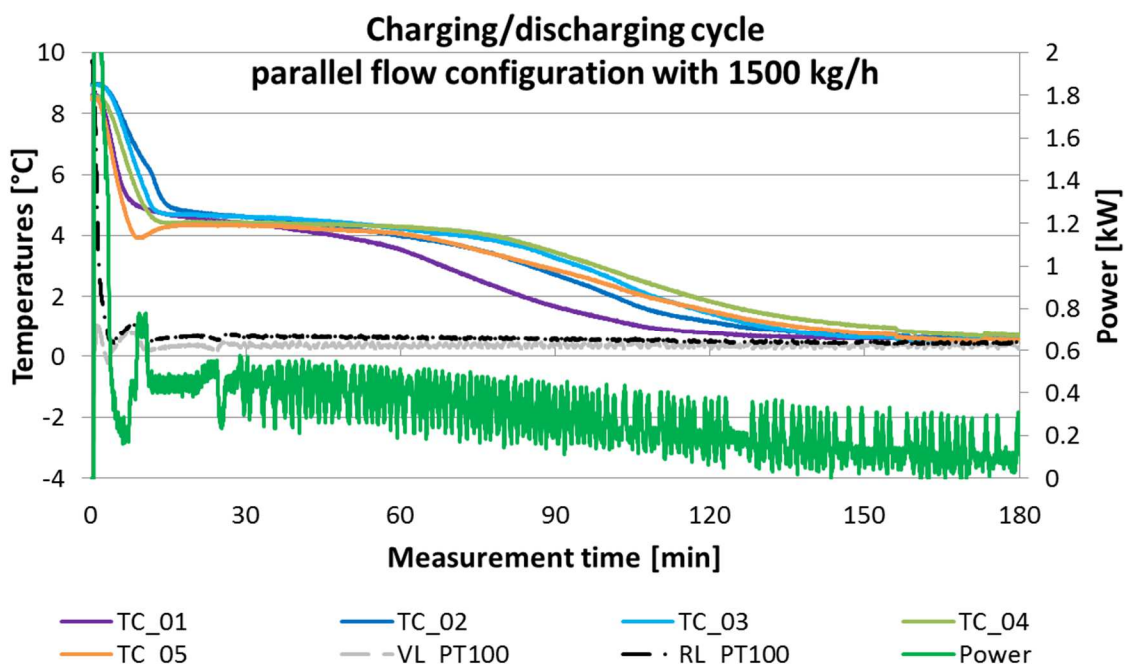


Figure 4-7: Charging heat delivery of experimental box in parallel flow configuration with a mass flow of 1500 kg/h

The large fluctuations in thermal heat delivery can be explained by the controller behaviour of the “MegaLauda” and by the small temperature difference between flow and return stream. The average temperature difference between flow and return stream during charging cycle with a mass flow rate of 1500 kg/h is about 0.28 K and the temperature difference during discharging is about 0.3 K. The average Reynolds number of the individual measurements is low, so the flow situation inside the tube is expected to be laminar. This results in low heat delivery and long measurement durations of charging and discharging cycle. The charging duration can be estimated by measuring the time that it takes to cool down the experimental box from starting temperature until all surface temperatures have reached +1 °C. The discharging duration can be estimated by measuring the time that it takes to heat up the experimental box from +1 °C to +9 °C. The calculated heat delivery according to equation (2-13) and the corresponding relative measurement uncertainty of the heat delivery for charging and discharging cycle in parallel flow configuration can be shown in Table 4-2. For determining the relative measurement error of heat delivery, the Gauß propagation of uncertainties has been used and it considers a combination of measurement uncertainties of temperature sensors and the relative error of the magnetic inductive flow meter. The propagation of error method for the heat delivery is explained in chapter 4.10.

Table 4-2: Average heat delivery of charging and discharging cycle in parallel flow configuration with the according measurement duration in relation to the chosen mass flow rate

charging / discharging	Mass flow	Initial temperature	average heat delivery	error of heat delivery	Measurement duration	average Reynolds
	[kg/h]	[°C]	[kW]	±[%]	[min]	[-]
charging	600	8.6	0.27	2.97	185	243
charging	1500	8.7	0.42	5.65	132.1	609
charging	3000	9.1	0.48	8.85	106.9	1217
charging	5000	8.9	0.72	14.49	96.1	2370
discharging	600	1.3	0.24	3.08	135.7	243
discharging	1500	1.1	0.25	5.98	108.1	609
discharging	3000	1.2	0.24	11.15	98.3	1217
discharging	5000	1.0	0.26	17.56	72.1	2370

A comparison of the measurements with the simulation in parallel flow configuration is discussed in the chapter 4.4.

4.4 Measurement VS simulation for parallel flow configuration

The main aspect for parametrization of the TRNSYS type 842 was to achieve a proper abstraction of heat delivery as well as temperature distribution of the whole charging cycle in both parallel and serial flow configuration. But as the thermal conductivity within the simulation could not be changed for liquid and solid state separately, and due the fact that only surface temperatures have been measured, it has been intended to abstract the measurement at least from the liquid state to the end of the phase change, as the main amount of latent heat occurs within this range. When comparing the measurement with the TRNSYS simulation type 842 it is obvious that the measurement does match the simulation in certain time intervals. When the paraffin is still liquid, the abstraction is quite good. Big discrepancies between measurement and simulation occur when the paraffin is in solid state (measurement time >90 minutes according to Figure 4-8). Core temperatures of the PCM have reached temperatures of +1 °C whereas the surface temperatures of the measurements are well above that temperature. Figure 4-8 gives a quick overview of temperature distribution of simulation and measurement. When the simulation type 842 is parametrized with the parameters in Table 3-1 the abstraction

between simulation and the measured surface temperatures is quite good for the liquid state until the end of the phase change, but weak when the paraffin is in solid state.

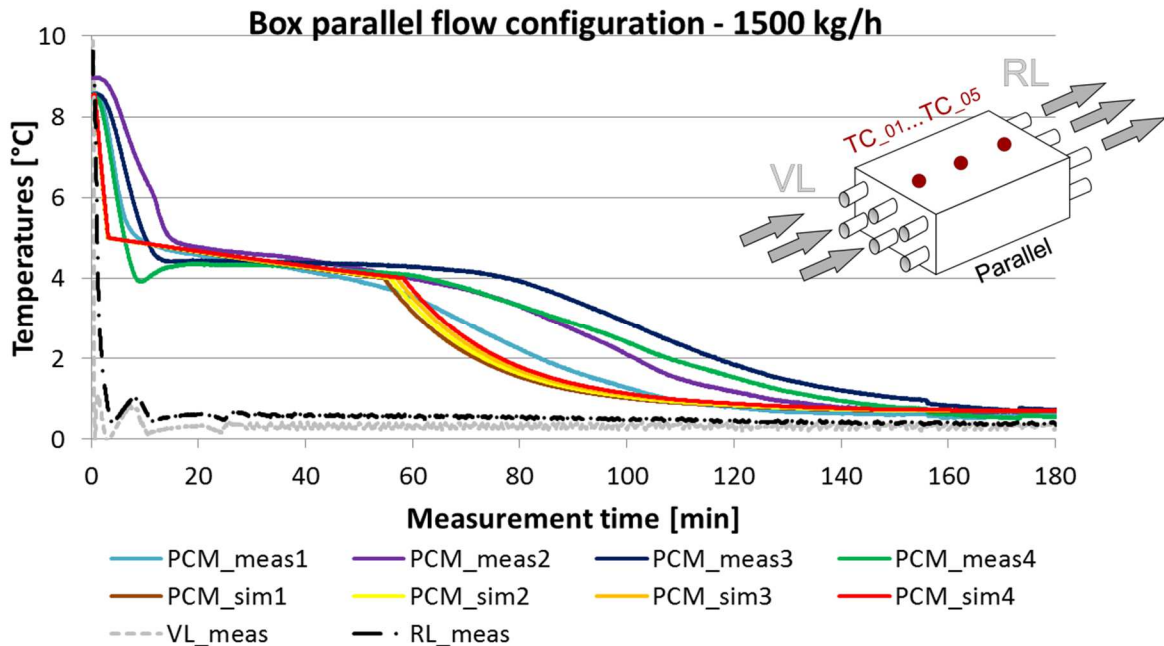


Figure 4-8: Comparison of measurement and simulation of parallel box measurements during charging cycle and a mass flow of 1500 kg/h

The brown, yellow and red curves indicate the simulated core temperatures and the blue, green and purple temperature curves indicate the surface temperatures out of the measurements. An analysis of heat delivery in Figure 4-9 shows the same behaviour. Figure 4-9 is comparing an averaged surface temperature of the measurement as well as an averaged core temperature out of the simulation. The heat delivery of both simulation and measurement is also shown. The Reynolds numbers (dependent on the temperature of the heat transfer fluid) show, that the flow situation inside the tube is laminar.

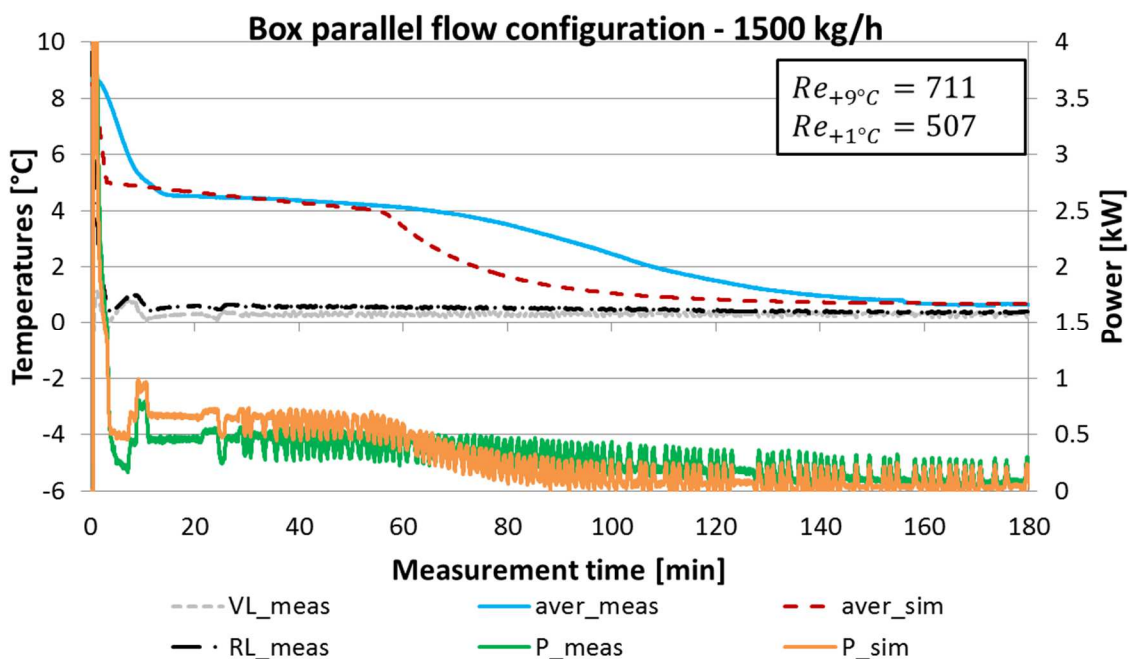


Figure 4-9: Heat delivery and average temperatures of parallel box measurement and simulation during charging cycle

The discrepancy in temperature distribution at the start of the measurement until the beginning of phase change can be explained by the fact, that the simulation model considers core temperatures while as during the measurement only surface temperatures have been collected. Comparing the measurements with the simulations for the mass flow rates 600, 1500, 3000 kg/h and 5000 kg/h (Figure 4-10, Figure 4-11 and Figure 4-12) show the same behaviour of good abstraction from liquid state to the end of phase change but decreased heat delivery and increased charging durations when in solid state.

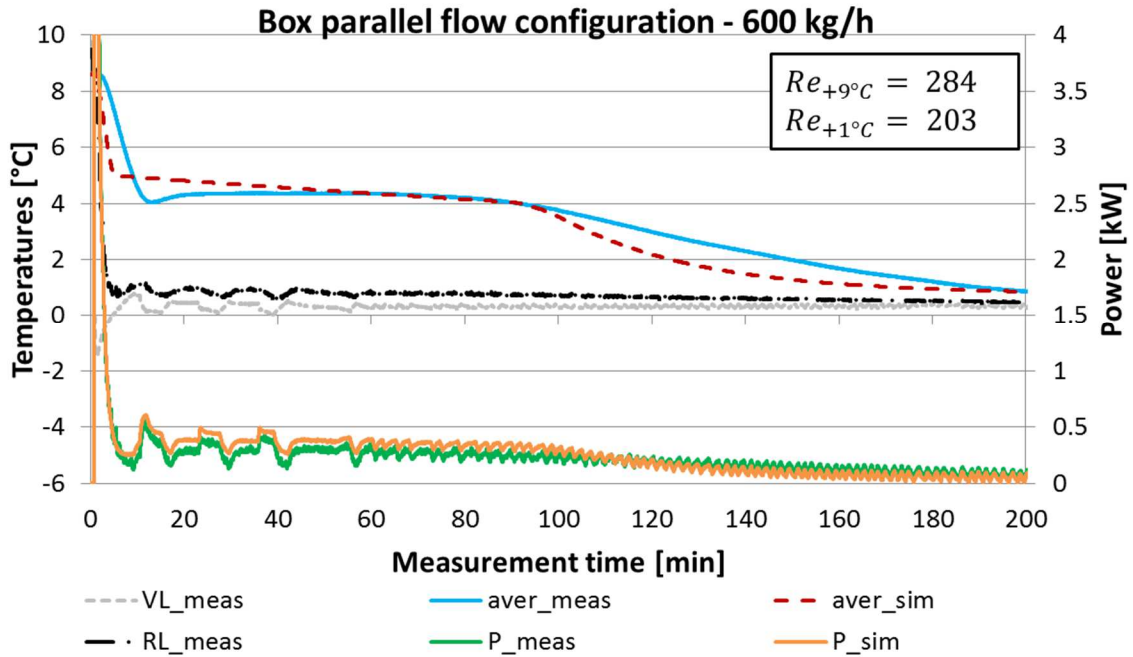


Figure 4-10: Heat delivery and average temperatures of parallel box measurement and simulation during charging cycle

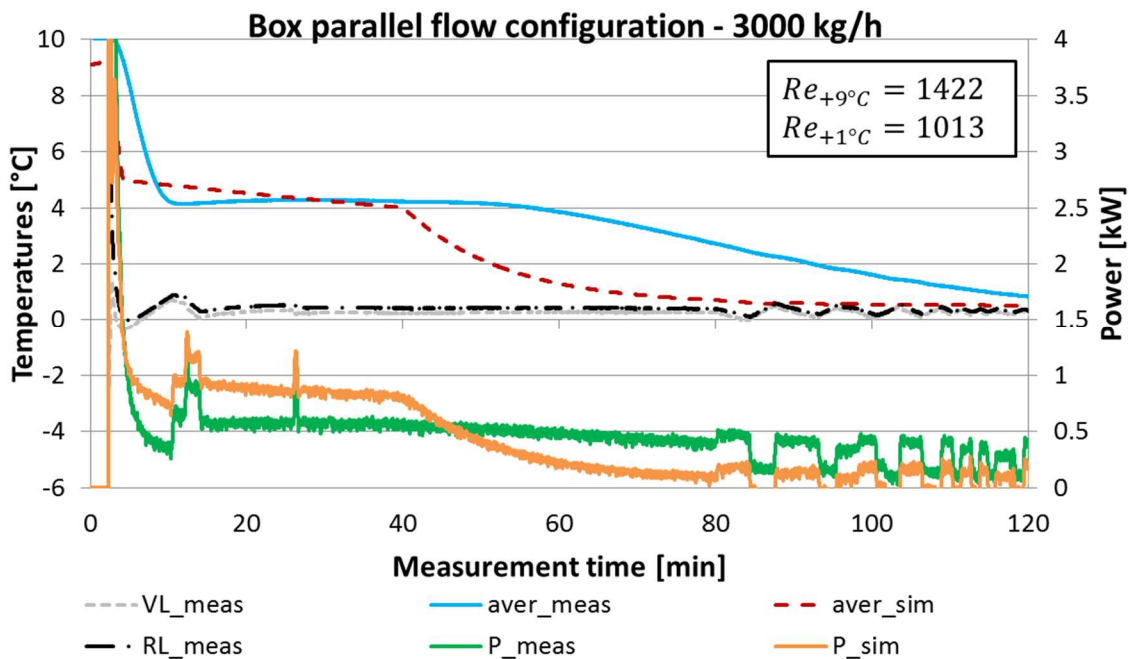


Figure 4-11: Heat delivery and average temperatures of parallel box measurement and simulation during charging cycle

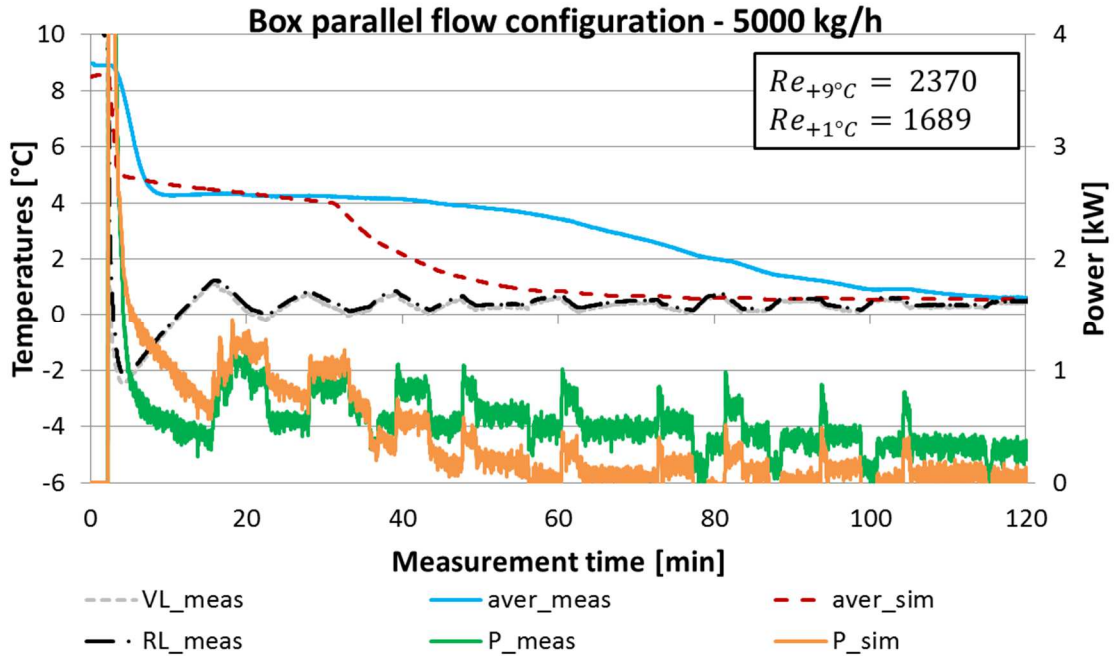


Figure 4-12: Heat delivery and average temperatures of parallel box measurement and simulation during charging cycle

Accumulated energies of the experimental box in parallel flow configuration are shown in Figure 4-13 to Figure 4-16.

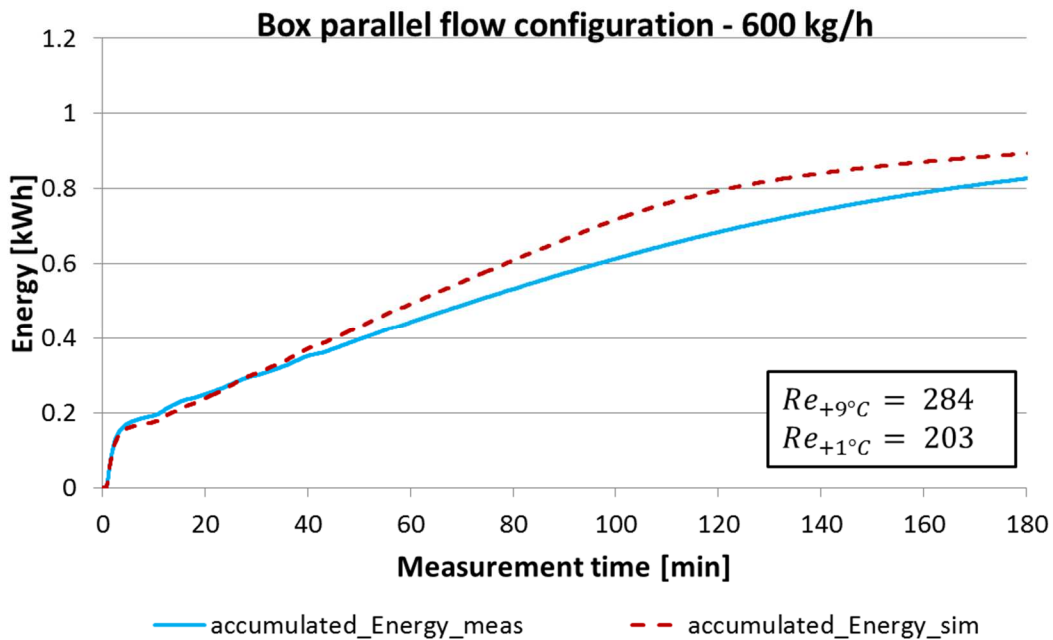


Figure 4-13: Accumulated energy of parallel box measurement and simulation during charging cycle

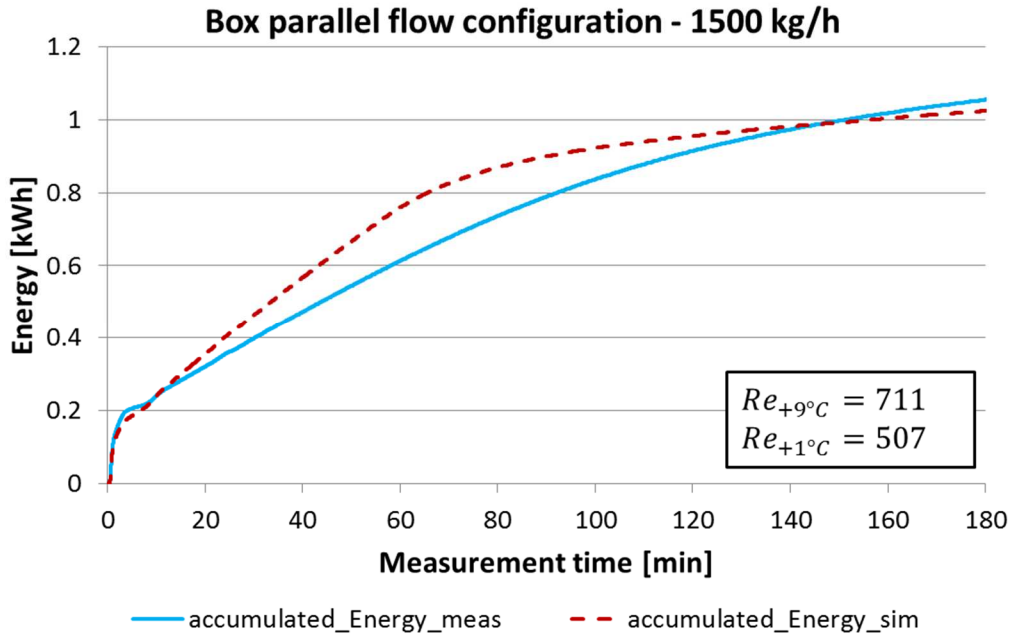


Figure 4-14: Accumulated energy of parallel box measurement and simulation during charging cycle

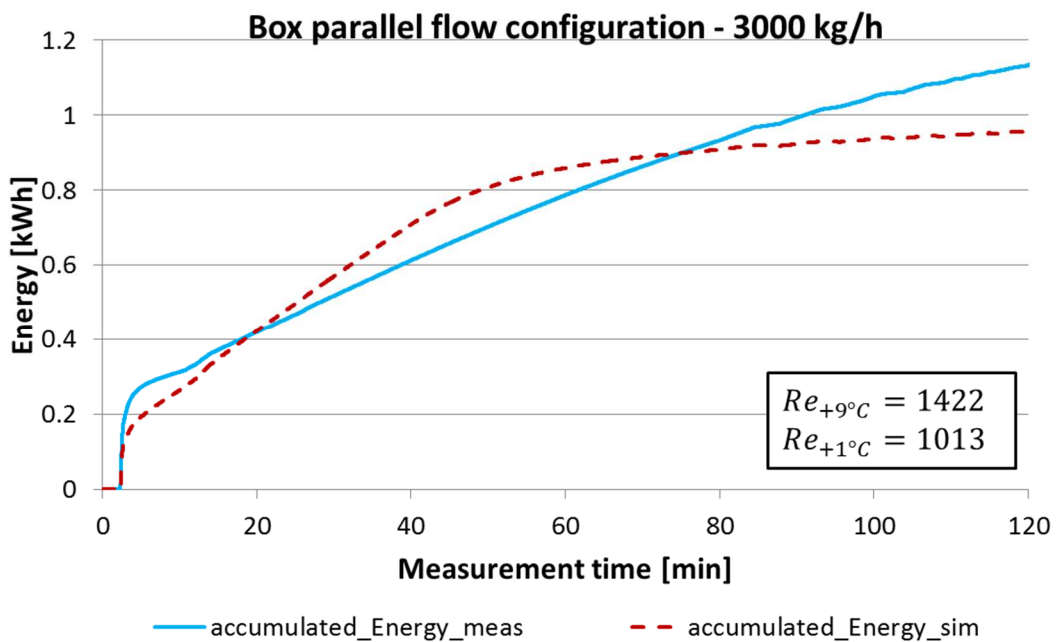


Figure 4-15: Accumulated energy of parallel box measurement and simulation during charging cycle

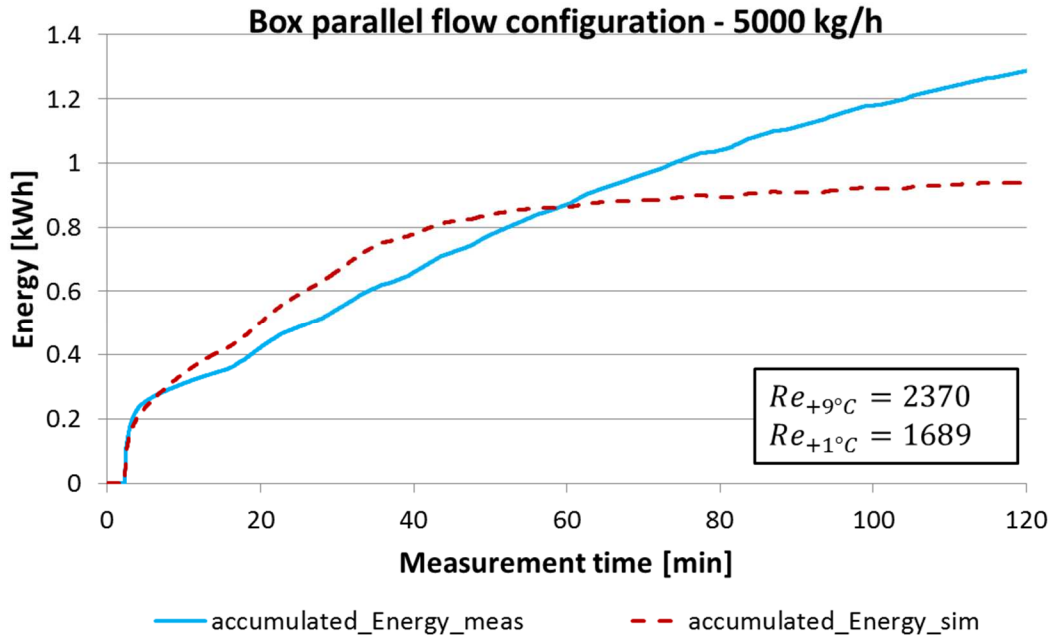


Figure 4-16: Accumulated energy of parallel box measurement and simulation during charging cycle

A comparison of all measurements is shown in Figure 4-17.

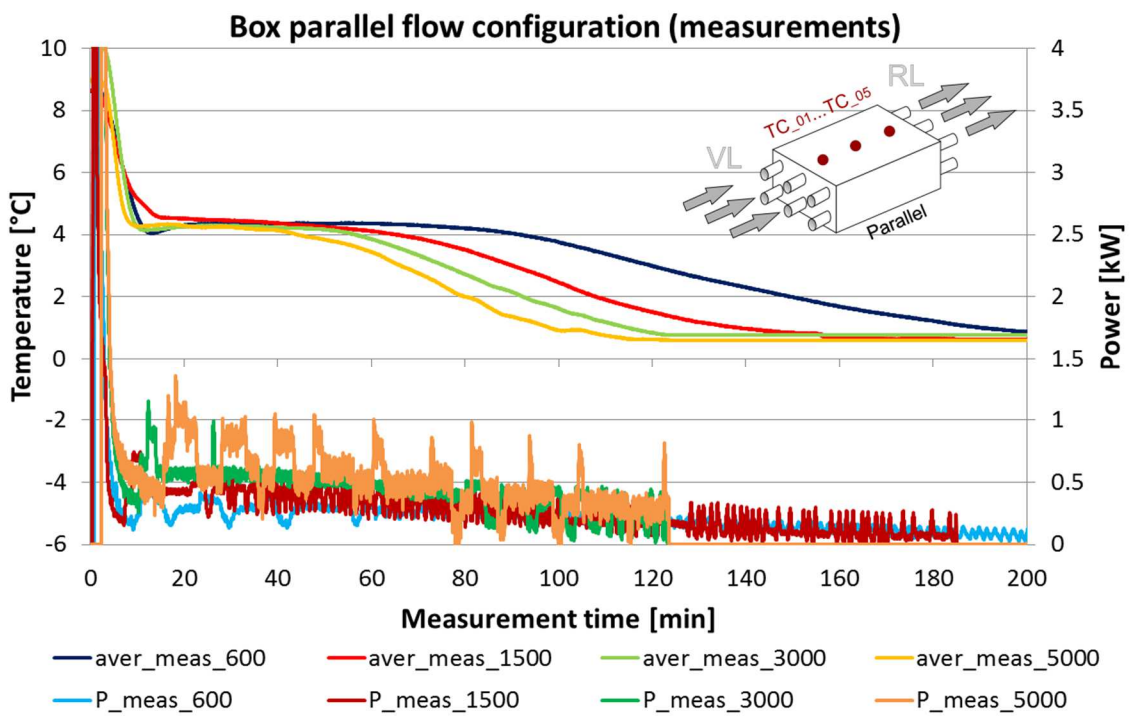


Figure 4-17: Comparison of all measurements in parallel flow configuration

A comparison of all box simulation results is shown in Figure 4-18.

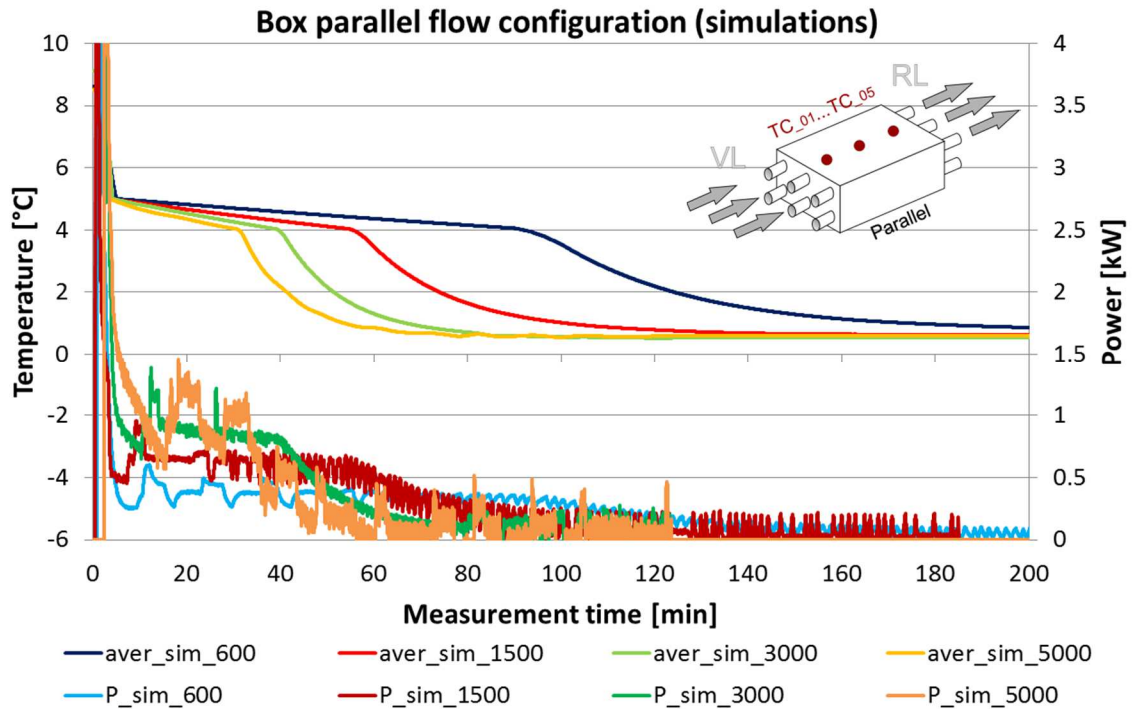


Figure 4-18: Comparison of all simulations in parallel flow configuration

According to Table 4-2 and the outcome of the comparison between measurements and simulations in parallel flow configuration it is evident that with laminar flow situation inside the tube, the average heat delivery is low due to a small heat transfer coefficient on the inside of the pipes. Therefore the heat deliveries of measurement and simulation are not showing the same results for all mass flow rates, except for the measurement with a mass flow rate of 600 kg/h. Unfortunately the build in circulating pump of the “MegaLauda” is reaching its maximum performance, limiting the maximum mass flow to 5000 kg/h. So it was decided to change the hydraulic flow setting through the box into serial flow configuration with the intention of reaching turbulent flow situation and gaining higher heat delivery.

4.5 Serial tests

As second test setting the experimental box was investigated in serial flow configuration according to Figure 4-19. The first hydraulics connection was on the top left side of the experimental box and the box was flown through the 14 tubes starting with the top layer, than the middle layer and finishing with the bottom layer. The return stream ended on the bottom right side of the box. An overview of flow configuration as well as temperature sensor positioning is shown in Figure 4-19.

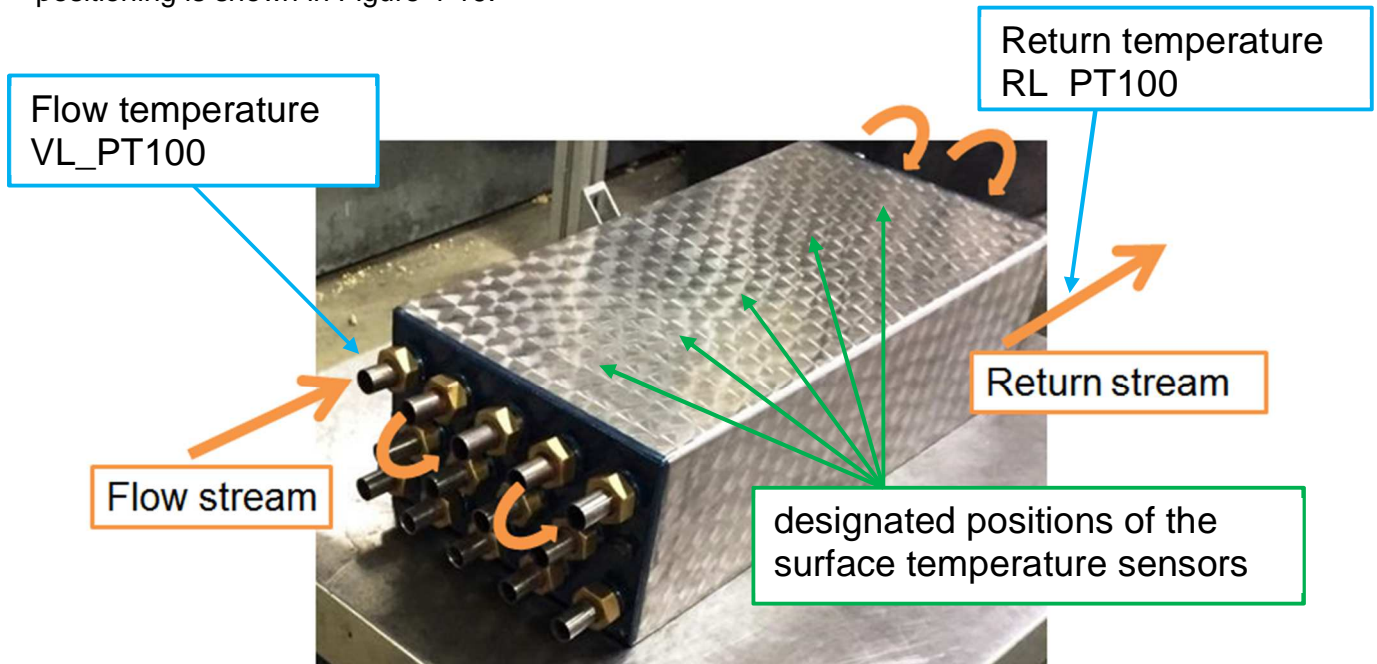


Figure 4-19: Experimental setup of serial flow configuration measurements

To estimate the heat delivery flow and return temperatures as well as mass flow rates have been measured. As only the flowing configuration of the box was modified, the surface temperatures have been kept on the same positions as during the parallel measurements. To connect the fittings in serial flow configuration 13 PVC tubes (inside diameter 3/4") with same length have been slid over the pipes and sealed with hose clamps. The volume of the heat transfer fluid inside all serial PVC tubes is about 3.6 dm³. As this volume cannot be abstracted within the simulation, a small error is made when comparing the measurements with the simulation, but as the energy content of the heat transfer fluid inside the PVC tubes is small compared with the total energy of the experimental box (equals 3.4 % of the total energy content), this simplification is acceptable.

An exemplary charging/discharging cycle in serial flow configuration is shown in Figure 4-20. The charging cycle takes about 80 minutes and the discharging cycle takes about 70 minutes. The mass flow rate was about 1500 kg/h and the initial temperature of the box prior to the measurement was set to 8.5 °C. In the time interval from 80 min to 84 min the heat transfer fluid was set to +9 °C via the bypass (according to Figure 4-4) to prepare for the discharging cycle.

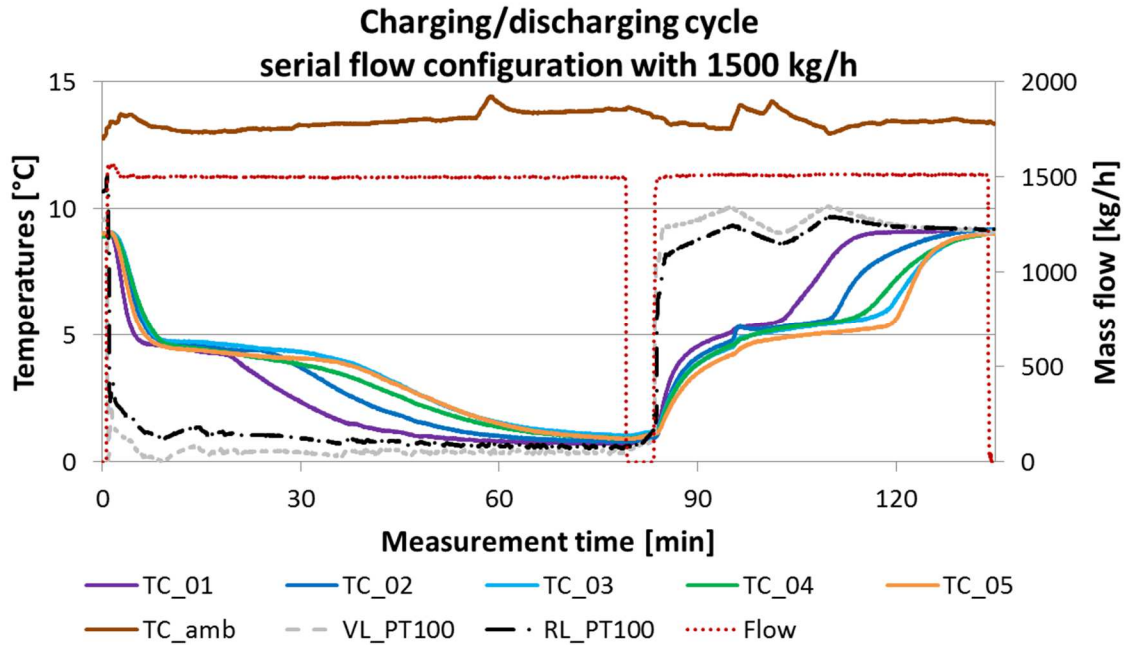


Figure 4-20: Exemplary charging/discharging cycle of serial box measurements

It has to be mentioned again that the discharging cycle is highly influenced by the slow behaviour of the controller of the “MegaLauda”, as the temperature of flow stream is varying about ± 0.6 K. But as the charging cycle is more relevant for the HVAC subway application the discharging cycle will be neglected and only charging cycles are shown in further diagrams.

The heat delivery can be estimated by measuring the temperatures of flow and return stream and the mass flow rate. As the specific heat capacity of the glycol/water mixture is well known the heat delivery can be calculated. According to Figure 4-21, the heat delivery to the experimental box is significantly higher than the heat delivery of the parallel measurements. This can be explained by the fact, that the higher velocity of the heat transfer fluid results in higher overall heat transfer coefficients. The mass flow rate inside the pipes is now turbulent for all measurements of serial flow configuration. The mass flow rates and the according Reynolds numbers can be seen in Table 4-3.

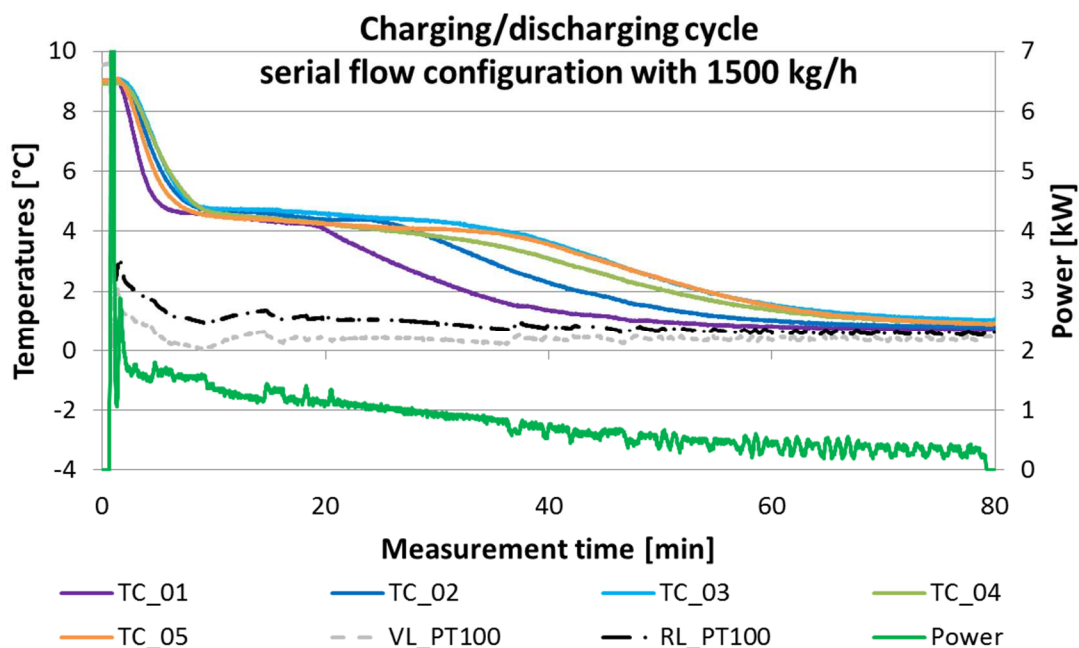


Figure 4-21: Charging heat delivery of experimental box in serial flow configuration with a mass flow of 1500 kg/h

Due to a bigger temperature difference between flow and return stream, also the fluctuations in thermal heat delivery are smaller than at the measurements of parallel flow configuration. The average temperature difference between flow and return stream during charging cycle is about 0.49 K and the temperature difference during discharging is about 0.43 K (the temperature differences of charging cycle with parallel flow configurations have been about 0.29 K, see chapter 4.3). This increased temperature difference has direct effect on measurement error of heat delivery of the individual measurements. These temperature differences for the exemplary charging/discharging cycle correspond to 5.13 % of the measurement uncertainties of the heat delivery during charging cycle (according to the propagation of uncertainties according chapter 4.10). A summarization of average heat delivery and charging/discharging durations for all parallel tests are shown in shown in Table 4-3.

Table 4-3: Average heat delivery of charging and discharging cycle in serial flow configuration with the according measurement duration in relation to the chosen mass flow rate

charging / discharging	Mass flow [°C]	Initial temperature [°C]	average heat delivery [kW]	error of heat delivery ±[%]	Measurement duration [min]	average Reynolds [-]
charging	600	8.3	0.57	3.16	63.4	3409
charging	1000	8.9	0.74	4.39	44.7	5683
charging	1500	8.5	0.91	5.13	41.9	8525
charging	2000	9.0	0.93	6.45	38.1	11367
discharging	600	1.0	0.53	3.2	93.1	3409
discharging	1000	1.0	0.7	4.38	66.3	5683
discharging	1500	1.2	0.72	6.25	54.1	8525
discharging	2000	1.0	0.76	8.16	54.5	11367

A comparison of the measurements with the simulation in serial flow configuration is discussed in the chapter 4.6.

4.6 Measurement VS simulation for serial flow configuration

Within this chapter a comparison of measurements of serial flow configuration with the TRNSYS simulation type 842 for the charging cycle is discussed. But as mentioned before, it has to be taken into account that during measurement only surface temperatures and not core temperatures have been measured. Figure 4-22 gives a quick overview of temperature distribution of simulation and measurement. The simulation type 842 has been parametrized with the parameter out of Table 3-1.

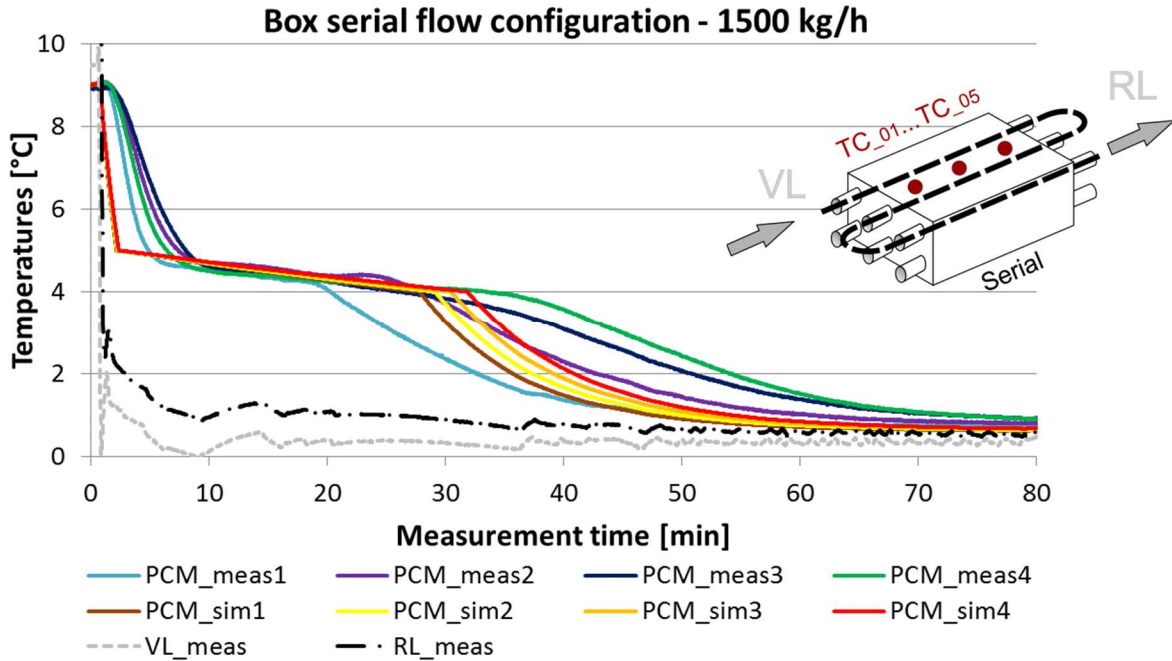


Figure 4-22: Comparison of measurement and simulation of serial box measurements during charging cycle and a mass flow of 1500 kg/h

The brown, yellow and red curves indicate the simulated core temperatures and the blue, green and purple temperature curves indicate the surface temperatures out of the measurements.

Figure 4-23 is comparing average surface temperatures of the measurement as well as average temperatures from the simulation. Also the heat delivery of both simulation and measurement is shown below in Figure 4-23. The Reynolds numbers (dependent on the temperature of the heat transfer fluid) show, that the flow situation inside the tube is turbulent.

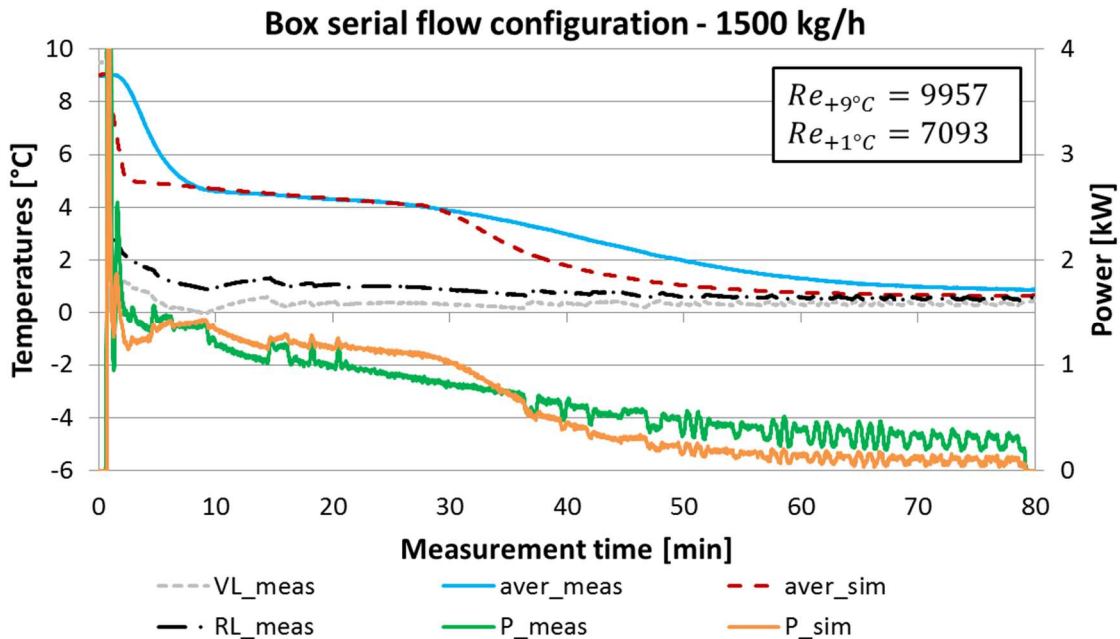


Figure 4-23: Heat delivery and average temperatures of serial box measurement and simulation during charging cycle

The small discrepancy in temperature distribution at the start of the measurement until the beginning of phase change can be explained by the fact, that the simulation model considers

core temperatures while as during the measurement only surface temperatures have been recorded. Comparing the measurements with the simulation for the mass flow rates 600 kg/h, 1000 kg/h, 1500 kg/h and 2000 kg/h (Figure 4-24, Figure 4-25 and Figure 4-26) shows a good fit between measurement and simulation.

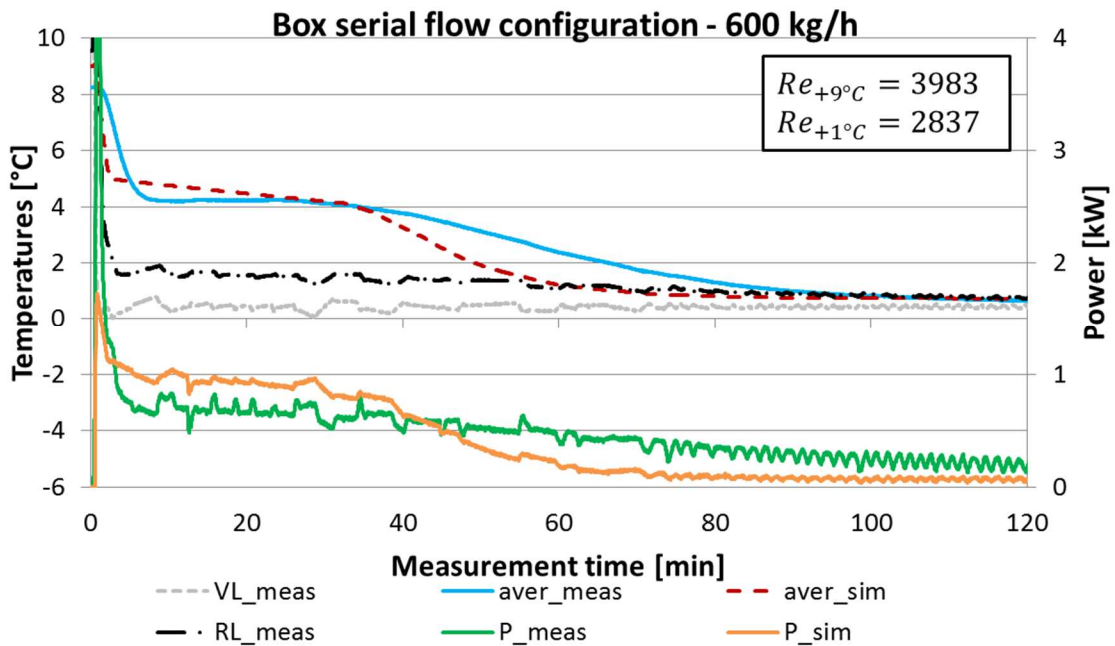


Figure 4-24: Heat delivery and average temperatures of serial box measurement and simulation during charging cycle

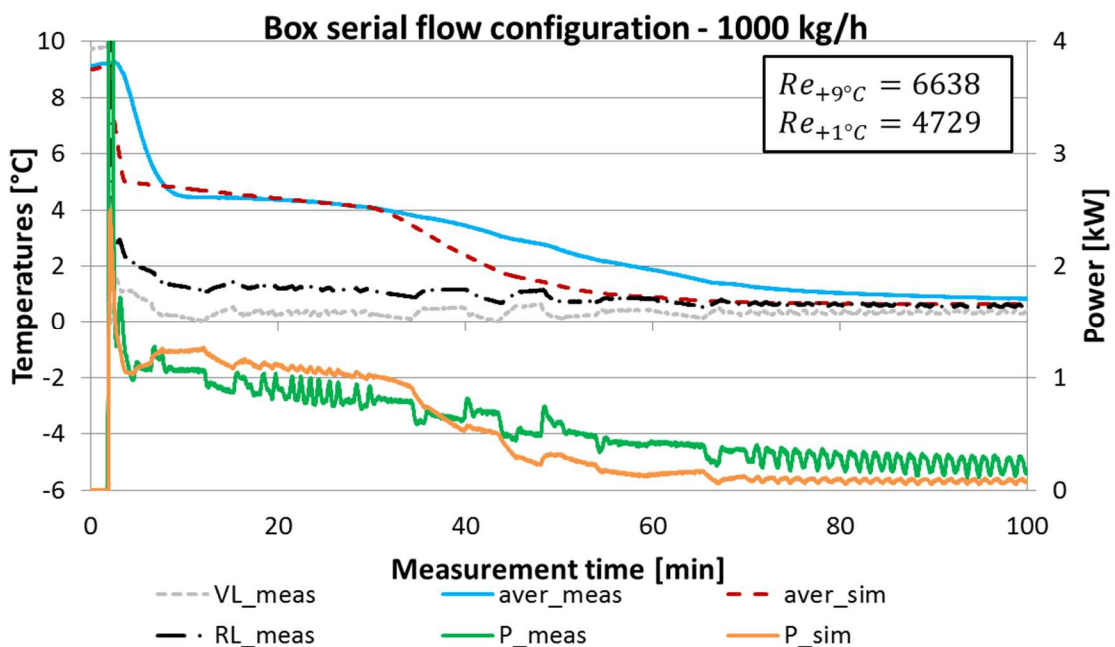


Figure 4-25: Heat delivery and average temperatures of serial box measurement and simulation during charging cycle

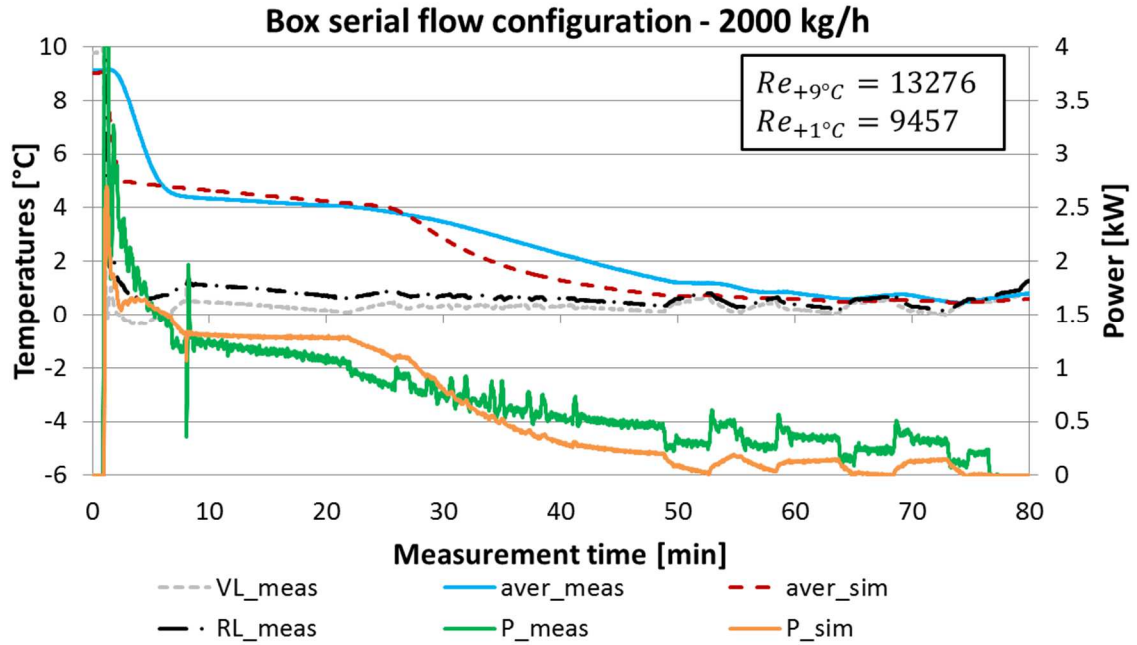


Figure 4-26: Heat delivery and average temperatures of serial box measurement and simulation during charging cycle

Accumulated energies of experimental box measurements in serial flow configuration are shown in Figure 4-27 to Figure 4-28.

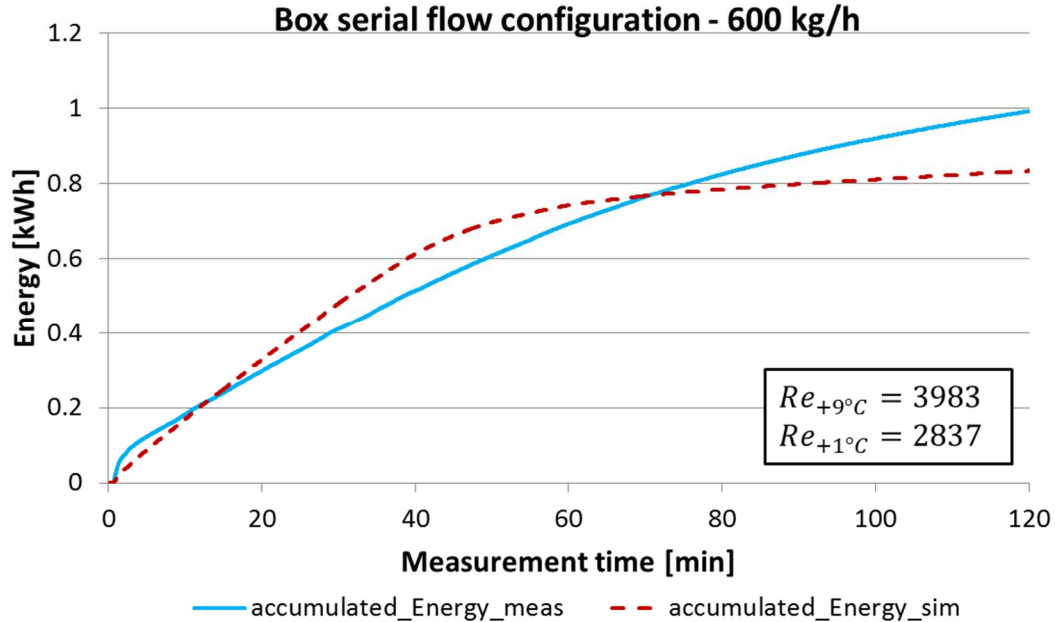


Figure 4-27: Accumulated energy of serial box measurement and simulation during charging cycle

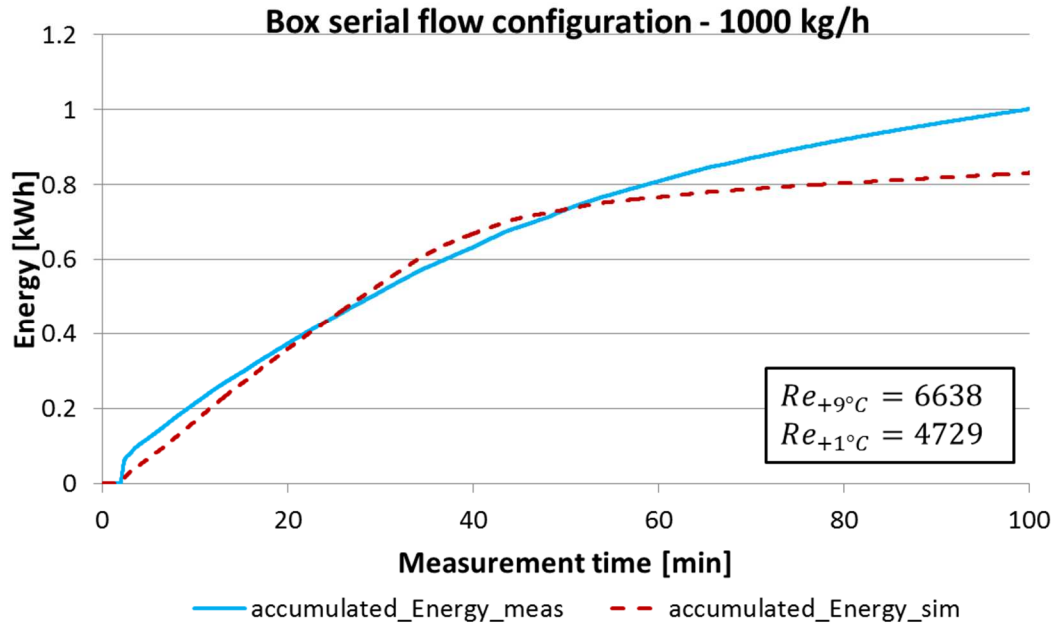


Figure 4-28: Accumulated energy of serial box measurement and simulation during charging cycle

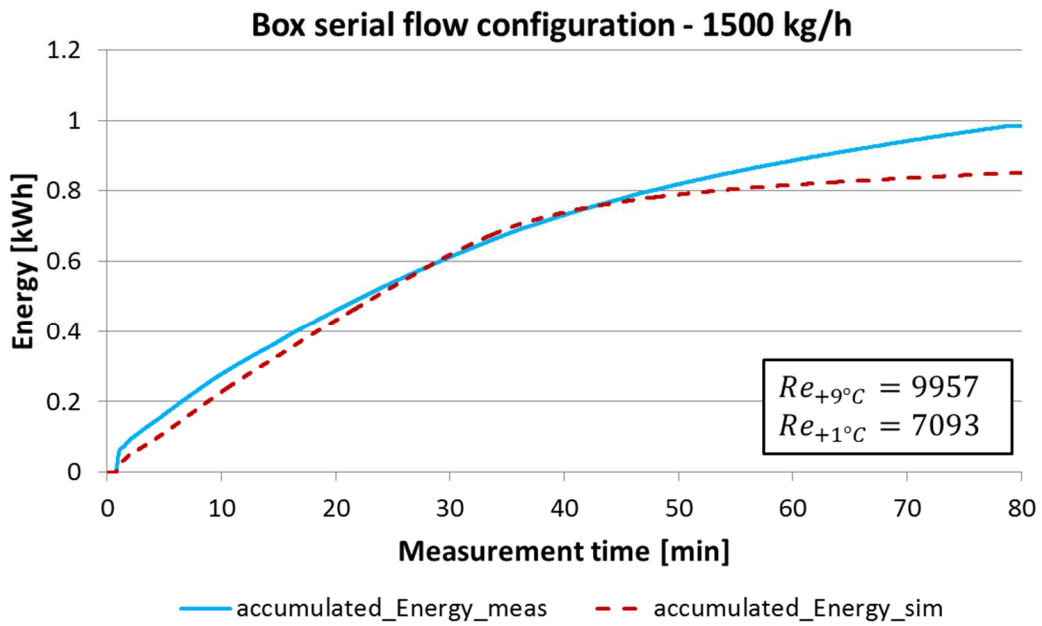


Figure 4-29: Accumulated energy of serial box measurement and simulation during charging cycle

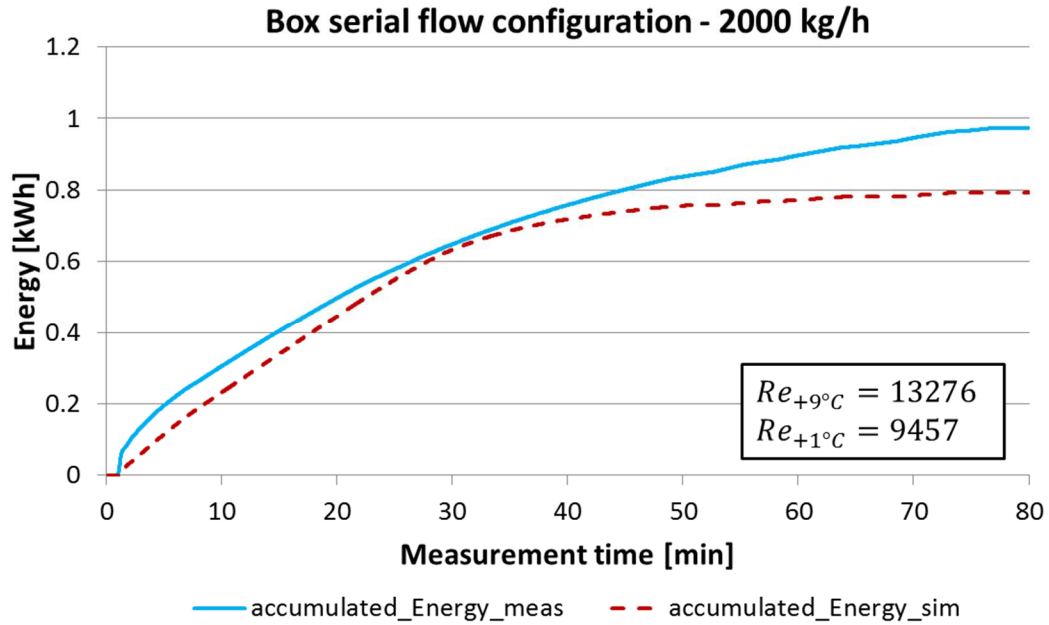


Figure 4-30: Accumulated energy of serial box measurement and simulation during charging cycle

A comparison of all measurement is shown in Figure 4-31.

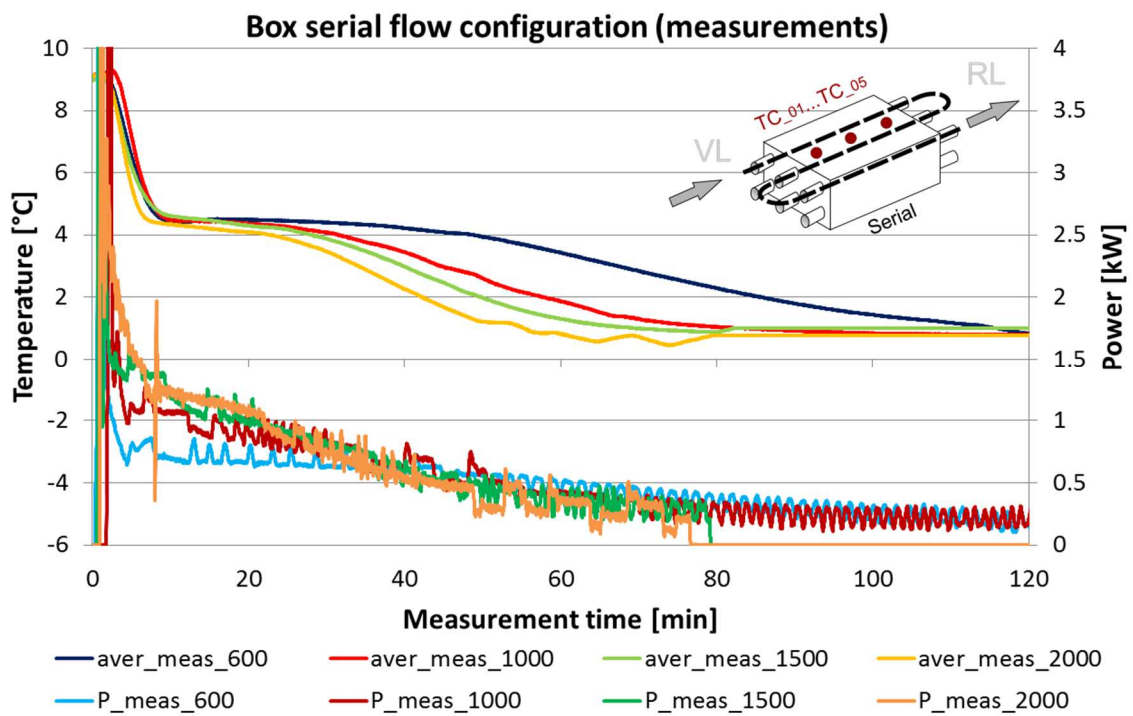


Figure 4-31: Comparison of all serial box measurements

A comparison of all simulation results is shown in Figure 4-32.

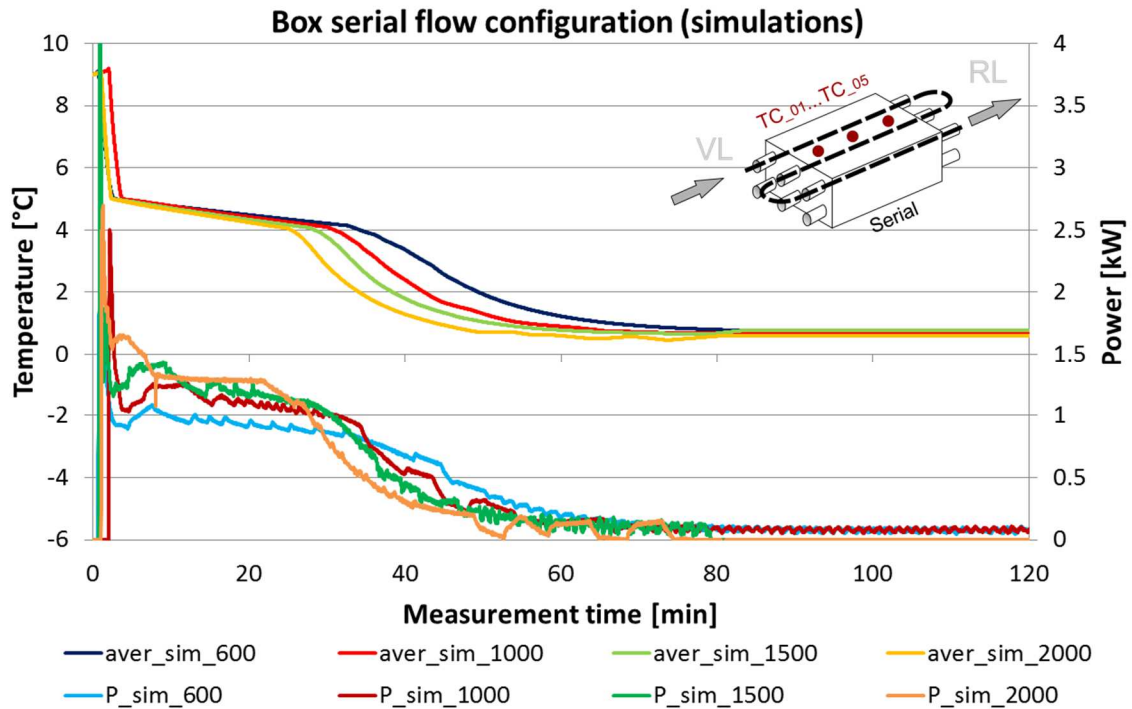


Figure 4-32: Comparison of all serial box simulations

After analysing average heat delivery of the serial box measurements compared with the parallel box measurements it could be shown, that the heat delivery as well as charging durations could be well improved. According to Table 4-3 and the outcome of the simulations it is evident that with turbulent flow situation inside the tube the average heat delivery is increasing due to improved heat transfer coefficients inside of the pipes. The circulating pump of the “MegaLauda” is reaching its maximum performance at mass flow rates of 2000 kg/h. Therefore mass flow rates above 2000 kg/h cannot be achieved.

4.7 Thermal gains of parallel and serial box experiments

Thermal gains can be estimated during charging or discharging cycle when flow and return as well as the surface temperatures are near equilibrium which means the temperature gradient within the box does not change significantly. The thermal gains are increasing if the difference between ambient temperature and box temperature is getting bigger. When determining the thermal gains during phase change several measures have to be considered to avoid significant errors. The reason for this error is related on the fact that during phase change it is difficult to achieve isothermal state, because any energy to or from the PCM (when charging temperatures are not equal to the phase change temperature of the PCM) will change the temperature and therefore the physical state of the PCM. Additionally the estimation of thermal gains during phase change has to take very long time (to ensure isothermal state) and the surface temperatures may detect the influence of ambient temperature as well. So the decision has been made to determine thermal gains at the end of the charging cycle, when the controller of the “MegaLauda” is fluctuating within small aberrations and thermal energy is stored in sensible heat according to Figure 4-33.

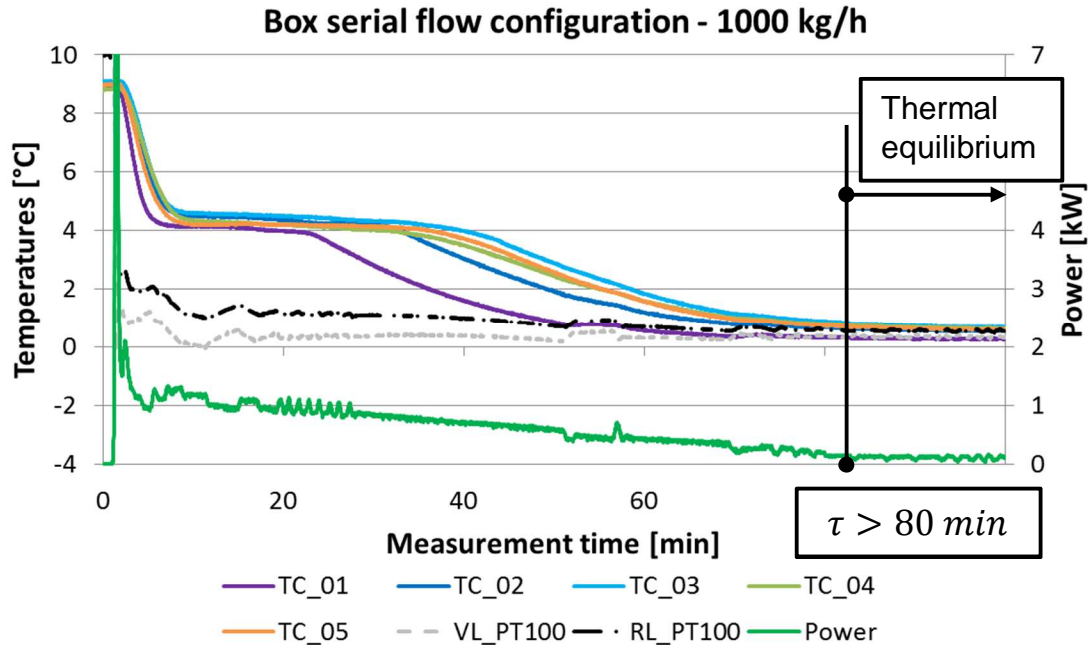


Figure 4-33: Estimating thermal gains at the end of the charging cycle

At measurement time >80 minutes the surface temperatures of the experimental box has reached +1 °C and it can be assumed, that the module is fully charged. The surface temperatures as well as the flow and return temperatures do not change significantly so that no temperature gradient is predominant. Any additional heat delivery from the heat transfer fluid to the experimental box can then be identified as thermal gains from the ambient as the box has reached its thermal equilibrium and does not cool down any further. Thermal gains of parallel and serial box measurements according to equation (2-14) are shown in Table 4-4. Two datasets have been analysed, where the thermal equilibrium has been reached.

Table 4-4: Thermal gains of parallel and serial box measurements

	m_{Flow} [kg/h]	P_{gain} [W]	T_{amb} [°C]	T_{box} [°C]	UA [W/K]
Parallel flow	5000	76.3...94.7	19.1...19.14	1.1...1.14	4.24...5.26
Serial flow	1000	59.1...82.4	23.5...23.63	0.76...0.81	2.6...3.61

The higher thermal gains of parallel tests in comparison to the serial tests can be explained by the additional flow distributor in the flow and return stream. The calculated heat loss rate has been used to parametrize the TRNSYS type 842.

4.8 Comparison of PCM/Aluminium modules with initial parametrization of type 842

Out of 6 parallel and 9 serial box measurements the geometric and thermal parameter for the TRNSYS simulation with the type 842 has been determined according to Table 3-1. With these parameter it is possible to reproduce the measurements of the experimental PCM/Aluminium module within the TRNSYS simulation. But it has not been analysed how the PCM/Aluminium module is performing against a different storage concept. As the TRNSYS type 842 is representing an air heat exchanger which is submerged in PCM, it basically represents the experimental PCM/Aluminium module. So for cross-comparison it is intended to parametrize the type 842 with its initial fin material parameter and check how good/bad it would perform when providing the same input data (flow temperature, ambient temperature and mass flow rate) as

for the simulation of the PCM/Aluminium modules. So when the parameter of the fin material of TRNSYS type 842 are changed to its initial settings than a comparison of the PCM/Aluminium modules with an air heat exchanger, which is submerged in PCM, in serial and parallel flow configuration in terms of heat delivery and charging duration can be made. The properties of the PCM and the heat transfer fluid have not been modified. The parameters which are changed to its initial settings for serial and parallel flow configuration are shown in Table 4-5 and are highlighted in yellow colour.

Table 4-5: Changed parameter of TRNSYS type 842 to the initial values for cross-comparison of the PCM/Aluminium module with an submerged air heat exchanger

Masses contained in the module			Thermal properties of the used materials		
m_{PCM}	10.7	kg	λ_t	15 210	W/(m.K)
m_{add}	18	kg	ρ_t	7850 8960	kg/m ³
			cp_t	477 385	J/(kg.K)
			λ_f	70.6 210	W/(m.K)
			ρ_f	660 2700	kg/m ³
			cp_f	897 942	J/(kg.K)
Dimensions of the module					
length of the tubes	0.5	m	cp_{add}	477	J/(kg.K)
Nr. of parallel tubes	1 or 14*	-	ρ_{PCM}	760	g/dm ³
Nr. of serial tubes	1 or 14*	-	λ_{PCM}	0.2	W/(m.K)
d	18	mm	$cp_{s_{PCM}}$	15	kJ/(kg.K)
t_w	1	mm	$cp_{l_{PCM}}$	2	kJ/(kg.K)
t_l	41.667	mm	$\Delta h_{m_{PCM}}$	163	kJ/kg
t_q	37.5	mm	T_{start}	8.3...9.1	°C
t_f	5 3.3	mm	T_{m1}	4	°C
s_f	2 0.3	mm	T_{m2}	5	°C

* depending on parametrizing the experimental box in parallel or serial flow configuration

t represents parameter considering the tube

f represents parameter considering the fin

cp_{add} specific heat of additional thermal capacity

PCM represents parameter considering the PCM material

T_{start} initial temperature of the module

T_{m1} temperature at which melting of the storage medium begins

T_{m2} temperature at which storage medium is fully melted

The flow temperature, as well as the mass flow rate and the diameter of the heat exchanger tubes were kept the same. So the hydraulic flow situation does not change. If the PCM aluminium module is now compared to the original fin parameter of the air heat exchanger, which is submerged in PCM, in serial and parallel flow configuration for two exemplary mass flow rates of parallel and serial flow configuration (Figure 4-34 and Figure 4-35) it can be shown that the PCM/Aluminium storage concept is lacking in thermal heat delivery. The average heat delivery according to Table 4-6 is about 11.4 % to 14.4 % higher for the simulated air heat exchanger and the charging duration could be reduced.

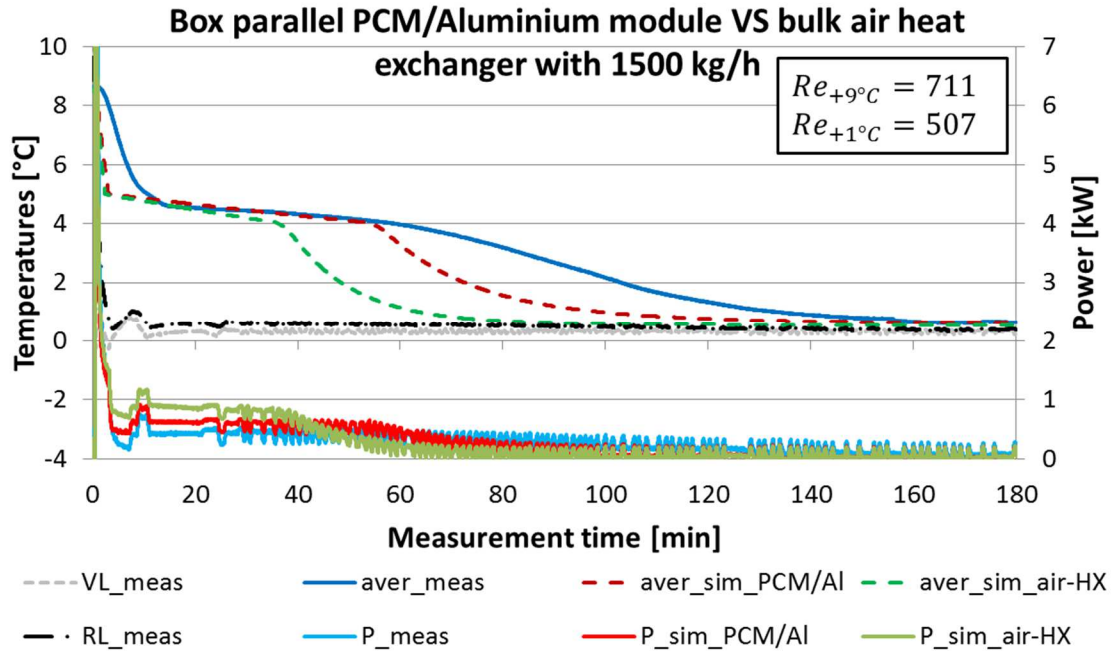


Figure 4-34: Comparison of simulation of PCM Aluminium foam module with submerged air heat exchanger in parallel flow configuration

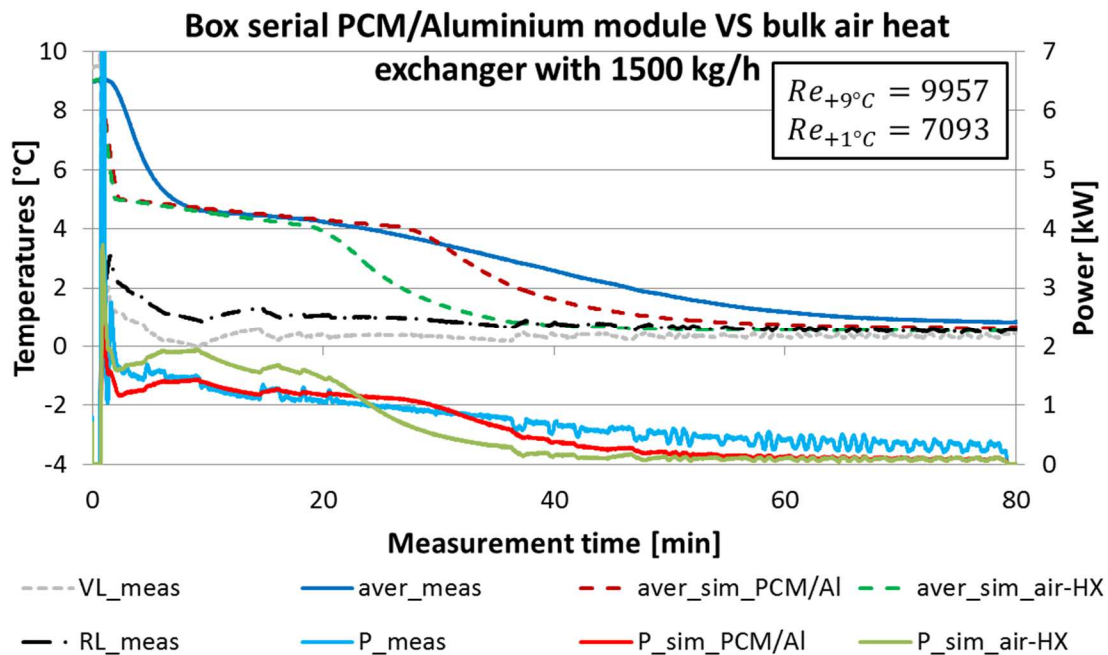


Figure 4-35: Comparison of simulation of PCM Aluminium foam module with submerged air heat exchanger in serial flow configuration

Figure 4-34 and Figure 4-35 show a comparison of two simulations with the experimental measurement for a serial and a parallel flow configuration with a mass flow rate of 1500 kg/h. The red curves indicate the simulations of the parametrized PCM/Aluminium module according to Table 3-1 and the green curves represent the simulations of an submerged air heat exchanger with same PCM mass according to Table 4-5.

Table 4-6 gives an overview of the improvement on heat delivery and charging durations of either parallel and serial flow configuration depending on the chosen mass flow and the parametrization within the simulation.

Table 4-6: Comparison of average charging heat delivery and duration in serial and parallel flow configuration between PCM/Aluminium and air heat exchanger parametrization

parallel / serial flow	Mass flow rate	average $P_{sim_{PCM/Al}}$	average $P_{sim_{air-HX}}$	charging duration PCM/Al foam	charging duration air heat exchanger	improvement
	[kg/h]	[kW]	[kW]	[min]	[min]	[%]
parallel	600	0.32	0.36	178.2	160.7	11.4
parallel	1500	0.46	0.51	141.8	124.2	11.6
parallel	3000	0.52	0.58	99.5	81.8	11.8
parallel	5000	0.76	0.85	79.7	62.2	11.5
serial	600	0.62	0.71	81.2	68.7	14.4
serial	1000	0.79	0.90	74.6	62.1	14.2
serial	1500	0.96	1.10	68.7	56.2	14.2
serial	2000	0.99	1.13	61.4	48.9	14.1

The improvement in percent is a fraction of the simulated average heat delivery of the submerged air heat exchanger $P_{sim_{air-HX}}$ and the simulated average heat delivery of the PCM/Aluminium module $P_{sim_{PCM/AL}}$.

$$Improvement = \left(\frac{P_{sim_{air-HX}}}{P_{sim_{PCM/AL}}} - 1 \right) \cdot 100 \% \quad (4-1)$$

After comparing the simulated PCM/Aluminium module with a simulated submerged air heat exchanger the average heat delivery has been improved by values ranging from 11.4 % to 14.4 %. It is assumed that the narrower dimensions between each fin and the thinner fin itself (which increases the surface area) is increasing the heat delivery and showing better thermal performance in comparison to the aluminium foam. A different foam structure or a variation in porosity of the aluminium foam could improve the thermal output.

4.9 Tube tests

Measurements to specify the size and influence of several “elementary cells” within an experimental box have been performed in addition to the tests of the experimental box in serial and parallel flow configuration (according to chapter 4.3 and 4.5). For this purpose, PCM/Aluminium tubes have been designed and fabricated. As the measurement cycle is expected to be much faster than the measurements of the box, much more measurement data can be collected in the same time. Also manufacturing these tubes can be performed in much shorter time and in addition these tubes are much cheaper and less complicated. These PCM/Aluminium tubes have then been measured and analysed in the laboratory of the Institute of Thermal Engineering.

4.9.1 Theoretical background

Several tube tests have been performed but the length and the inside pipe diameter d of the “elementary cell” have been kept constant whereas the outside diameter D , and therefore the diameter of the aluminium foam matrix and the mass of the encapsulated paraffin has been varied.

The experimental PCM tube consists of a stainless steel pipe, with an outside diameter of $d = 18 \text{ mm}$ and a wall thickness of 1 mm. The stainless steel pipe is surrounded by a cylindrical aluminium foam ring with varying outside diameter D of 32 mm, 50 mm and 78 mm. These varying outside diameter of the aluminium matrix represent different sizes of the “elementary cell” and can be seen in Figure 4-36 and Figure 4-37. The aluminium foam ring is used as matrix for absorbing the PCM material RT5HC Rubitherm (2016). To illustrate the technical capabilities of the PCM tube, charging and discharging cycles have been performed with fluid temperatures of $+1 \text{ }^\circ\text{C}$ and $+9 \text{ }^\circ\text{C}$ and with mass flow rates of 3000 kg/h. This means that the flow situation inside the stainless steel pipe is turbulent and provides therefore optimum heat transfer rates. The reason for changing the outside diameter D of the aluminium matrix is, to vary the radial distance between the “elementary cells” to enhance the geometry and the dimensions of future experimental boxes. When the distance between the tubes is decreasing the ratio between encapsulated paraffin and tube surface area is decreasing as well. On the other hand, if the distance between the tubes is increasing the mass of paraffin is increasing which leads to higher storable energy content of the “elementary cell”. But the heat delivery to the paraffin decreases as there is less surface area of the heat changing fluid. To reproduce this effect with minimum technical effort one variable is kept constant and the other variable can be changed. As it causes much more effort to change the inside diameter d of the pipe it is easier to change the outside diameter D of the “elementary cell” to reproduce the effect of interference of multiple parallel tubes (according to Figure 4-36). Experimental tube UC12-MB/MC for example has an inside pipe diameter of 18 mm and an outside diameter of 78 mm, whereas UC30-MB/MC has an inside pipe diameter of 18 mm and an outside diameter of 32 mm. The denotation of the different “elementary cells” (UC12-MB/MC, UC18-MB/MC and UC30-MB/MC) is dependent on the ratio of the encapsulated PCM and the ratio between inside and outside tube diameter. A specific explanation of the encoding of the experimental tubes is not intended as it is not relevant for the outcome of the measurements. If the ratio D/d is changed several times an optimum constellation, where the maximum heat delivery occurs, can be extrapolated.

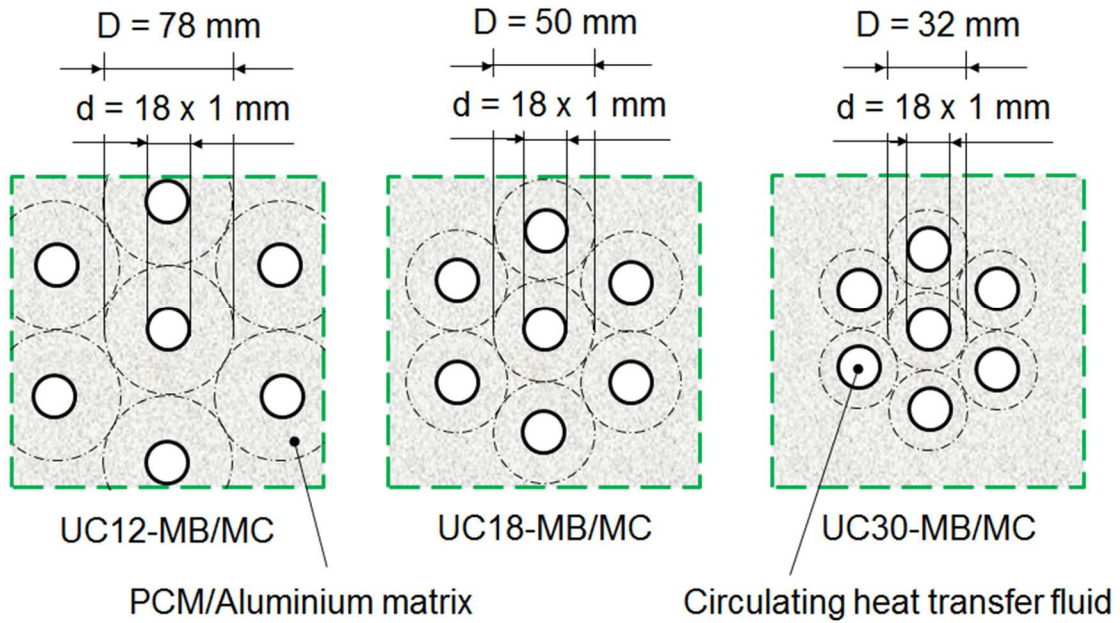


Figure 4-36: Different sizes of “elementary cells” depending on varying outside diameter D

To evaluate the effect of maximising the heat transfer coefficient by increasing the fluid turbulence inside the heat transfer pipe, corrugated pipes (Figure 4-37 and Figure 4-38) with the same diameter d have been manufactured and tested as well. These corrugated pipes have a bigger roughness and lead therefore to an increased drag coefficient.

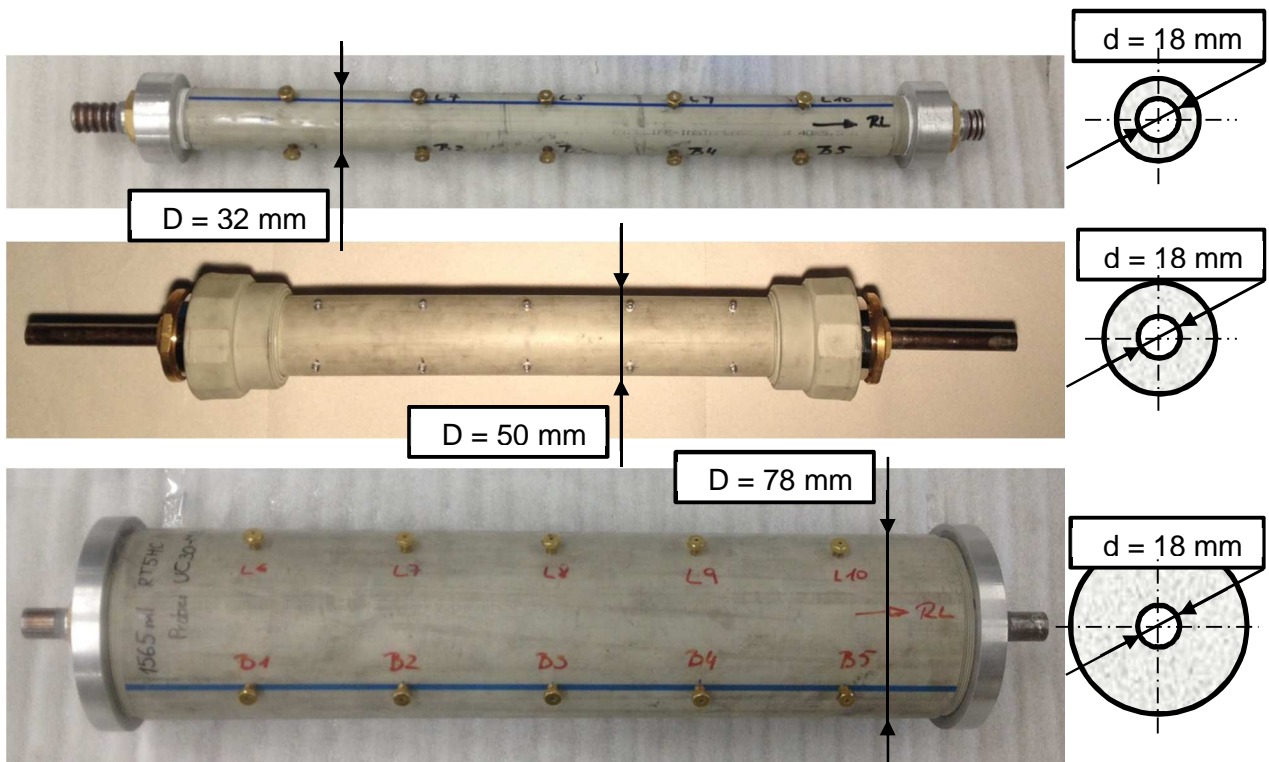


Figure 4-37: Corrugated and bare experimental tubes with varied outside diameter D

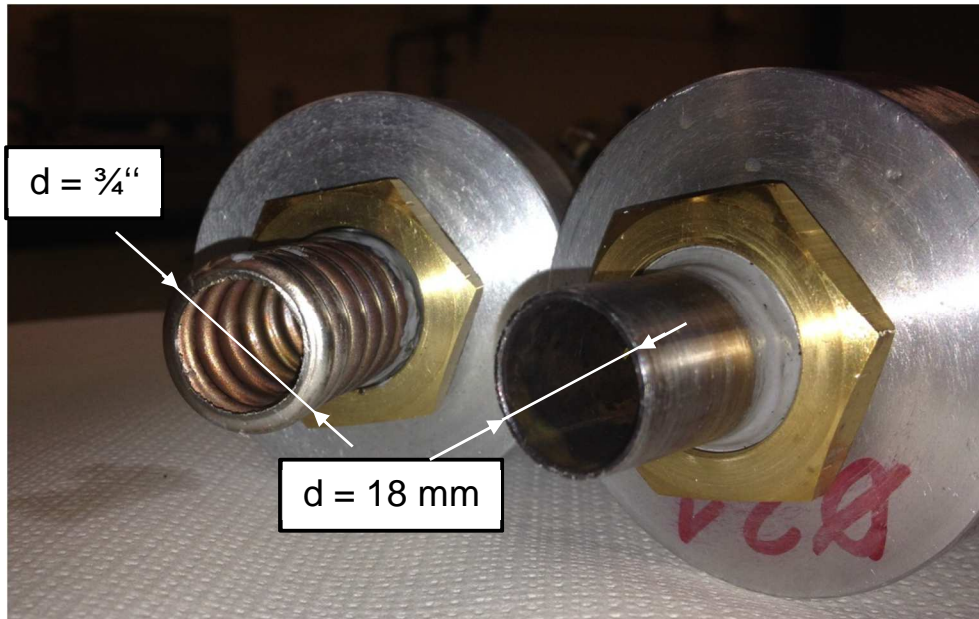


Figure 4-38: Corrugated pipe on the left and bare pipe on the right side of the picture

An overview of all experimental test tubes with its main dimensions and thermal masses are shown in Table 4-7.

Table 4-7: List of properties of the individual experimental tubes

	Bare pipe			Corrugated pipe		
Denotation	UC12-MB	UC18-MB	UC30-MB	UC12-MC	UC-18-MC	UC30-MC
Porosity	Medium	Medium	Medium	Medium	Medium	Medium
Length	498 mm	500 mm	497 mm	498 mm	498 mm	497 mm
Inside Diameter d	18 mm	18 mm	18 mm	$\frac{3}{4}$ "	$\frac{3}{4}$ "	$\frac{3}{4}$ "
Outside Diameter D	78 mm	50 mm	32 mm	78 mm	51 mm	32 mm
Mass PCM	1.207 kg	0.555 kg	0.169 kg	1.147 kg	0.548 kg	0.154 kg
Mass of the aluminium	1.451 kg	0.564 kg	0.176 kg	1.448 kg	0.641 kg	0.235 kg

The six experimental tubes vary in outside diameter D as well as shape of the stainless steel pipe (corrugated or bare pipe) but the porosity level of all six tubes consists of aluminium foam with medium porosity which means the pore diameter varies between 3 to 12 mm.

4.9.2 Tube composition

The tubes consist of straight stainless steel pipes with an outside diameter of 18 mm for the bar pipes an outside diameter of $\frac{3}{4}$ " for the corrugated pipes (see Figure 4-38). The aluminium foam is casted onto the outside of the stainless steel pipe providing optimum heat transfer from the inside of the stainless steel pipe over the aluminium foam matrix to the paraffin. A PVC tube surrounding the aluminium foam ring provides either proper sealing as well as housing for up to 10 immersion sleeves, which are screwed into the PVC pipe. The immersion sleeves are brass screws M6x30 with a centre hole ($d_i = 1$ mm; $l = 25$ mm deep) and are used to insert the thermocouple temperature sensors. To provide optimum heat transfer from the brass screw to the surface temperature sensors a heat transfer paste ($\lambda_{paste} = 2.9 \frac{W}{m \cdot K}$, RS Components (2014), a tech data sheet can be found in the appendix chapter) was filled inside the immersion sleeves.

A cross-sectional view of an experimental test tube is shown in Figure 4-39.

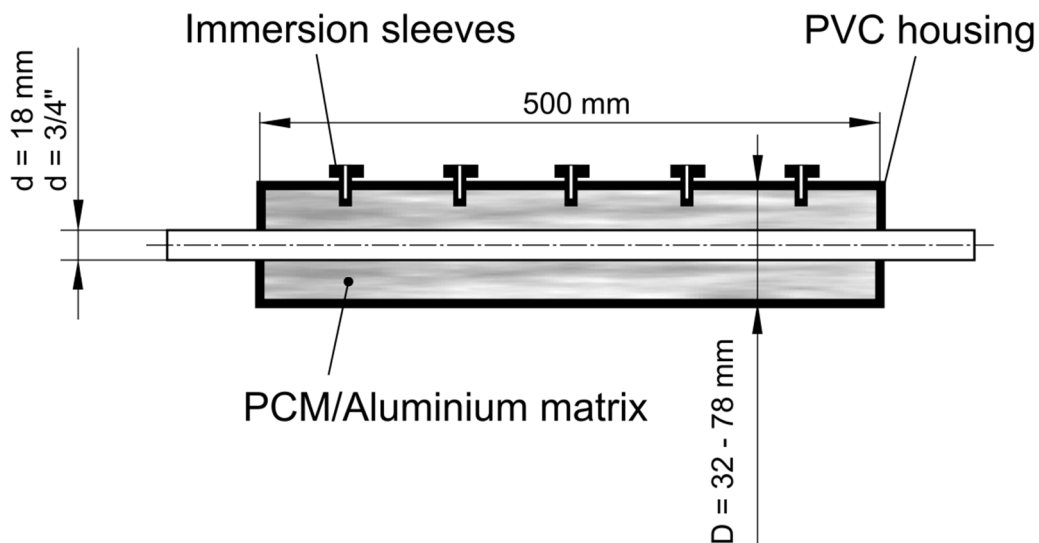


Figure 4-39: Cross-sectional view of the experimental test tube

To ensure measuring a nearly three dimensional temperature distribution 5 temperature sensors cover the temperature distribution on the bottom and 5 temperature sensors on the lateral side of the tube over its length. A detailed view of the positioning of the surface temperature sensors can be seen in Figure 4-41. To fill the paraffin inside the aluminium foam, air is sucked out through one of the measurement sleeves and the liquid paraffin flows inside the experimental tube over another measurement sleeve. Additionally to the tube experiments with bare stainless steel pipe, experiments with $3/4 \text{ inch}$ corrugated stainless steel pipes have been performed. It is expected that the corrugated pipes increase the turbulence inside the pipe significantly, so that the heat transfer coefficient and the heat delivery increase which results in reduced charging/discharging durations. As side-effect an increased pressure drop could be noticed. The circulation pump of the "MegaLauda", during the measurements of the experimental tubes with corrugated pipes, had to be operated at 90 % of its maximum rotation speed, which limits future experiments to mass flow rates of 3200 kg/h.

4.9.3 Measurement setup

The measurement setup (shown in Figure 4-40) consists of the mobile heat source/sink-system "MegaLauda", an internal pump in the return stream, a magnetic inductive flow meter (Endress Hauser Promag 50P25) as well as a bypass valve to set the mass flow rate to 3000 kg/h. Two PT100 temperature sensors (VL_PT100 and RL_PT100) are used to measure the flow and return temperature of the experimental tube.

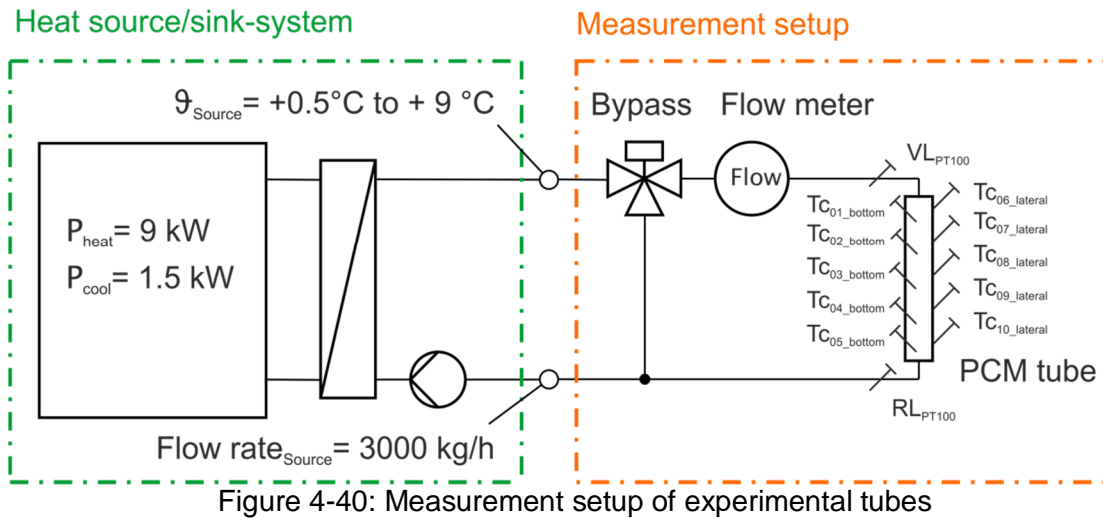


Figure 4-40: Measurement setup of experimental tubes

The “MegaLauda” is capable of providing a heating temperature of +9 °C at 9 kW and a cooling temperature of +0.5 °C with at heat output of 1.5 kW. The flow rate of the “MegaLauda” is 3000 kg/h. To prevent freezing of the heat transfer fluid, a mixture of 70 % water and 30 % Glysofor N (2016) was used. Physical properties of the heat transfer fluid are shown in Table 4-1.

10 immersion sleeves are equally positioned in two lines over the length of the surface of the tube; 5 at the bottom and 5 at the side position and 10 Thermocouple sensors are used to measure surface temperatures of the PCM tube (see Figure 4-41). The thermocouple sensors measuring the bottom temperatures are named B_1, B_2, \dots, B_5 and the thermocouples measuring lateral temperature are named L_1, L_2, \dots, L_5 . A cross-sectional view of an experimental tube can be seen in Figure 4-39.

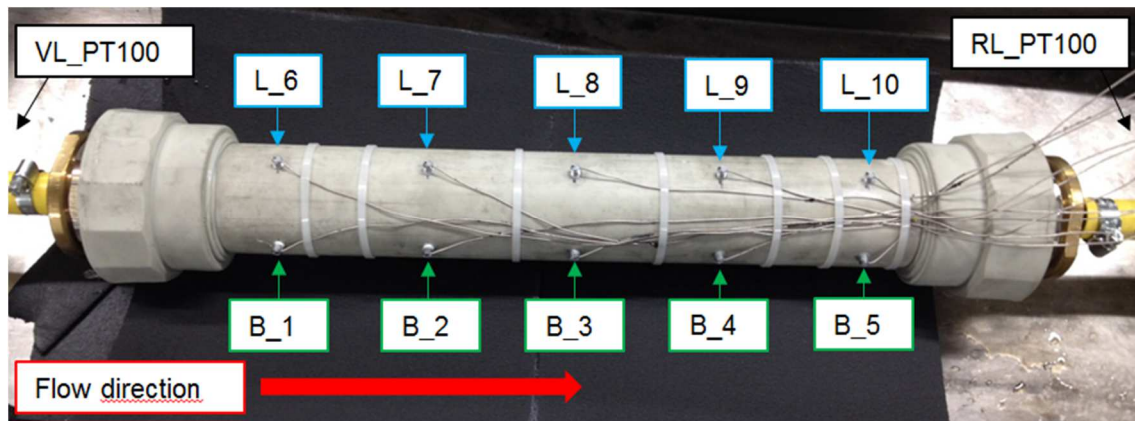


Figure 4-41: Alignment of the thermocouple sensors on the experimental tube (without insulation)

The experimental tube has been insulated with AF/Armaflex (2015) with a thickness of 19 mm. The thermal conductivity of the AF/Armaflex material is $\lambda_{ARMAFLEX} \leq 0.033 \frac{W}{m \cdot K}$. The flow configuration through the tube is shown in Figure 4-41. To ensure reproducible charging and discharging cycles the heat transfer fluid was preconditioned to the same temperature level by circulating over the bypass channel. Data recording was carried out by the measurement equipment Solartron IMP UNIVERSAL 3595J and a calibration protocol can be found in appendix chapter 7. The sampling rate of the IMP 3595J was set to 1 second for all tube measurements.

4.9.4 Measurement strategy

All measurements have been performed with the mobile heat source/sink-system “MegaLauda” and an exemplary charging/discharging cycle is shown in Figure 4-42. Prior to the measurement the tube has been cooled down to a start temperature of +9 °C. The tube has then been charged with cooling temperatures of +0.5 °C (± 0.5 K) and a mass flow rate of 3000 kg/h (± 15 kg/h). When the temperatures of the surface sensors fall below +1 °C it can be assumed that the encapsulated paraffin performed its phase change and the charging cycle is finished. The charging duration is about 30 minutes and subsequent to the charging cycle the temperatures of the heat transfer fluid are set to +9 °C (± 0.5 K). This can be achieved via a bypass stream parallel to the measurement tube and takes about 4 minutes (according to Figure 4-40). The preconditioning of the heat transfer fluid occurs from minute 30 to minute 34. The bypass stream is not flowing over the magnetic inductive flow meter, so no mass flow can be measured during that time. Due to thermal gains from the ambient the surface temperatures rise about +0.5K. This small increase in surface temperature has to be accepted as it is assumed that the paraffin inside the tube is still in solid state. Discharging of the tube occurs again with a mass flow rate of 3000 kg/h (± 15 kg/h). The charging/discharging cycle takes about 60 minutes. The Reynolds number, by considering a mass flow rate of 3000 kg/h and an inside diameter of 16 mm can be found in Table 2-4 or in Figure 4-42.

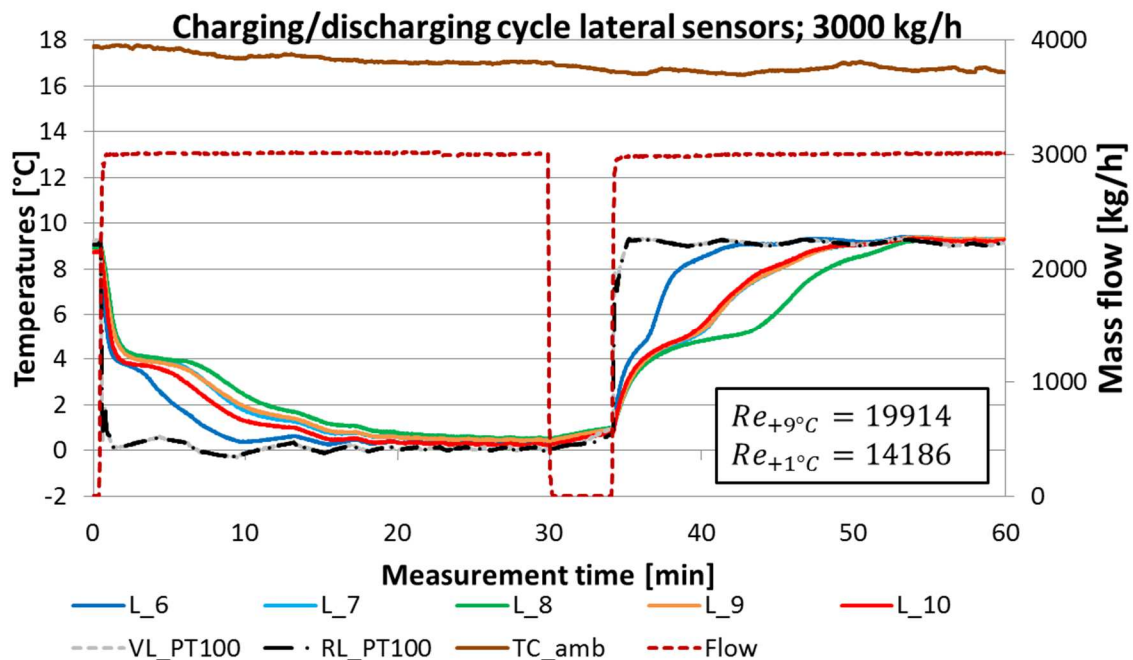


Figure 4-42: Exemplary charging/discharging cycle of the test tube UC-30MB showing lateral sensors with a mass flow rate of 3000 kg/h

Charging of the PCM tube was executed with temperatures below +1 °C whereas discharging temperatures were above +9 °C. Small variations in flow temperature were caused by the dead band of the controller of the “MegaLauda”. The charging temperatures varied between -0.3 °C and +0.8 °C and discharging temperatures varied between +9 °C and 9.3 °C. The measurements of the tubes (Figure 4-42) show an arbitrary temperature distribution over the tube length, especially during discharging process (lateral sensors L_6 and L_8). This behaviour could not be expected as there could not be noticed a significant temperature difference between flow and return stream. The fluctuations in flow and return temperature are within the measurement uncertainty of both sensors (± 0.07 K). When analysing the bottom temperature sensors the same behaviour in temperature distribution could be noticed (according to Figure 4-43). To verify if the flow direction over the experimental tube showing a different temperature distribution, the flow direction was inverted for 2 measurements. It could

be shown, that a conversion in streaming direction did not show different charging/discharging behaviour. Therefore surface temperatures do not represent the streaming direction but only provide the information when charging of the tube is finished. This discrepancy in surface temperature distribution could be explained by an inhomogeneous dispersion of paraffin over the length of the tube. Areas with less paraffin possess greater temperature gradients than areas with more paraffin. Also as the aluminium foam is not homogeneous it cannot be ensured that all aluminium pores are fully filled with paraffin, or that the encapsulated paraffin is diffusing over time into other porous voids. This circumstance can be proven by the fact that the temperature distribution over the length of the tube is slowly changing in time because after performing additional comparison measurements over a period of 4 days the temperature distribution of the individual surface temperature sensors is slightly changing. If the experimental tube is equally infiltrated with paraffin all temperature sensors would show the same temperature curves and would match perfectly, because the temperature difference between flow and return stream is nearly identical.

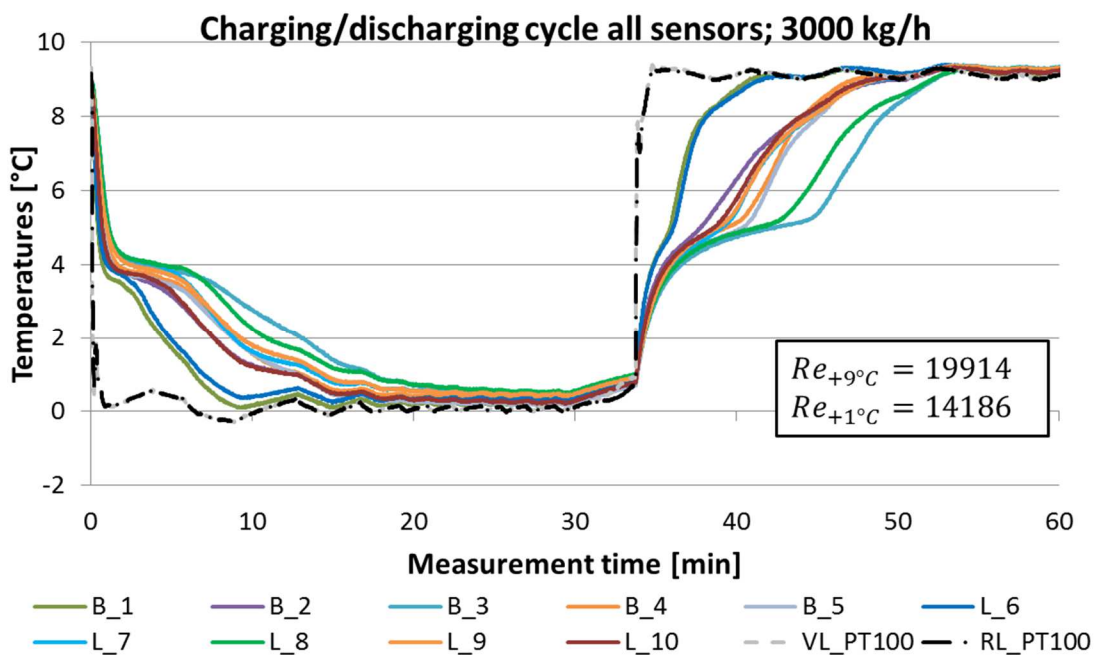


Figure 4-43: Exemplary charging/discharging cycle of the test tube UC-30MB showing all temperature sensors with a mass flow rate of 3000 kg/h

To estimate the heat delivery to the tube it is therefore best to determine an average temperature of all 10 temperature sensors \bar{x} , and calculate the standard deviation s_N of the average temperature distribution. The standard deviation of the 10 surface temperatures calculates by equation (4-2) according to DIN 1319-3 (1996) and regards the sample size N (this means all 10 surface temperature sensors), the individual surface temperature sensors that are used to calculate the standard deviation x_i and an average surface temperature \bar{x} .

$$s_N = \sqrt{\frac{1}{N} \cdot \sum_{i=1}^N (x_i - \bar{x})^2} \quad (4-2)$$

By adding and subtracting the standard deviation to and from the average surface temperature \bar{x} , an upper and lower boundary ($Std +$ and $Std -$) of the average surface temperature can be calculated according to equation (4-3) and (4-4).

$$Std += \bar{x} + s_N \quad (4-3)$$

$$Std- = \bar{x} - s_N \quad (4-4)$$

This method of determining the average surface temperature curve and the according upper and lower standard deviation is shown in Figure 4-44.

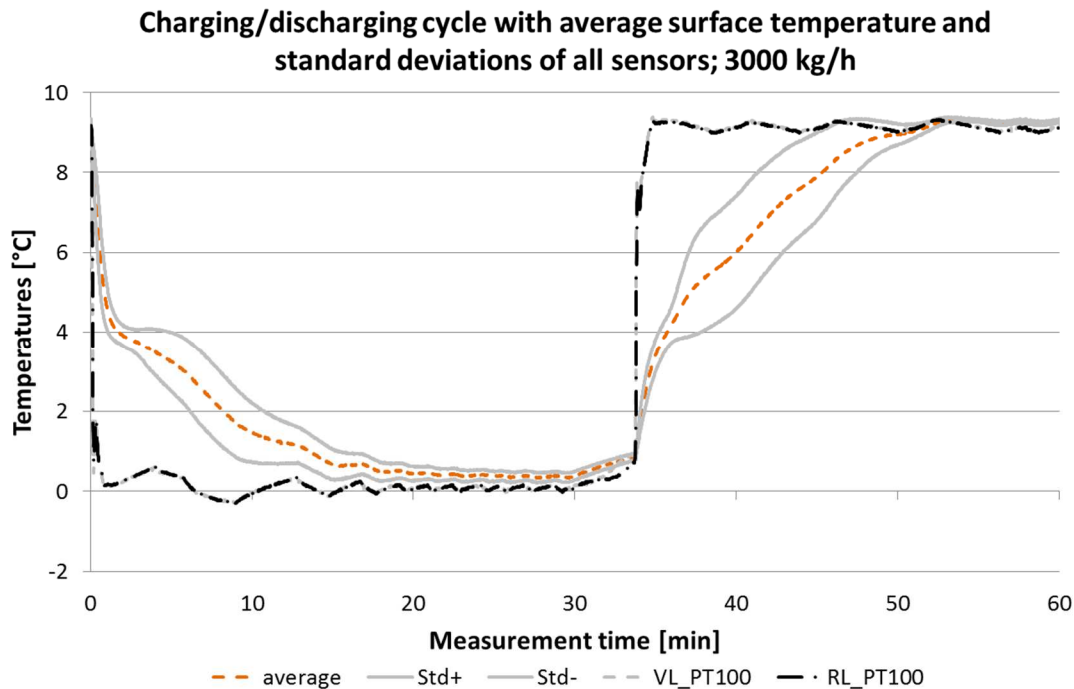


Figure 4-44: Average temperature distribution and standard deviations of all temperatures according to Figure 4-43

According to Figure 4-43 the surface temperatures B_1, B_3, L_6 and L_7 show abnormal behaviour which leads to big variances between the average surface temperature and the upper and lower standard deviation. Therefore these surface temperatures should be excluded from the calculations for determining the average surface temperature and the standard deviation. When eliminating arbitrary temperature curves out of the calculation of the standard deviation it minimizes the gap between upper and lower standard deviation. The adjusted temperature distribution (shown in Figure 4-45) displays a better approximation of real charging/discharging situation with minimal standard deviations.

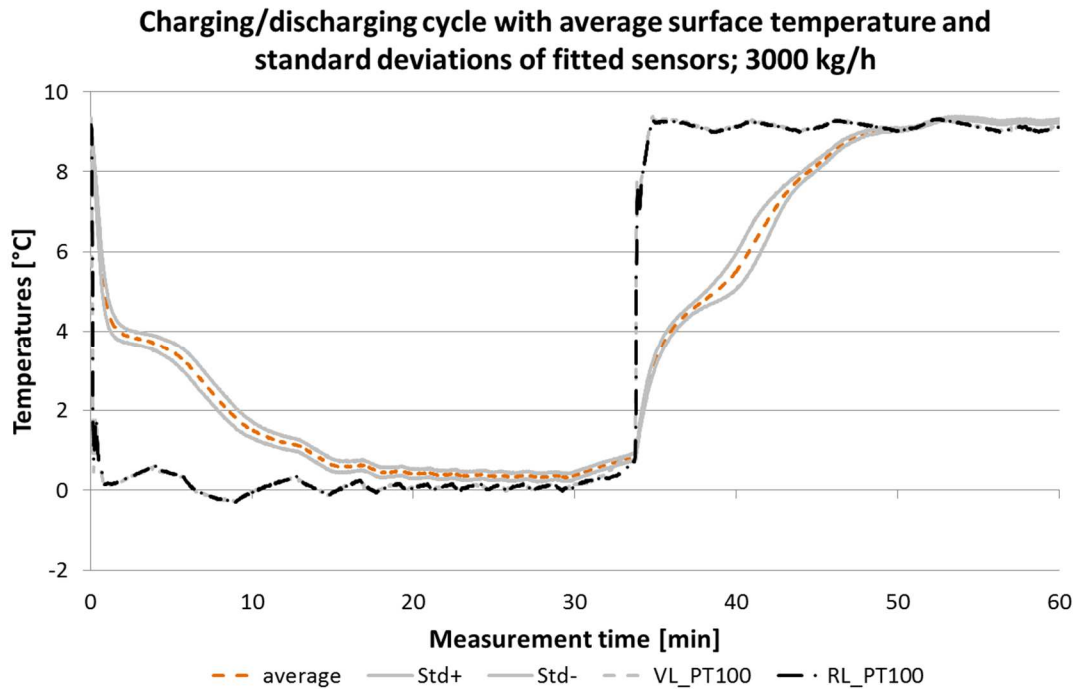


Figure 4-45: Adjusted average surface temperature distribution and standard deviations with excluded surface temperatures B_1, B_3, L_6 and L_7

4.9.5 Heat delivery of the tube tests

After the first measurements a very small temperature difference between flow and return stream (± 0.07 K) was detected. As the temperature difference was within the measurement uncertainties it was evident that an estimation of heat delivery would lead to unsatisfying results. Luckily the dimensions and masses of the tubes as well as the thermal properties of the paraffin are well known. So the total energy content can be calculated by defining a specific temperature boundary where the phase change, and therefore the main energy conversion occurs. Analysing the thermal properties of the used paraffin Rubitherm RT5HC (according to Figure 2-8) the phase changing process (from liquid to solid state) starts at a temperatures of $+6$ °C and is finished at $+3$ °C. The specific enthalpies at temperatures below $+3$ °C are small in comparison to the specific enthalpies between $+6$ °C and $+3$ °C, so the energy contents of temperatures below $+3$ °C are not being considered for estimating average heat delivery. An illustration of defining the boundary temperature is shown in Figure 4-46.

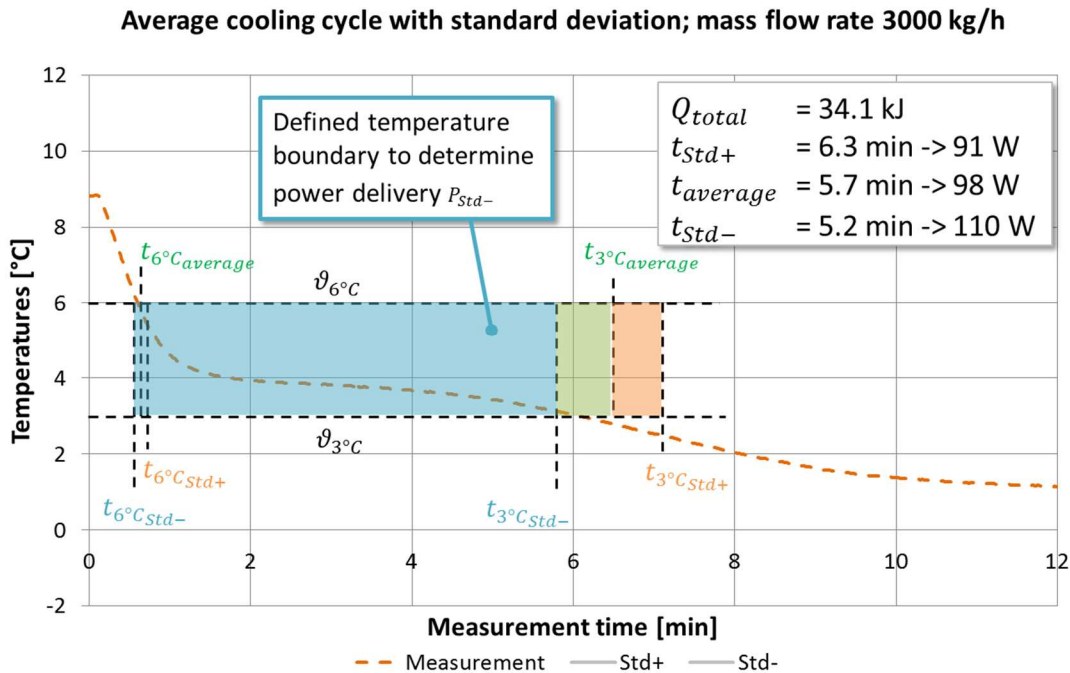


Figure 4-46: Definition of temperature boundary for estimating average heat delivery

Estimating charging durations is slightly more relevant in terms of usage of PCM/Aluminium storage systems for technical applications as the main intention is to cool down the PCM modules as fast as possible. Discharging durations are shorter because ambient thermal gains enhance melting of the paraffin leading to increased average heat delivery.

A step by step measurement instruction for estimating the average heat delivery of the experimental tube tests is shown below.

- a) Precondition the experimental tube to temperatures of about +9 °C
- b) Charging the tube with fluid temperatures between +0 °C and +1 °C (due to the deviation of the controller of the “MegaLauda”)
- c) Record the temperature distribution between +6 °C (the paraffin is still in liquid phase) and +3 °C (the paraffin has performed its phase change)
- d) Calculating an average temperature by considering all 10 temperature surface sensors
- e) Calculate the standard deviation by considering all 10 temperature surface sensors
- f) Generate charts of an average temperature and the upper and lower standard deviation of the surface temperatures (*Std +* and *Std -*)
- g) Minimize the upper and lower standard deviation by eliminating not more than 4 arbitrary temperature curves
- h) determining the duration (for average surface temperature as well as for upper and lower standard deviation) that it takes to pass the boundary where the main part of the phase change occurs (+6 °C to +3 °C)
- i) determining the total energy content of the tube
- j) calculate average heat delivery of average surface temperature as well as for the upper and lower standard deviation

By calculating the total energy content of the experimental tube Q_{total} and dividing it through the time it takes to undergo the temperature boundary ($t_{average}$, t_{Std+} and t_{Std-}) an average heat delivery for the average cooling curve and the according standard deviations *Std +* and *Std -* can be calculated (see equation (4-5), equation (4-6) and equation (4-7)).

$$P_{average} = \frac{Q_{total}}{t_{average}} \quad (4-5)$$

$$P_{Std+} = \frac{Q_{total}}{t_{Std+}} \quad (4-6)$$

$$P_{Std-} = \frac{Q_{total}}{t_{Std-}} \quad (4-7)$$

An average heat delivery for all experimental test tubes is shown in Table 4-8.

Table 4-8: Average heat delivery of the experimental tubes

sample	Q_{total} [kJ]	t_{Std-} [min]	$t_{average}$ [min]	t_{Std+} [min]	P_{Std-} [W]	$P_{average}$ [W]	P_{Std+} [W]	P_{gain} [W]
UC12-MB	241	42.7	55.1	70.7	94	73	57	2.1
UC18-MB	110.8	17.6	18.8	20.3	105	98	91	1.8...2.0
UC30-MB	34.1	5.2	5.7	6.3	110	98	91	1...1.6
UC12-MC	229.3	24	29.5	35.6	159	127	107	2.1...2.5
UC30-MC	31.4	3.3	3.9	4.3	158	134	121	1...1.6

4.9.6 Thermal gains

As the total energy content of the experimental tube is known, any temperature increase over a specific amount of time represents thermal gains, according to equation (2-14), driven by natural convection at the outside of the tube, within this duration (Figure 4-47). For determining the thermal gains of the experimental tubes a duration of 30 seconds, where an average surface temperature has been calculated, has been chosen. The thermal gains decrease when the average temperature of the tube is approaching ambient temperature. Thermal gains at operating temperatures can be evaluated by extrapolating the temperature difference in Figure 4-48.

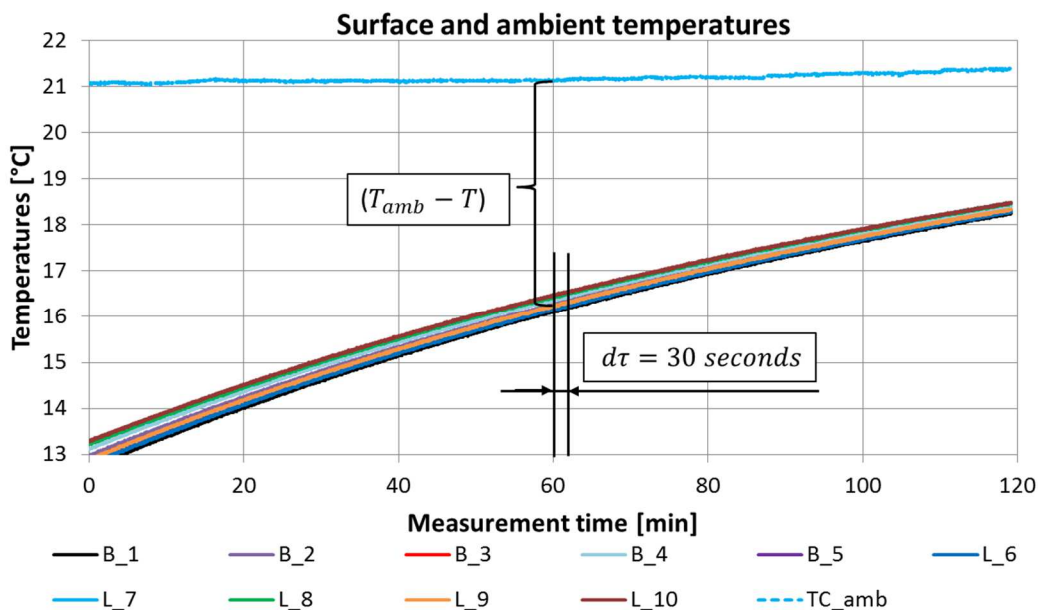


Figure 4-47: Temperature increase due to temperature difference to the ambient

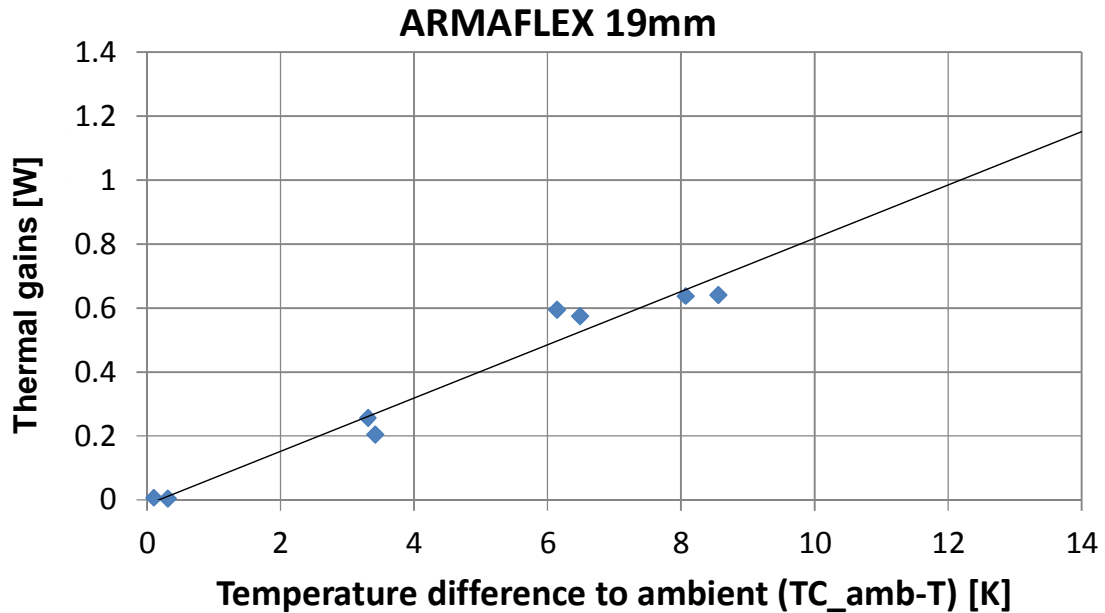


Figure 4-48: Estimated thermal gains depending on temperature difference to ambient when insulating the tubes with 19 mm AF/Armaflex

Figure 4-48 shows the estimated thermal gains if the test tubes are insulated with AF/Armaflex (2015) with a thickness of 19 mm. The greater the difference between ambient temperature and average temperature of the tube, the greater is the influence of ambient gains. Ambient gains at operating temperature +1 °C to +9 °C and an ambient temperature between 16.2 °C and 24.7 °C, dependent on tube dimension, vary between 1 W and 2.5 W.

4.9.7 Conclusion of the tube measurements

A wide distribution in surface temperatures could be noticed throughout the measurements of the experimental tube. As this behaviour can be reproduced with all tested tubes the conclusion leads to the fact that inhomogeneous fractions inside the tube lead to arbitrary temperature distribution over the length. Also the temperature sensors of bottom and lateral sensors show different temperature distribution. It is evident that the paraffin slowly diffuses to the bottom of the tube with decreasing amount of paraffin in upper parts of the tube. Additionally when the main amount of encapsulated paraffin is descending to the bottom of the tube it means that there is much available space left on the top of the tubes without containing any PCM. As there has no leakage been detected, this leads to the assumption that it was not possible to fill the experimental tubes completely with paraffin. Maybe the porosity of the aluminium foam is limiting the amount of paraffin that can be filled inside the tube and should be adjusted for future modules.

4.10 Measurement uncertainties

In technical experiments a lot of raw data is collected and the general idea of error estimation is that physical measurements are basically not exact and the real value of the measurement lies in between an estimated area. The basis of this uncertainty is the fact that each measurement device possesses deficiencies. The true value from the measurement parameter can therefore not be captured exactly but only with a certain aberration (for example indication errors or false reading of the measuring scale). During the measurement a deviance of the measuring object

cannot be excluded, so the possibility, that the measurement itself distorts the expected results cannot be neglected. Deviations from the true values to the values out of the measurements are called measurement errors. These measurement errors occur with every measurement and have to be considered in the analysis of the experimental outcome to meet the standards of meaningful and significant conclusions.

The methods to determine the qualitative error of measurements is denoted as uncertainty analysis and it has to be said that a comparison between different values is only correct when it displays the value and the according measurement error. The estimation of the error is therefore as important as the measurement itself and a reading without error indication does not allow any conclusions or statements.

4.10.1 Random errors

According to DIN 1319-3 (1996) errors due to unpredictable incidents are captured by statistical methods and are called random errors. If the measurement is repeated several times, fluctuations of the measurement values lie between an average boundary. Such errors are basically unavoidable.

4.10.2 Systematic errors

Unilateral deviations from the true value to the measured value are called systematic errors. They are generated by poorly calibrated instruments, crooked scales respectively buoyant effects during weighing, or poor agreement with the experimental conditions. Systematic errors can be corrected or minimized with a careful selection of the measurement and evaluation methods.

4.10.3 Error propagation

Error propagation is shown for an exemplary charging cycle of the box measurement and 1500 kg/h. The relative and absolute error of the heat delivery will be calculated at the time of 12 minutes and the time of 70 minutes within the measurement.

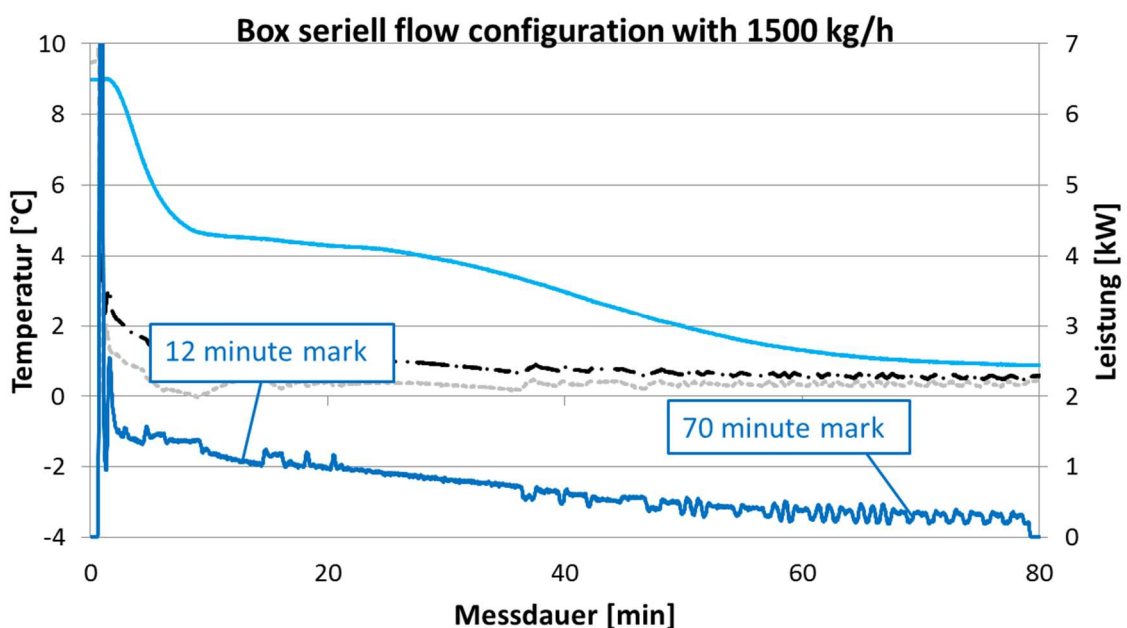


Figure 4-49: Overview of calculated measurement uncertainties of an exemplary measurement of serial flow configuration at 1500 kg/h

When charging the experimental box with a mass flow rate of 1500 kg/h the heat transfer fluid is flowing with a velocity of 1.97 m/s within the tubes. The relative error of the MID Endress Hauser Promag 50P25 for this velocity (according to Figure 4-50) denotes as 0.5 % of the actual volume flow. The relative error curve of 0.2 % can be achieved with optional accuracy calibration, but the Endress Hauser Promag 50P25 does have normal accuracy of 0.5 %.

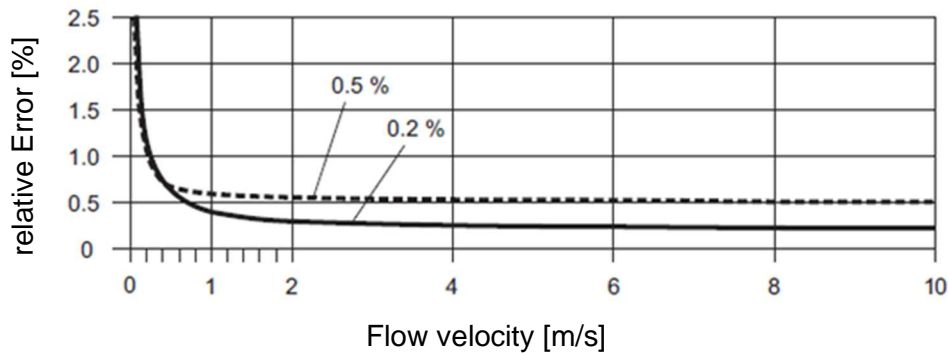


Figure 4-50: Relative error of MID Endress Hauser Promag 50P25 depending on flow velocity
source: Endress + Hauser (2009)

The systematic error for the selected mass flow rate is therefore 1500 kg/h \pm 7.5 kg/h.

The systematic error for the combination of PT100 sensors and the Solartron IMP UNIVERSAL 3595J denotes as \pm 0.025 K within the selected temperature range (see appendix chapter). This deviancy has been determined out of the raw data of the calibration file. It has to be mentioned that during time step 12 the temperature difference between flow and return stream is 0.76 K and at time step 70 the temperature difference decreased to 0.23 K. This results in an increasing relative error at that certain point of time.

The heat transfer fluid is a mixture of 70vol% water and 30vol% glycol. It is assumed that there can be a parallax error of determining the freezing point (when using the refractometer) of \pm 4 K. This results in a possibility of having either a mixture of 65%water 35%glycol or 75%water and 25%glycol within the circulation stream. This error has an influence on determining the specific heat capacity of the heat transfer fluid and can therefore vary within a range of 3800 J/(kg.K) \pm 107.5 J/(kg.K).

A list of all measurement variables and the according uncertainties is shown in Table 4-9.

Table 4-9: Uncertainties of the used components

Component	Freezing point	Value	Absolute Error	Relative error
Volume flow meter				
E+H Promag 50P25		1500 kg/h	\pm 7.5 kg/h	0.5 %
PT100 and IMP3595J				
$\Delta\vartheta$ between flow and return stream		0.76 K...0.23 K	\pm 0.025 K	3.3 %...10.9 %
Heat transferring fluid				
70%water 30%glycol	-16 °C	3800 J/(kg.K)	\pm 107.5 J/(kg.K)	2.8 %
75%water 25%glycol	-12 °C	3880 J/(kg.K)		
65%water 35%glycol	-20 °C	3665 J/(kg.K)		

4.10.4 Propagation of uncertainties

To estimate the absolute/relative error of the calculated heat delivery the Gauß propagation of uncertainties according to DIN 1319-3 (1996) is used because it is a common method for determining the error of the heat delivery. This error method considers the second order of the individual error of the partial differentiation of the heat delivery calculation according to equation (4-8).

$$s_{\bar{z}} = \sqrt{\sum \left[\left(\frac{\partial z}{\partial x} \right) \cdot s_{\bar{x}} \right]^2} \quad (4-8)$$

The uncertainty $s_{\bar{z}}$ is dependent on the amount of partial differentiations $\left(\frac{\partial z}{\partial x} \right)^2$ and the uncertainty of the individual derived variable $s_{\bar{x}}$. The error uncertainty denotes according to equation (4-9)

$$s_{\overline{power}} = \sqrt{\left[\left((\dot{m} \cdot cp) \cdot s_{\Delta\vartheta} \right)^2 + \left((\dot{m} \cdot \Delta\vartheta) \cdot s_{c\overline{p}} \right)^2 + \left((cp \cdot \Delta\vartheta) \cdot s_{\overline{m}} \right)^2 \right]} \quad (4-9)$$

When calculating the partial derivatives and multiplying it with the individual errors of the derived variables the heat delivery with the according absolute and relative error can be calculated. The outcome of this error estimation is shown in Table 4-10.

Table 4-10: Heat delivery with absolute and relative error for 2 specific moment in time

Measurement time [min]	Heat delivery [W]	Absolute error [W]	Relative error [%]
12	1084.1	52.4	4.48
70	318.2	40.9	12.85

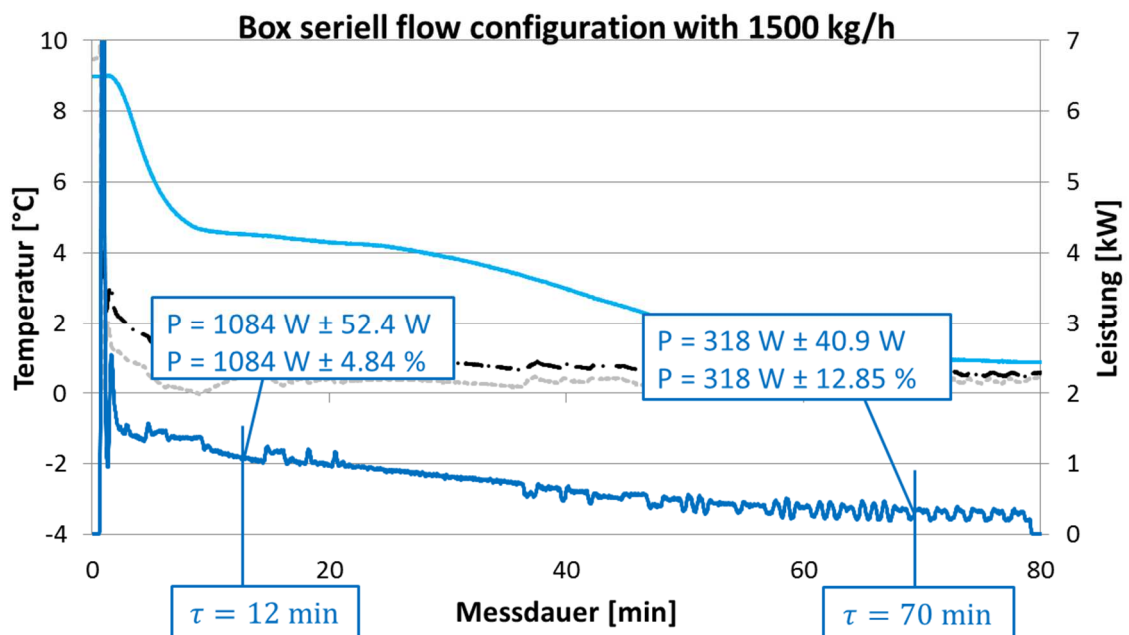


Figure 4-51: Measurement uncertainties of the heat delivery at 12 and 70 minutes after the measurement started

Figure 4-51 shows the summarization of heat delivery and the uncertainty values for the two measurement at the time of 12 and 70 minutes.

With assistance of the Gauß propagation of uncertainties it is now possible to determine the heat delivery of all experimental measurements with the information of its systematic absolute and relative error. The uncertainties of the flow meter, the temperature sensors or the specific heat capacity of the heat transfer fluid can be estimated and taken into consideration when analysing the outcome of the experiments. The relative errors of the calculated heat delivery have been denoted in Table 4-2 and Table 4-3.

5 CONCLUSION

After performing several measurements with the experimental box in either serial or parallel flow configuration it could be shown that the thermal output and the surface temperature distribution could be reproduced within an individually parametrized TRNSYS simulation. The measurements of the experimental box have been performed for laminar (parallel flow configuration) and turbulent flow of the heat transfer fluid (serial flow configuration). Also the progression of heat delivery as well as the expected charging/discharging durations does match with the outcome of the simulation. This has the advantage of accelerating development of future experimental modules as well as minimizing costs and effort in time by applying simulations. But it has to be mentioned that the simulation has its downsides in terms of correct abstraction of the experimental modules. This is caused by the fact that only surface temperatures could be measured within the experiments while the simulation calculates node temperatures. And it could not be shown, that using an aluminium matrix instead of an air heat exchanger, which is submerged in PCM, is enhancing the thermal conductivity resulting in increased heat delivery and faster charging/discharging durations. It is assumed that the aluminium foam with medium porosity is suppressing the natural convection within the storage module and therefore reducing the convective heat transfer performance. Changing the aluminium foam porosity level to values, where both convection as well as heat conduction is increasing the melting process of the encapsulated paraffin, could indeed lead to enhanced thermal performance. Variations in porosity level of the used aluminium foam are part of future development, but not covered within this master thesis. Another reason for lacking thermal performance could be reduced contact surface between the heat exchanger tubes and the aluminium foam. It cannot be excluded that during the casting process the aluminium is not in full contact to the stainless steel pipe and does therefore not provide optimum heat transfer from the heat transfer fluid to the PCM. A comparison in terms of heat delivery and charging duration shows that the submerged air heat exchanger is performing better than the experimental PCM/Aluminium storage modules.

After experimenting excessively with the experimental tubes, an alternative approach of determining the average heat delivery could be worked out. This could be achieved by calculating the energy content of the experimental tubes and determining the charging durations of an average surface temperature and upper and lower standard deviation of the average surface temperature. Unfortunately these measurements could not be compared with the TRNSYS simulation as the measurement uncertainties of the temperature sensors in comparison with the small temperature difference between flow and return stream would lead to false results. Also an arbitrary distribution of surface temperatures could be noticed throughout the measurements despite the fact that the temperature of flow and return stream is almost identical. As this behaviour could be reproduced several times with nearly all measurements it could be excluded that a temperature sensor is in bad contact to the measurement sleeve. This leads to the assumption that there are a few areas within the experimental tube that are not properly filled with paraffin. So it is assumed that areas with less encapsulated paraffin behave differently as areas with more encapsulated paraffin.

Within this master thesis the combination of PCM with aluminium foam as matrix material has been investigated and analysed and it could be shown, that this concept has some potential in storing energy within compact storage modules. But unfortunately the effort of constructing and manufacturing these modules is in contrast to its limited thermal performance for HVAC applications. Additionally, the heat delivery is rather low which is leading to long charging durations.

6 REFERENCES

- Armacell. (21. 04. 2015). *AF/Armaflex*. Abgerufen am 05. 09. 2016 von www.armacell.de: <http://local.armacell.com/de/armacell-deutschland/produkte/afarmaflex/>
- Atal, A., Wang, Y., Harsha, M., & Sengupta, S. (15. 04. 2015). Effect of porosity of conducting matrix on a phase change energy storage device. *International Journal of Heat and Mass Transfer* 93 (2015) 9–16, S. 8.
- Banhart, J., & Seelinger, H.-W. (01. 09. 2008). Aluminium foam sandwich panels: Manufacture, metallurgy and applications. *Advanced engineering materials*, S. 793-802.
- Bauer, C., & Wirtz, R. (5. 11. 2000). Thermal characteristics of a compact, passive thermal energy storage device. *2000 ASME IMECE*, S. 7.
- Cao, P. (24. 04. 2013). *PCM price challenge*. Abgerufen am 01. 05. 2017 von https://cdn2.hubspot.net:https://cdn2.hubspot.net/hub/55819/file-30934935-pdf/docs/pcm_price_challenge.pdf
- DIN 1319-3:1996-05. (1996). Evaluation of measurements of a single measurand, measurement uncertainty Part3. In D. I. Normung, *Fundamentals of metrology*. Beuth Verlag GmbH, Berlin Wien Zürich.
- Endress + Hauser. (28. 10. 2009). www.endress.com. Abgerufen am 30. 05. 2017 von www.endress.com.
- Furbo, S., Fan, J., Andersen, E., Chen, Z., & Perers, B. (2012). Development of seasonal heat storage based on stable supercooling of a sodium acetate water mixture. *Energy Procedia* 30, S. 260-269.
- Gao, D., Chen, Z., Zhang, D., & Chen, L. (12. 01. 2017). Lattice Boltzmann modeling of melting of phase change materials in. *Applied Thermal Engineering* 118, S. 315-327.
- Glysofor-N. (11. 05. 2016). www.westfalen-ag.de. Abgerufen am 10. 02. 2017 von www.westfalen-ag.de: <https://www.westfalen-ag.de/geschaeftskunden/gase-fuer-industrie-und-handwerk/waermetraeger/glysofor-n.html>
- Gnielinski, V., Kabelac, S., Kind, M., Martin, H., Mewes, D., Schaber, K., et al. (2006). *VDI-Wärmeatlas*. Heidelberg Deutschland: Verein deutscher Ingenieure Gesellschaft Verfahrenstechnik und Chemieingenieurwesen.
- Han, X., Tian, Y., & Zhao, C. (11. 06. 2012). An effectiveness study of enhanced heat transfer in phase change materials (PCMs). *International Journal of Heat and Mass Transfer* 60 (2013) 459–468, S. 10.
- Heinz, A. (01. 04. 2007). Application of Thermal Energy Storage with Phase Change Materials in Heating Systems. *Doctoral thesis at the Institute of Thermal Engineering TU GRAZ*, S. 169.
- IEA. (01. 02. 2005). Inventory of Phase Change Materials (PCM) - Advanced storage concepts for solar and low energy buildings. *IEA Solar Heating and Cooling Programm Task 32*.
- Jade, B. (31. 07. 2014). *Silicone heat transfer paste*. Abgerufen am 04. 04. 2017 von www.rs-components.com: <http://at.rs-online.com/web/p/warmeleitpaste/2173835/>
- Kim, K.-b., Choi, K.-w., Kim, Y.-j., Lee, K.-h., & Lee, K.-s. (26. 12. 2008). Feasibility study on a novel cooling technique using a phase change material in an automotive engine. *Energy* 35, S. 487-484.
- Lynch, G. (22. 10. 2014). *How Londons amazing new subway trains were designed*. Abgerufen am 16. 11. 2016 von <http://gizmodo.com>: <http://gizmodo.com/how-londons-amazing-new-subway-trains-were-designed-1649257928>
- Mahdi, J., & Nsofor, E. (20. 06. 2016). Melting enhancement in triplex-tube latent heat energy storage system using nanoparticles-metal foam combination. *Applied Energy* 191 (2017) 22–34, S. 13.
- Mehling, H., & Cabeza, L. (2008). *Heat and cold storage- An up to date introduction into basics and applications*. 85748 Garching: Springer Verlag Berlin Heidelberg.
- Nada, S., & Alshaer, W. (13. 05. 2015). Comprehensive parametric study of using carbon foam structures saturated with PCMs in thermal management of electronic systems. *Energy Conversion and Management* 105 (2015) 93–102, S. 10.

- Nagano, K., Takeda, S., Mochida, T., Shimakura, K., & Nakamura, T. (10. 05. 2006). Study of a floor supply air conditioning system using granular phase change material to augment building mass thermal storage—Heat response in small scale experiments. *Energy and Buildings* 38, S. 436-446.
- Plant engineer. (01. 11. 2007). *Cooling the tube*. Abgerufen am 01. 05. 2017 von <http://www.plantengineer.org.uk>: <http://www.plantengineer.org.uk/article-images/23757%5Ccooling.pdf>
- Rubitherm. (31. 05. 2016). *Rubitherm RT5HC*. Abgerufen am 12. 06. 2016 von www.rubitherm.eu: <https://www.rubitherm.eu/en/index.php/productcategory/organische-pcm-rt>
- Tomizawa, Y., Sasaki, K., Kuroda, A., Takeda, R., & Kaito, Y. (30. 09. 2015). Experimental and numerical study on phase change material (PCM) for thermal management of mobile devices. *Applied Thermal Engineering* 98, S. 320-329.
- Wang, Z., Zhang, Z., Jia, L., & Yang, L. (19. 08. 2014). Paraffin and paraffin/aluminum foam composite phase change material heat storage experimental study based on thermal management of Li-ion battery. *Applied Thermal Engineering*, S. 9.
- Xiao, X., Zhang, P., & Li, M. (21. 05. 2013). Effective thermal conductivity of open-cell metal foams impregnated with pure paraffin for latent heat storage. *International Journal of Thermal Sciences* 81, S. 94-105.
- Zhang, Z., & He, X. (24. 03. 2016). Three-dimensional numerical study on solid-liquid phase change within open-celled aluminum foam with porosity gradient. *Applied Thermal Engineering* 113 (2016) 298–308, S. 11.

7 APPENDIX

7.1 Parametrization of the TRNSYS type 842

Parameter	Value	Unit	Parameter	Value	Unit
nr_nodes	10	-	mass_PCM	10.7	kg
UA_loss	2.6...3.6	W/K	lambda_PCM	0.2	W/(m.K)
l_tubes	0.5	m	rho_PCM	820	kg/m ³
a_tubes	1	-	cps_PCM	15000	J/(kg.K)
nr_tubes_ser	1 or 14*	-	cpl_PCM	2000	J/(kg.K)
nr_tubes_par	1 or 14*	-	hm_PCM	163000	J/kg
d	18	mm	Tm1	4	°C
dw	1	mm	Tm2	5	°C
lambda_t	15	W/(m.K)	dT_sc	0	deltaC
rho_t	7850	kg/m ³	dT_hyst	0	deltaC
cp_t	477	J/(kg.K)	mass_add_cap	18	kg
tf	5	mm	cp_add	477	J/(kg.K)
sf	2	mm	lambda_m	0	W/(m.K)
tl	41.666	mm	lambda_n	0	W/(m.K)
tq	37.5	mm	T_start	8.3...9.1	°C
lambda_f	70.6	W/(m.K)	Pos_T1	0.2	-
cp_f	897	J/(kg.K)	Pos_T2	0.4	-
rho_f	660	kg/m ³	Pos_T3	0.6	-
rho_fhx	1052	kg/m ³	Pos_T4	0.8	-
cp_fhx	3800	J/(kg.K)			

*.....depending on parametrizing the experimental box in parallel or serial flow configuration

7.2 Parametrization of the flow distributor within the simulation

Parameter	Value	Unit	Parameter	Value	Unit
Variable inlet positions	2	-	Deadband for heating element-1	5	deltaC
Tank volume	0.1...6.8	l	Maximum heating rate of element -1	0	kJ/hr
Fluid specific heat	3800	J/(kg.K)	Node containing heating element -2	1	-
Fluid density	1052	kg/m ³	Node containing thermostat -2	1	-
Tank loss coefficient	0.7	W/(m ² .K)	Set point temperature for element-2	60	C
Height of node	0.25	m	Deadband for heating element-2	5	deltaC
Auxiliary heater mode	1	-	Maximum heating rate of element -2	0	kJ/hr
Node containing heating element -1	1	-	Not used (Flue UA)	0	W/K
Node containing thermostat -1	1	-	Not used (Tflue)	20	C
Set point temperature for element-1	60	C	Boiling point	100	C

7.3 Calibration protocol of the PT100 temperature sensors

Calibration protocoll

Job: Kalibrierprotokoll TES4SET
 Datum: 08.02.2017
 Von: Brandstätter Christian
 DataLog: 2017-02-08_cali_PT100s_control.csv

Correctional factors

k			0.9993	0.9991	0.9991	0.9988
d			0.0995	0.1201	0.0909	0.0213

Calibration values

	Sensor	Kelvimat	PT_01	PT_02	PT_03	PT_04
	Channel		12:3	12:7	12:11	12:15
		[°C]	[°C]	[°C]	[°C]	[°C]
1		-9.94	-9.93	-9.93	-9.93	-9.93
2		0.08	0.10	0.10	0.09	0.09
3		10.10	10.11	10.11	10.11	10.11
4		20.02	20.03	20.04	20.03	20.02

Absolute measurement uncertainties

	Sensor	Kelvimat	PT_01	PT_02	PT_03	PT_04
	Channel		12:3	12:7	12:11	12:15
		[°C]	[°C]	[°C]	[°C]	[°C]
1		-9.94	0.01	0.01	0.01	0.01
2		0.08	0.02	0.02	0.01	0.01
3		10.10	0.01	0.01	0.01	0.01
4		20.02	0.01	0.02	0.01	0.00

max. measurement uncertainty

	Sensor		PT_01	PT_02	PT_03	PT_04
	Channel		12:3	12:7	12:11	12:15
		[°C]	[°C]	[°C]	[°C]	[°C]
max			0.02	0.025	0.01	0.01
min			0.01	0.01	0.01	0.00

7.4 Calibration protocol of the Thermocouple sensors

Calibration protocol

Job: Kalibrierprotokoll TES4SET
 Datum: 07.02.2017
 Von: Brandstätter Christian
 DataLog: 2017-02-07_cal_i_TC10s_control.csv

Correctional factors													
k		1.0046	0.9963	0.9978	0.9992	1.0012	0.9971	0.9973	1.0002	1.0012	0.9965	0.9982	0.9993
d		0.0157	0.3226	0.3334	0.4033	0.4269	0.3018	0.3345	0.3817	0.4153	0.2708	0.2717	0.3471

Calibration values													
Sensor	Kelvinat	PT_100_r	B_1	B_2	B_3	B_4	B_5	L_6	L_7	L_8	L_9	L_10	K_11
Channel		12:1	12:3	12:5	12:7	12:9	12:11	12:13	12:15	12:17	12:19	12:21	12:22
	[°C]	[°C]	[°C]	[°C]	[°C]	[°C]	[°C]	[°C]	[°C]	[°C]	[°C]	[°C]	[°C]
1	-9.97	-9.96	-9.92	-9.94	-9.98	-10.00	-9.92	-9.95	-9.98	-10.01	-9.92	-9.95	-9.98
2	0.02	0.03	0.05	0.05	0.03	0.02	0.05	0.04	0.03	0.02	0.04	0.05	0.03
3	10.00	10.01	9.98	9.99	10.01	10.01	9.98	10.00	10.01	10.02	9.98	9.99	10.01
4	19.95	19.96	19.89	19.90	19.94	19.97	19.89	19.91	19.95	19.97	19.90	19.91	19.94

absolute measurement uncertainties													
Sensor	Kelvinat	PT_100_r	B_1	B_2	B_3	B_4	B_5	L_6	L_7	L_8	L_9	L_10	K_11
Channel		12:1	12:3	12:5	12:7	12:9	12:11	12:13	12:15	12:17	12:19	12:21	12:22
	[°C]	[°C]	[°C]	[°C]	[°C]	[°C]	[°C]	[°C]	[°C]	[°C]	[°C]	[°C]	[°C]
1	-9.97	0.01	0.05	0.03	-0.01	-0.03	0.05	0.02	-0.01	-0.04	0.05	0.02	-0.01
2	0.02	0.01	0.03	0.03	0.01	0.00	0.03	0.02	0.01	0.00	0.02	0.03	0.01
3	10.00	0.01	-0.02	-0.01	0.01	0.01	-0.02	0.00	0.01	0.02	-0.02	-0.01	0.01
4	19.95	0.01	-0.06	-0.05	-0.01	0.02	-0.06	-0.04	0.00	0.02	-0.05	-0.04	-0.01

max. measurement uncertainty													
Sensor	Kelvinat	PT_100_r	B_1	B_2	B_3	B_4	B_5	L_6	L_7	L_8	L_9	L_10	K_11
Channel		12:1	12:3	12:5	12:7	12:9	12:11	12:13	12:15	12:17	12:19	12:21	12:22
	[°C]	[°C]	[°C]	[°C]	[°C]	[°C]	[°C]	[°C]	[°C]	[°C]	[°C]	[°C]	[°C]
max		0.01	0.05	0.03	0.01	0.02	0.05	0.02	0.01	0.02	0.05	0.03	0.01
min		0.01	-0.06	-0.05	-0.01	-0.03	-0.06	-0.04	-0.01	-0.04	-0.05	-0.04	-0.01

7.5 Error estimation of the flow meter Endress + Hauser Promag 50P25

Error estimation

Date 07.12.2016

MID Endress Hauser Promag 50P25; inventory number: 0171427

Scales Mettler Toledo KC120 and ID1 Multirange; inventory number: 0012558

Temperature Water	v_dot_water	v_MID	Density water	mass water	Volume	Volume MID	relative error
[°C]	[l/h]	[m/s]	[kg/dm ³]	[kg]	[dm ³]	[dm ³]	[%]
15.4	674	0.363	0.999041	100.54	100.637	100	0.63

7.6 Tech data sheet Rubitherm RT5HC

source: Rubitherm (2016)

Data sheet



RT5HC



RUBITHERM® RT is a pure PCM, this heat storage material utilising the processes of phase change between solid and liquid (melting and congealing) to store and release large quantities of thermal energy at nearly constant temperature. The RUBITHERM® phase change materials (PCM's) provide a very effective means for storing heat and cold, even when limited volumes and low differences in operating temperature are applicable.

We look forward to discussing your particular questions, needs and interests with you.

Properties:

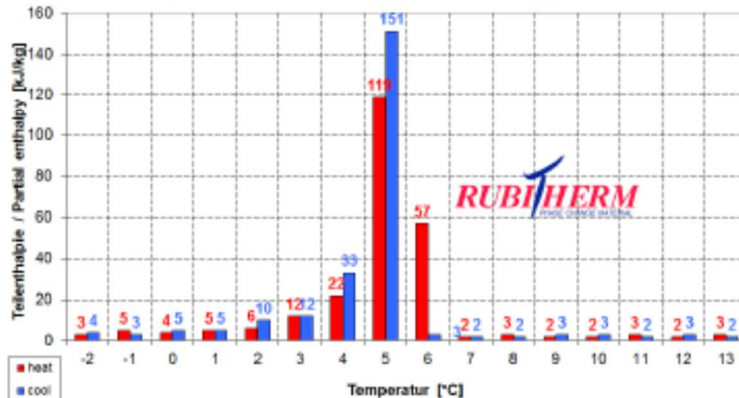
- high thermal energy storage capacity
- heat storage and release take place at relatively constant temperatures
- no supercooling effect, chemically inert
- long life product, with stable performance through the phase change cycles
- melting temperature range between -4 °C and 100 °C

The most important data:

	Typical Values	
Melting area	5-6	[°C]
	main peak: 6	
Congeealing area	6-5	[°C]
	main peak: 5	
Heat storage capacity ± 7,5%	250	[kJ/kg]*
Combination of latent and sensible heat in a temperatur range of -2 °C to 13°C.	70	[Wh/kg]*
Specific heat capacity	2	[kJ/kg·K]
Density solid at -15°C	0,88	[kg/l]
Density liquid at 20 °C	0,76	[kg/l]
Heat conductivity (both phases)	0,2	[W/(m·K)]
Volume expansion	13	[%]
Flash point	115	[°C]
Max. operation temperature	30	[°C]



Beispiel: RT5HC Teilenthalpie / Partial enthalpy distribution



*Measured with 3-layer-calorimeter.

Rubitherm Technologies GmbH
 Sperenberger Str. 5a
 D-12277 Berlin
 Tel: +49 30 720004-62
 Fax: +49 30 720004-99
 E-Mail: info@rubitherm.com
 Internet: www.rubitherm.com

The product information given is a non-binding planning aid, subject to technical changes without notice. Version: 31.03.2016

7.7 Glysofor N – Specifications part I

source: Glysofor N (2016)

Frostschutzmittel

Auf der Basis von Glykol (Monoethylenglykol) setzt Glysofor N den Gefrierpunkt von Wasser deutlich herab und verhindert, z. B. in Heizungssystemen oder Kühlsystemen, das Gefrieren der Flüssigkeit. Heizungsanlagen können mit Glysofor N auch bei Frost vorübergehend abgeschaltet werden, bleiben jedoch jederzeit funktionsbereit. In temporär genutzten Einrichtungen wie Sporthallen, Wochenendhäusern, Kirchen, Schulen oder Veranstaltungsräumen kann dies zu einer erheblichen Einsparung von Brennstoffen führen. Eine frostbedingte Beschädigung des Systems durch eine Sprengwirkung wird durch Glysofor N sicher vermieden.

Glysofor N – Aktivgehalt (Volumen)	Frostschutz bis °C
20 %	-9
25 %	-12
30 %	-16
35 %	-20
40 %	-25
45 %	-31
50 %	-38
55 %	-45
58 %	-51

7.8 Glysofor N – Specifications part II

source: Glysofor N (2016)



Konzentration [Vol.-%]	Frostschutz [°C]	Temperatur [°C]	Wärmeleitfähigkeit [W/m K]	Spezifische Wärme [kJ/kg K]	Dichte [g/cm ³]	Kinemat. Viskosität [mm ² /s]	Kub. Wärmeausdehnungskoeffizient [K ⁻¹]	Relativer Drukverlust [Faktor]
20	-9	0	0,490	3,92	1,035	3,34	0,00021	1,28
		10	0,501	3,98	1,032	2,44	0,00028	1,18
		20	0,512	3,99	1,029	1,82	0,00034	1,07
		30	0,523	4,02	1,025	1,40	0,00039	1,00
		40	0,535	4,04	1,021	1,11	0,00045	0,95
		50	0,548	4,06	1,016	0,90	0,00050	0,90
		60	0,557	4,07	1,010	0,75	0,00055	0,87
		70	0,568	4,08	1,005	0,64	0,00059	0,84
		80	0,580	4,08	0,998	0,57	0,00063	0,81
		90	0,591	4,09	0,992	0,51	0,00067	0,78
		100	0,602	4,08	0,985	0,47	0,00071	0,76
		-10	0,458	3,82	1,048	5,51	0,00022	1,49
25	-12	0	0,489	3,88	1,044	3,88	0,00027	1,34
		10	0,479	3,90	1,040	2,78	0,00033	1,22
		20	0,490	3,93	1,037	2,08	0,00038	1,13
		30	0,501	3,98	1,032	1,57	0,00043	1,05
		40	0,511	3,99	1,028	1,23	0,00047	1,00
		50	0,522	4,01	1,022	0,99	0,00052	0,94
		60	0,533	4,02	1,017	0,82	0,00056	0,90
		70	0,544	4,04	1,011	0,70	0,00061	0,87
		80	0,554	4,04	1,004	0,62	0,00065	0,83
		90	0,565	4,04	0,998	0,56	0,00069	0,80
		100	0,576	4,04	0,990	0,51	0,00072	0,77
		-10	0,438	3,73	1,056	6,43	0,00028	1,58
30	-18	0	0,448	3,78	1,052	4,45	0,00033	1,39
		10	0,458	3,82	1,049	3,17	0,00037	1,28
		20	0,468	3,86	1,044	2,33	0,00041	1,18
		30	0,479	3,89	1,040	1,78	0,00045	1,10
		40	0,489	3,92	1,035	1,37	0,00049	1,04
		50	0,499	3,94	1,029	1,10	0,00053	0,98
		60	0,509	3,98	1,024	0,90	0,00057	0,93
		70	0,519	3,97	1,017	0,77	0,00061	0,89
		80	0,530	3,98	1,011	0,67	0,00064	0,85
		90	0,540	3,98	1,004	0,61	0,00068	0,82
		100	0,550	3,98	0,997	0,56	0,00071	0,79
		-20	0,414	3,52	1,068	12,49	0,00030	1,84
-10	0,423	3,58	1,064	8,18	0,00034	1,62		
35	-20	0	0,431	3,64	1,061	5,48	0,00037	1,44
		10	0,440	3,69	1,056	3,79	0,00041	1,32
		20	0,449	3,73	1,052	2,71	0,00044	1,22
		30	0,458	3,76	1,047	2,00	0,00047	1,13
		40	0,468	3,81	1,042	1,53	0,00050	1,06
		50	0,475	3,84	1,038	1,20	0,00053	1,00
		60	0,484	3,88	1,030	0,98	0,00056	0,95
		70	0,493	3,88	1,024	0,83	0,00059	0,91
		80	0,501	3,89	1,018	0,72	0,00062	0,87
		90	0,510	3,90	1,012	0,65	0,00065	0,83
		100	0,519	3,91	1,005	0,60	0,00067	0,80
		-20	0,400	3,34	1,077	17,09	0,00036	1,91
-10	0,407	3,41	1,073	10,59	0,00038	1,67		
40	-25	0	0,415	3,47	1,068	6,84	0,00041	1,49
		10	0,422	3,53	1,064	4,57	0,00044	1,37
		20	0,430	3,58	1,059	3,18	0,00048	1,27
		30	0,437	3,63	1,054	2,30	0,00048	1,17
		40	0,445	3,67	1,049	1,72	0,00051	1,09
		50	0,452	3,71	1,043	1,33	0,00056	1,03
		60	0,460	3,74	1,037	1,07	0,00058	0,98
		70	0,467	3,77	1,031	0,90	0,00062	0,93
		80	0,475	3,79	1,025	0,78	0,00065	0,89
		90	0,482	3,80	1,019	0,71	0,00068	0,85
		100	0,490	3,81	1,013	0,66	0,00072	0,82
		-30	0,376	3,09	1,090	38,90	0,00039	
-20	0,383	3,18	1,085	21,09	0,00041	1,98		
-10	0,390	3,25	1,081	12,29	0,00043	1,73		
45	-31	0	0,397	3,32	1,076	7,74	0,00044	1,55
		10	0,404	3,39	1,071	5,15	0,00048	1,41
		20	0,411	3,45	1,066	3,61	0,00048	1,31
		30	0,417	3,50	1,060	2,63	0,00050	1,21
		40	0,424	3,55	1,055	1,99	0,00053	1,13
		50	0,431	3,60	1,049	1,55	0,00055	1,06
		60	0,438	3,64	1,043	1,25	0,00058	1,01
		70	0,445	3,67	1,037	1,04	0,00060	0,96
		80	0,452	3,70	1,030	0,90	0,00063	0,92
		90	0,459	3,72	1,024	0,79	0,00065	0,88
		100	0,466	3,74	1,017	0,73	0,00068	0,84

7.9 AF/Armaflex insulation material

source: AF/Armaflex (2015)

Leistungserklärung Nr. 0543-CPR-2013-001

Eindeutiger Kenncode des Produkttyps:	AF/Armaflex
Verwendungszweck(e):	Wärmedämmprodukt für die technische Gebäudeausrüstung und für betriebstechnische Anlagen in der Industrie (ThiBEII)
Hersteller:	Armacell GmbH Robert-Bosch-Str. 10 D-48153 Münster
Systeme zur Bewertung und Überprüfung der Leistungsbeständigkeit:	1 und 3
Harmonisierte Norm:	EN 14304:2009+A1:2013
Notifizierte Stelle/Stelle(n):	NB 0919, NB 0751, NB 0432
Erklärte Leistung(en):	

Wesentliche Merkmale	Leistung		
Wärmedurchlasswiderstand/ Wärmeleitfähigkeit	Schläuche Platten, Band	$d_M = 7 - 25 \text{ mm (AF1-AF4)}$ $d_M = 3 - 32 \text{ mm}$	$\lambda_{\vartheta_{\text{C}}} \leq 0,033 \text{ W/(m}\cdot\text{K)},$ $\lambda(\vartheta_m) = (33 + 0,1 \cdot \vartheta_m + 0,0008 \cdot \vartheta_m^2) / 1000$
	Schläuche Schläuche Platten	$d_M = 25 - 45 \text{ mm (AF5-AF6)}$ $d_M = 54 \text{ mm}$ $d_M = 36 - 50 \text{ mm}$	$\lambda_{\vartheta_{\text{C}}} \leq 0,036 \text{ W/(m}\cdot\text{K)},$ $\lambda(\vartheta_m) = (36 + 0,1 \cdot \vartheta_m + 0,0008 \cdot \vartheta_m^2) / 1000$
Brandverhalten	Schläuche Platten, Band Schläuche	$d_M = 7 - 45 \text{ mm (AF-1-AF6)}$ $d_M = 3 - 50 \text{ mm}$ $d_M = 54 \text{ mm}$	B _L -s3,d0 B-s3,d0 E
Dauerhaftigkeit des Wärmedurchlasswiderstandes unter Einfluss von Alterung / Abbau	Dimensionsstabilität ¹⁾ Untere Anwendungsgrenztemperatur ST(-)50 (= -50 °C)		
Dauerhaftigkeit des Wärmedurchlasswiderstandes unter Einfluss von hohen Temperaturen	Obere Anwendungsgrenztemperatur ST(+)110 (=110 °C)		
Dauerhaftigkeit des Brandverhaltens unter Einfluss von Alterung / Abbau	Eigenschaften der Dauerhaftigkeit ²⁾		
Dauerhaftigkeit des Brandverhaltens unter Einfluss von hohen Temperaturen	Eigenschaften der Dauerhaftigkeit ²⁾		
Wasseraufnahme	NPD		

7.10RS Components – Heat transfer paste RS217-3835

source: RS Components (2014)



Professionally approved products

TECHNICAL DATA SHEET

RS 217-3835 Silicone Heat Transfer Paste

RS 217-3835 should be used where a large amount of heat needs to be dissipated quickly and effectively. RS 217-3835 is a non-setting compound which allows easy rework of the components should this be necessary.

- Superior thermal conductivity even at high temperatures.
- Wide operating temperature range.
- Low evaporation weight loss.
- Economic in use.
- Low in toxicity.

Approvals	RoHS-2 Compliant (2011/65/EU):	Yes
Typical Properties:	Colour: Base Thermo-conductive Component: Thermal Conductivity: Density @ 20°C: Temperature Range: Weight Loss after 96 hours @ 100°C: Specific Resistance: Dielectric Strength: Viscosity (Pa*s):	Pale Gray Silicone Oil Powdered metal oxides 2.9 W/m*K 3 g/cm ³ -40°C to +200°C <0.8% 1 x 10 ¹⁴ Ohms/cm 16 kV/mm 45 at 1 rpm

<u>Packaging</u>	<u>Order Code</u>
20 ml Tube	RS 217-3835

Directions for Use

Apply a thin layer of compound to one of the contact surfaces using brush, spatula, roller, automated systems or screen printing techniques. Ensure that the entire interface is covered otherwise hot-spots can form and place the surfaces together. Any excess paste squeezed out during the mounting process should be removed. Best results are achieved when a uniform, thin coat is applied between the mating surfaces.

WLF745869